# Forced regression in rift shoulder derived deltas

**Anders Hågenvik**

Master thesis in Basin and Reservoir studies

Department of Earth Science

University of Bergen

June 2018

# Abstract

Footwall uplift and migration of fault activity have led to the preservation of spectacular down-stepping Gilbert-type deltas at the southern margin of the Corinth Rift. It is the purpose of this thesis to present the architecture and sedimentology of the down-stepping deltas to better understand the geological processes controlling this type of delta deposits. This study contributes with sedimentary and sequence stratigraphic analysis to better constrain the Late Pleistocene evolution of the southern margin of the Corinth Rift. Several studies have been conducted on the giant Gilbert-type deltas at the southern margin of the Corinth Rift; however there are no detailed studies on the Late Pleistocene deltas investigated in this study. Sedimentological and sequence stratigraphic data was obtained by combining traditional fieldwork techniques with digital acquisition techniques. Virtual outcrop models were generated from UAV data obtained during the field work and from an already existing LiDAR dataset. Six different delta bodies were mapped in the study area (Delta 1, Delta 2, Delta 3, Delta 4, Delta 5 and Delta 6). Eleven different facies were identified in the delta deposits, which are organized in four main facies associations: (1) topset, (2) foreset, (3) toeset and (4) bottomset. The sedimentology of the deltas is similar to previously studied giant Gilbert-type deltas at the southern margin of the Corinth Rif.  The dimensions of the investigated deltas differ from the giant-Gilbert type deltas, which is interpreted to be due to their location on the footwall crest rather than in the immediate hangingwall. In general, the younger deltas are deposited topographically lower than the older deltas, except Delta 5 and Delta 6, which are deposited on top of Delta 4. Based on the analysis of shoreline trajectories and stratal termination surfaces recorded in the delta deposits, a significant relative sea-level rise from Delta 4 to Delta 6 is interpreted, which has not been described in previous work.

**Keywords** Corinth Rift, Gilbert-type deltas, facies analysis, sequence stratigraphy, shoreline trajectories, Pleistocene

# Acknowledgements

This thesis is part of a master's degree in basin and reservoir studies at the Department of Earth Science at the University of Bergen.

First and foremost, I will like to thank my main supervisor Dr. Martin Muravchik for great guidance during fieldwork and in the process of writing this thesis. Thank you for great discussions, constructive feedback and for processing the LiDAR and UAV data utilized in this study.

I will also like to thank my co-supervisors Dr. Gijs Allard Henstra and Prof. Rob Gawthorpe, and PhD Candidate Gauti Trygvason Eliassen for great discussions in the field and for always answering my questions. I will like to thank my field partner Sandra Eriksson for good teamwork during two field seasons and for the work we performed together in the seismic lab. I will also like to thank you all for good times in Loutraki and especially for memorable evenings at the "Five brothers" restaurant.

I will also like to thank Prof. Rob Gawthorpe for letting me take part in the Syn-Rift Systems Project. Thanks to the sponsors of the project: The National Research Council Norway, Faroe Petroleum, Conoco Phillips, AkerBP, Equinor and VNG Norge for funding the project.

Thanks to my fellow students and friends at the University of Bergen for five memorable years. A special thanks to the people in "Hjørnerommet" and the seismic lab "Grotten" for great discussions and for always being helpful.

Last but not least, I will like to thank my family and girlfriend for always being supportive. You are eternally appreciated.

<div align="center">

Anders Hågenvik

Bergen, 01.06.2018

</div>

# Table of Contents

# 1 Introduction

## 1.1 Rationale and background

The Corinth Rift is one of the world's most rapidly extending continental rift systems (e.g., Taylor et al., 2011, Gawthorpe et al., 2017a, Ford et al., 2013). It is an outstanding area to investigate the early development of rift basins (e.g., Taylor et al., 2011, Nixon et al., 2016). Migration of fault activity and footwall uplift (e.g., Backert et al., 2010, Gawthorpe et al., 2017a) have led to the preservation of spectacular down-stepping Gilbert-type deltas at the southeastern margin of the Corinth Rift.

Gilbert-type deltas play an important role in basin analysis as they are considered to be sensitive recorders of relative sea-level changes, especially in tectonic active areas (e.g., Gawthorpe et al., 1990, Breda et al., 2007, Gobo et al., 2015). The transition from topset to foreset can be used to interpret the variations in accommodation space and sediment supply (e.g., Gawthorpe et al., 1994, García-García et al., 2006, Rohais et al., 2008). The accommodation space is controlled by eustatic sea-level changes, climate and local tectonics (e.g., Van Wagoner et al., 1988, Emery et al., 1996, Catuneanu, 2006). Sedimentological and sequence stratigraphic analysis of Gilbert-type deltas can therefore be very valuable when it comes to understanding the evolution of a rift system.

The deltas investigated in this study are located on the southeastern margin of the Corinth Rift, in the proximity of the city of Xylokastro (Fig. 1.1). There have been conducted several studies on giant Gilbert-type deltas in the central and western part of the Corinth Rift (e.g., Ori, 1989, Rohais et al., 2008, Backert et al., 2010, Gobo et al., 2015), but there are no detailed studies on the Late Pleistocene deltas of the study area. However, Armijo et al. (1996) have conducted a study on marine terraces and paleo-shorelines between Corinth and Xylokastro.

Nine marine terraces have been mapped in the study area by Armijo et al. (1996), using aerial and SPOT imagery combined with field observations. As a result of the detailed mapping conducted in this study, it was found that some of the marine terraces interpreted by Armijo et al. (1996) partly correspond to delta topsets.

It is the purpose of this study to present the architecture and sedimentology of the down-stepping Gilbert-type deltas to better understand the geological processes controlling this type of delta deposits. This study contributes with sedimentary and sequence stratigraphic analysis to better constrain the Late Pleistocene evolution of the southern margin of the Corinth Rift.
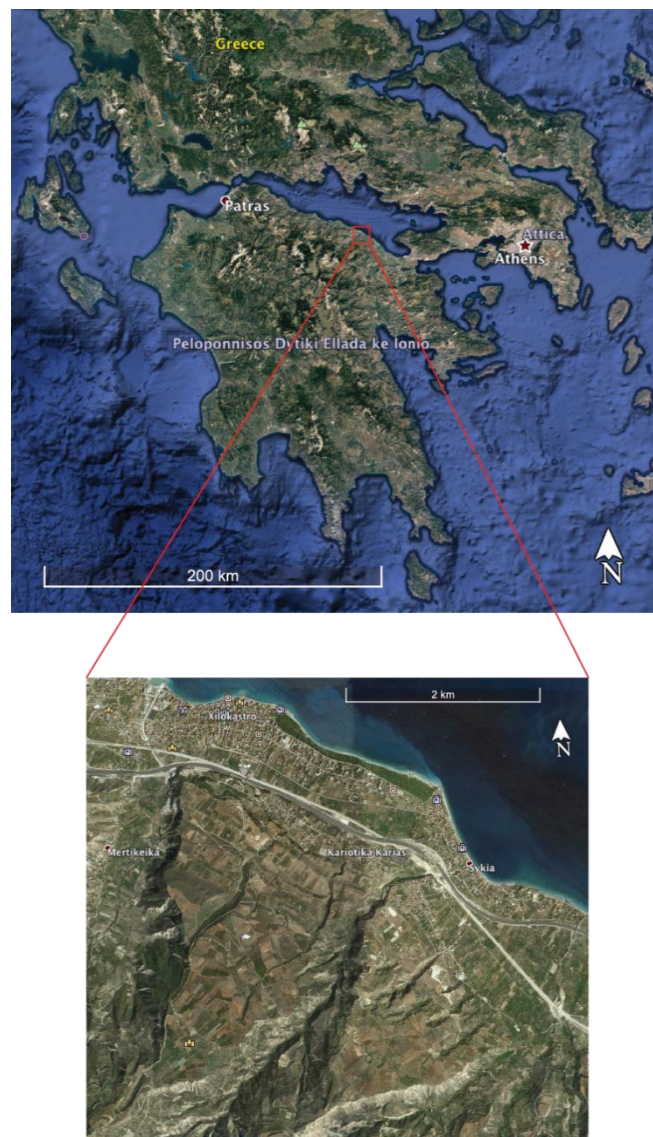


**Fig. 1.1:** Location of the study area. Maps are modified from Google Earth.

## 1.2 Aims and objectives

The aim of this thesis is to analyze the sedimentology and sequence stratigraphy and generate detailed maps of the Late Pleistocene deltas of the study area, to better constrain the evolution of the southern margin of the Corinth Rift. The objectives for this study are:

i.      Analyze the sedimentology and the architecture of the deltaic system

ii.     Map the delta bodies and physically correlate the different delta units

iii.    Study the relation between the different deltas and determine their relative age

iv.     Use shoreline trajectory analysis to better understand the role of accommodation space as a controlling factor on the deposition of these deltas and its link with eustatic and tectonic processes

# 2 Theoretical background

## 2.1 Sedimentology of Gilbert-type deltas

Gilbert-type deltas were first described by Gilbert (1885) and later named after him. They are characterized by high-angle delta front slopes and steeply inclined profiles (e.g., Postma and Roep, 1985, Reading, 1996a, Kleinhans, 2005). Gilbert-type deltas are generally coarse-grained (e.g., Gawthorpe et al., 1990, Longhitano, 2008) and ideally, they have a tripartite depositional geometry with topset, foreset and bottomset (Fig. 2.1) (e.g., Postma and Roep, 1985, Nemec, 1990, Rojas and Le Roux, 2010). Gilbert-type deltas typically form where a fluvial system prograde into a relatively deep body of water (e.g., Sohn et al., 1997, Kleinhans, 2005, Gobo et al., 2014). They were initially described as lacustrine features (e.g., Stanley and Surdam, 1978, Falk and Dorsey, 1998), but in the last decades Gilbert-type deltas have been recognized in marine settings (e.g., Prior et al., 1981, Postma, 1984, Colella et al., 1987). Gilbert-type deltas are typically observed in tectonic active areas (e.g., Gawthorpe et al., 1990, Ford et al., 2007, Rohais et al., 2008, Backert et al., 2010, Gobo et al., 2015) but they are also common in proglacial settings (e.g., Nemec et al., 1999, Lønne et al., 2001, Lønne and Nemec, 2004).

Gilbert-type topsets are predominantly defined as gently inclined (<6°) fluvial deposits on top of the delta (e.g., Postma and Roep, 1985, Colella, 1988a, Backert et al., 2010). The topsets are generally dominated by fluvial traction sedimentation and mass flow deposits (Falk and Dorsey, 1998). The foreset deposits are dominated by gravity driven processes and may reach slope gradients up to 35° (Colella, 1988b, Sohn et al., 1997). They may consist of both sand and gravel-dominated deposits (e.g., Sohn et al., 1997, Rohais et al., 2008, Backert et al., 2010, Gobo et al., 2015, Gawthorpe et al., 2017a). The sand-dominated foresets are commonly intercalated with silt beds and they are usually interpreted to form during deposition of turbidity-currents (Sohn et al., 1997). The gravel-dominated foresets commonly consists of poorly sorted, massive or crudely stratified, matrix to clast-supported conglomerates (e.g., Rohais et al., 2008, Backert et al., 2010, Gobo et al., 2015). The gravel-dominated foresets are commonly interpreted as debris flow deposits (e.g., Rohais et al.,

2008, Backert et al., 2010, Gobo et al., 2015). The topset to foreset transition is commonly referred to as the delta-brink (Gobo et al., 2015). The break in slope between the topset and foreset is  called the offlap break (Vail, 1991). Gilbert-type bottomsets are typically described as gently inclined deposits (<10°) originated from suspension load and gravity flows (e.g., Reading, 1996b, Backert et al., 2010). The transition from foreset to bottomset is usually referred to as the delta toeset (e.g., Massari, 1996, Sohn et al., 1997, Breda et al., 2007).
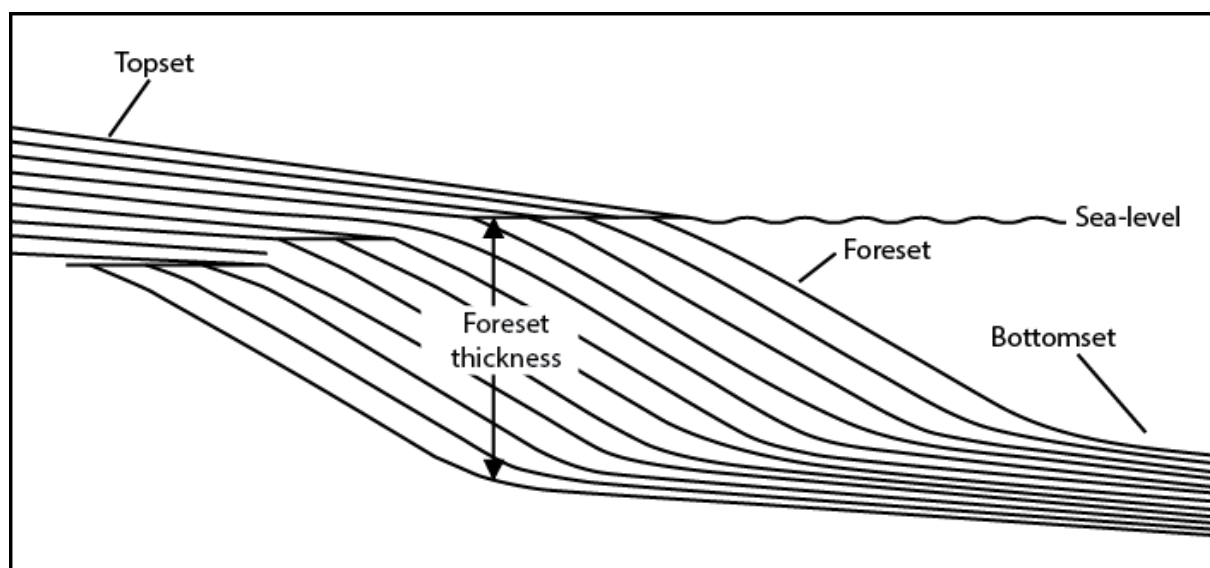


**Fig. 2.1:** Idealized cross-section of a Gilbert-type delta with topset, foreset and bottomset. Modified from Postma and Roep (1985).

## 2.2 Gilbert-type deltas in rift basins

The formation of Gilbert-type deltas are dependent on conditions with high sediment supply, high water flux and high creation of accommodation space (Backert et al., 2010). Gilbert-type deltas are favored by steep subaqueous slopes, which are frequent in small fault controlled basins (Colella, 1988a). Gilbert-type deltas are frequently found in many lacustrine and marine rift basins, for example, the Crati Basin (Colella, 1988a) the Gulf of Corinth (e.g., Rohais et al., 2008, Backert et al., 2010, Gobo et al., 2015, Gawthorpe et al., 2017a) and the Gulf of Suez (e.g., Gawthorpe et al., 1990, Gupta et al., 1999).

On a basin scale, sediment sources and depocenters are created by footwall uplift and hangingwall subsidence respectively (Gawthorpe et al., 1990). The location of the Gilbert-type delta with respect to major normal faults may have great impact on the internal architecture and sequence geometry (Gawthorpe et al., 2017b). Giant Gilbert-type deltas are commonly found on the immediate hangingwall of major normal faults (e.g., Gupta et al., 1999, Gawthorpe et al., 2017a), where subsidence may outpace eustatic sea-level fall, resulting in an aggrading and prograding system (Gawthorpe and Leeder, 2000). Various stacking patterns may develop along-strike of normal faults due to different rates of displacement from the fault center towards the fault tip (Fig. 2.2) (Gawthorpe et al., 2003). High rates of displacement near fault center of a normal fault may cause a relative sea-level rise and more accommodation space available, which can result in the deposition of aggradationally stacked deltas (e.g., Gawthorpe and Leeder, 2000, Young et al., 2000). The stacking pattern will change from aggradational to progradational if the rate of sediment supply becomes greater than the rate of accommodation space generated (e.g., Gawthorpe and Leeder, 2000, Young et al., 2000).
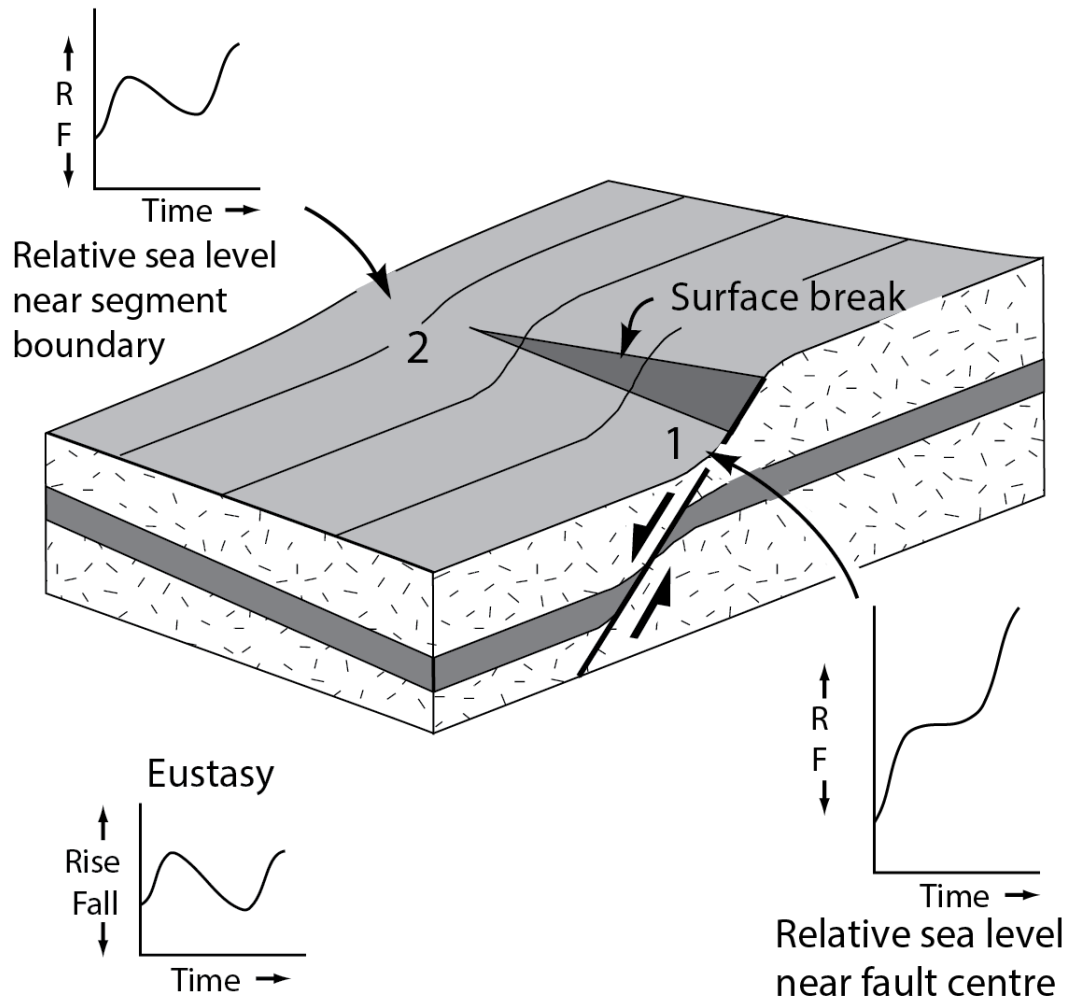
**Fig. 2.2:** Along-strike variations for an idealized half fault segment. The graphs are illustrating the along-strike differences in relative sea-level changes as a consequence to different displacement rates. The displacement rates are higher close to the fault centre than close to the fault tip. Modified from Gawthorpe and Leeder (2000).

## 2.3 Sequence stratigraphy and architectural elements in Gilbert-type deltas

Sequence stratigraphy is in a simple way defined as the subdivision of sedimentary deposits into genetically related packages bounded by unconformities and their correlative conformities (Emery et al., 1996). The term sequence is fundamental in sequence stratigraphy (Van Wagoner et al., 1988) and it was first defined by Mitchum et al. (1977) as a genetically related and relatively conformable succession of strata bounded by unconformities or correlative conformities at its top and base. A sequence is composed of several parasequence sets, which is defined as genetically related parasequences stacked in a distinctive pattern, bounded by major flooding surfaces (Van Wagoner et al., 1988). A parasequence is defined as a genetically related and relatively conformable succession of beds bounded by flooding surfaces (Van Wagoner et al., 1988).

In sequence stratigraphy it is important to differentiate between eustatic and relative sea-level. Eustatic sea-level (or eustasy) is the global sea-level and it is usually measured between the center of the Earth and the sea-surface (Emery et al., 1996). The relative sea-level is the local sea-level at a specific time (Kemp et al., 2015) and it is controlled by both the eustatic sea-level and local changes in the elevation of the sea-floor (Coe, 2003).

The depositional architecture in a sedimentary system is highly controlled by the balance between accommodation space and sediment supply (Coe, 2003). The term accommodation space was first defined by Jervey (1988) and is used to describe the space available for sediment accumulation below sea-level in marine settings (Viseras et al., 2003). By investigating the delta brink zone of a Gilbert-type delta, it is possible to say something about the balance between accommodation space and sediment supply (Rohais et al., 2008). In terms of the topset to foreset transition, (Mitchum Jr et al., 1977)differentiate between sigmoidal (transitional) and oblique (erosional) toplap geometries (Fig. 2.3). The term toplap describes a termination of inclined strata against an low-angle overlying surface (Fig. 2.4) (Catuneanu, 2006). Both sigmoidal and oblique toplap are interpreted to be due to clinoform progradation (Mitchum Jr et al., 1977). Sigmoidal toplap is associated with a relative sea-level rise and oblique toplap is associated with a decrease in accommodation space (Gobo et al., 2015). When strata is terminated by an overlying erosional surface it is referred to as an

erosional truncation (Fig. 2.4) (Emery et al., 1996). The transition from foreset to bottomset can either be tangential (e.g., Gilbert, 1885, Nemec et al., 1999) or sharply angular (fig. 2.3) (e.g., Colella, 1988b, Zelilidis and Kontopoulos, 1996). When inclined strata terminates downwards against a low-angle surface it is referred to as downlap (Fig. 2.4) (Catuneanu, 2006).
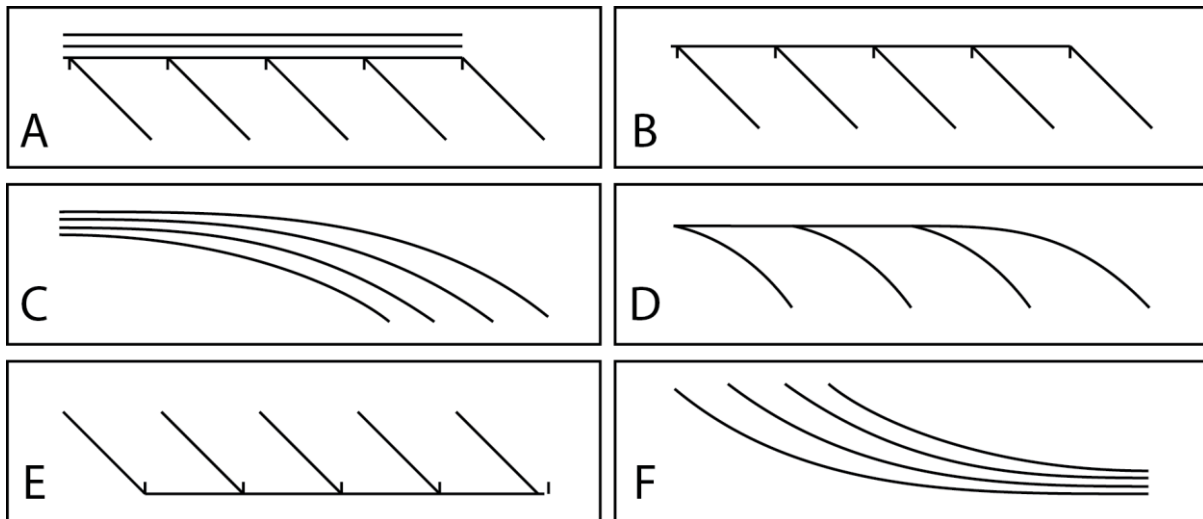


**Fig. 2.3:** Different types of toplap and downlap geometries. A: Oblique toplap with fluvial or marine deposits on top. B: Oblique toplap with no overlying deposits. C: Sigmoidal toplap with topset preserved. D: Sigmoidal toplap without topset.  E: Sharp/angular downlap. F: Tangential downlap.
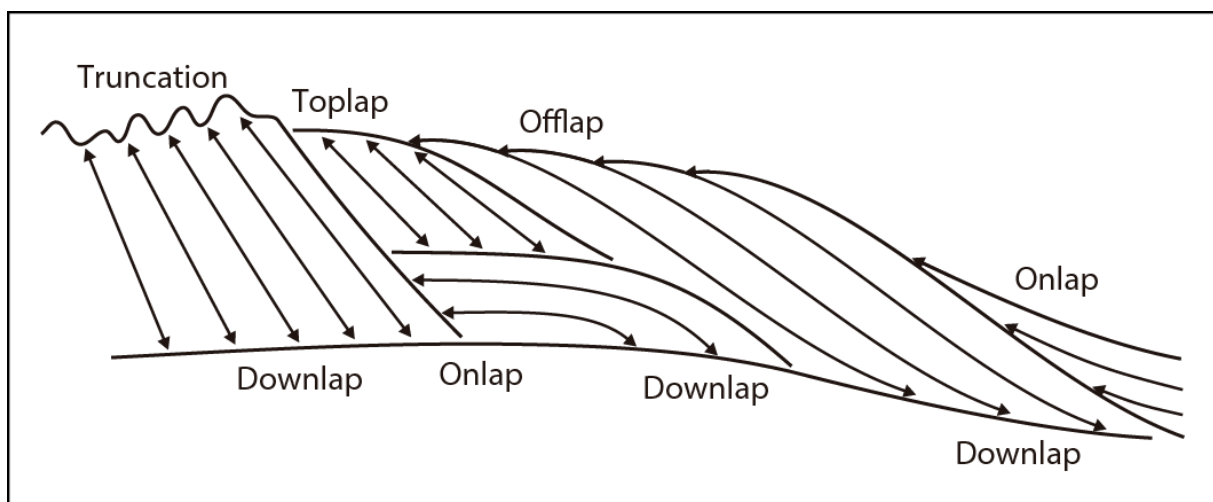


**Fig. 2.4:** Stratal terminations. Modified by Catuneanu (2006) from Emery et al. (1996).

In sequence stratigraphy depositional cycles are subdivided into systems tracts. System tracts were originally defined by Brown Jr and Fisher (1977) as the linkage of contemporaneous depositional systems. The boundaries of systems tracts are defined by the stratal termination surfaces (onlap, downlap, etc.) (Emery et al., 1996). The systems tracts can be divided into four cycles (Helland-Hansen and Martinsen, 1996): (1) the highstand systems tract (HST), (2) the falling stage systems tract (FSST), (3) the lowstand systems tract (LST), (4) the transgressive systems tract (TST) (Coe, 2003). During the highstand systems tract sediments are deposited in the late phase of an eustatic sea-level rise (Van Wagoner et al., 1988) and HST is characterized by an aggradational to progradational stacking pattern of parasequence sets (Coe, 2003). During the falling stage systems tract sediments are deposited when the sea-level is falling (Coe, 2003) and FSST is characterized by prograding, down stepping wedges (Posamentier et al., 1992). During the lowstand systems tract sediments are deposited in the late phase of eustatic sea-level fall or during the early rise (Van Wagoner et al., 1988). LST is characterized by progradational to aggradational stacking of parasequence sets (Coe, 2003). During the transgressive systems tract sediments are deposited when there is a rapid eustatic sea-level rise (Van Wagoner et al., 1988). TST is characterized by retrograding parasequences and if the sediment supply is low, the deposits may be thin or even absent (Coe, 2003). The systems tracts represent different portions of a relative sea-level curve (e.g., Helland-Hansen and Martinsen, 1996, Hampson et al., 2009). The more continuous spectrum of deposition during relative sea-level changes, can be investigated by applying the shoreline trajectory concept (Henriksen et al., 2009).

The shoreline trajectory concept was first described by Helland-Hansen and Martinsen (1996) and it can be used to describe the stratigraphic architecture observed in 2D and 3D data (Hampson et al., 2009). The shoreline trajectory describes the shoreline migration path in a cross-section and it is a function of relative sea-level changes, basin physiography and sediment supply (Helland-Hansen and Gjelberg, 1994, Helland-Hansen and Martinsen, 1996). The shoreline trajectory can be grouped into three main classes: 1. Transgressive, 2. Ascending regressive and 3. Descending regressive (Fig. 2.5) (Helland-Hansen and Hampson, 2009). The transgressive and descending regressive trajectory classes can be subdivided into accretionary and non-accretionary types (Helland-Hansen and Hampson, 2009). The accretionary trajectories are characterized by sediment accumulation at the shoreline

(Helland-Hansen and Martinsen, 1996). The non-accretionary trajectories are characterized by minor or no sediment supply and the shoreline trajectory coincides with the basin topography (Fig. 2.5) (Helland-Hansen and Martinsen, 1996).
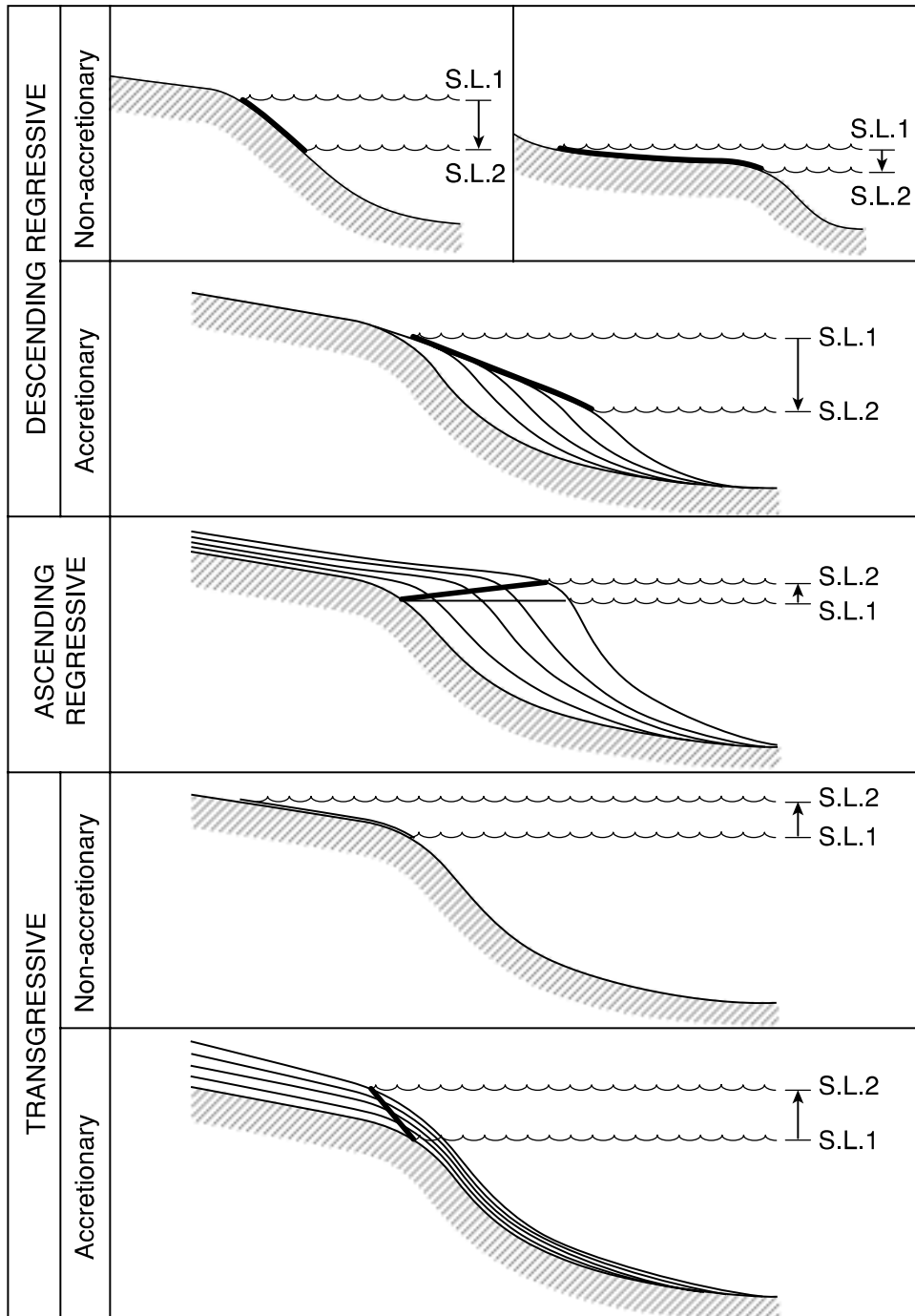


**Fig. 2.5:** The shoreline trajectory classes. Modified from Helland-Hansen and Hampson (2009).

# 3 Geological setting

## 3.1 Tectonic setting

### 3.1.1 Tectonic setting of the Aegean Region

The Corinth Rift is located in the north-western part of the Aegean region, one of the most active extensional regions in the world (e.g., McKenzie, 1972, McKenzie, 1978, Armijo et al., 1996). It is part of the Aegean microplate (Fig 3.1) (Kahle et al., 1998), which is dominantly affected by the plate motions of the Eurasian plate, the African plate and the Arabian plate (Fig. 3.1) (Le Pichon and Angelier, 1979). It is confined by the Anatolian microplate to the east, the Hellenic trench in the south and the North Anatolian fault in the north (Le Pourhiet et al., 2003). The Aegean and Anatolian microplates are driven westwards due to the northward collision of the Arabian plate with the Eurasian plate (Doutsos and Kokkalas, 2001). The westward motion is taken up by the subduction at the Hellenic Trench (Dewey and ŞENGÖR, 1979). The extension of the Aegean region started in Miocene times, but the relationship with the Gulf of Corinth are still unclear (Moretti et al., 2003, Rohais et al., 2007a). The Aegean Sea extension originates from a combination of back-arc extension due to rollback of the subducting African Plate (e.g., Le Pichon and Angelier, 1979, Doutsos et al., 1988), propagation of the North Antolian fault (Armijo et al., 1996) and gravitational collapse in the Hellenide orogeny (Le Pichon and Angelier, 1979).
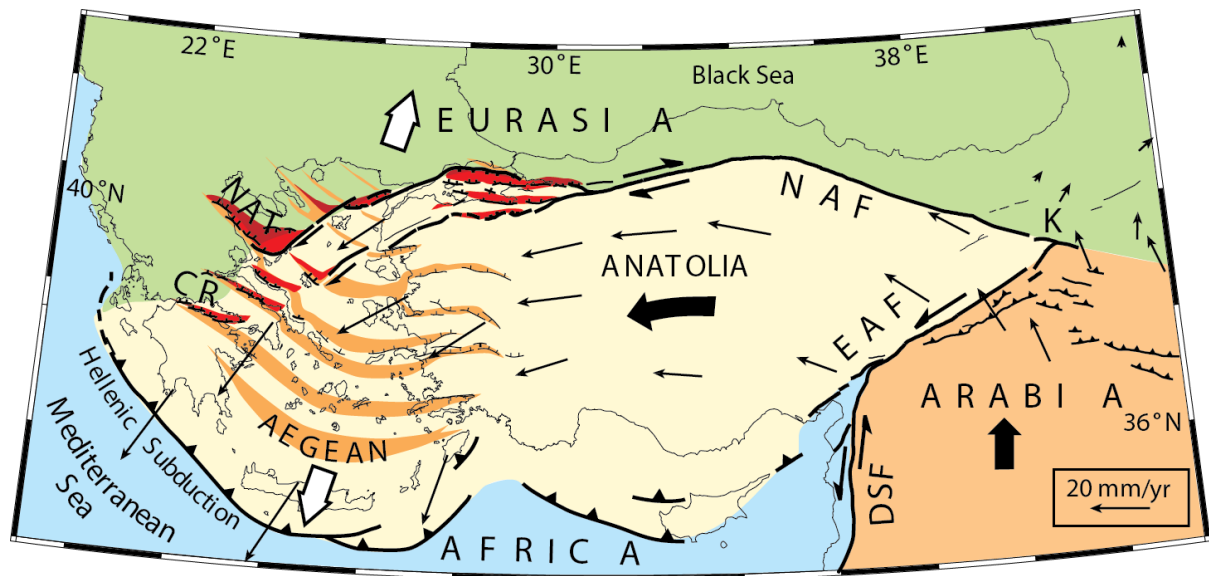
**Fig. 3.1:** Tectonic setting of the Aegean region. Abbreviations: NAF: North Anatolian fault, EAF: East Anatolian fault, DSF: Dead Sea fault, K: Karliova triple junction, CR: Corinth Rift. Modified from Armijo et al. (1999).

### 3.1.2 Tectonic setting of the Corinth Rift

The Corinth Rift is one of the most active continental rift systems in the world (e.g., Ford et al., 2013, Nixon et al., 2016) with extension rates of 5-15 mm/yr (Briole et al., 2000). It forms a high strain band with N-S extension and E-W strike (Fig. 3.2) (e.g., Nixon et al., 2016, Gawthorpe et al., 2017a). The rift is approximately 105 km long and 30 km at its widest point (Ford et al., 2013). It is considered an asymmetric graben with active normal faults on each side of the rift (Moretti et al., 2003). The current extension of the Corinth Rift is localized on the southern margin (Fig 3.2) (Bell et al., 2009, e.g., Gawthorpe et al., 2017a), which consist of series of N-dipping fault segments (e.g., Roberts and Jackson, 1991, Armijo et al., 1996).

It is generally agreed that the Corinth Rift developed during two phases of rifting (e.g., Doutsos and Piper, 1990, Rohais et al., 2007a, Gawthorpe et al., 2017a). The timing of the first phase of rifting is poorly constrained but is estimated to have started somewhere between 5.0-3.6 Ma and lasted until 2.2-1.8 Ma (e.g., Kissel and Laj, 1988, Ford et al., 2013, Gawthorpe et al., 2017a). The rift axis of the first rifting phase was located south of the present-day Gulf of Corinth (Gawthorpe et al., 2017a). The second phase of rifting started between 2.2-1.8 Ma and is still active today (e.g., Bell et al., 2009, Nixon et al., 2016, Gawthorpe et al., 2017a). During this phase, the fault activity migrated northwards to its present day location (Gawthorpe et al., 2017a).
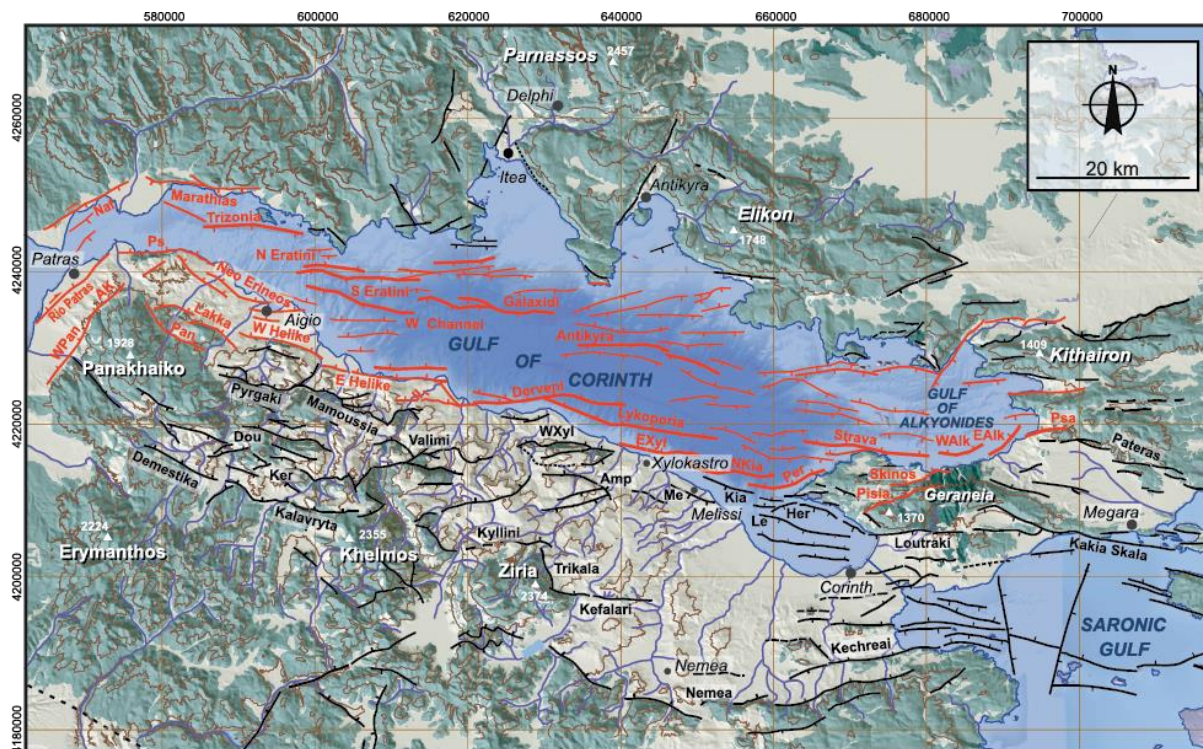


**Fig. 3.2:** Tectonic setting of the Corinth Rift. Black lines are illustrating inactive normal faults and the red lines are illustrating active normal faults. Modified from Gawthorpe et al. (2017a).

### 3.1.3 Tectonic setting of the study area

The study area is located on the footwall crest of the East Xylokastro fault (Fig. 3.3). The deltas are unconformably overlying the Rethi-Dendro formation and they are eroded by several marine terraces. The deltas investigated in this study are located north east of the Kefalari and Kryoneri Gilbert-type deltas (Fig. 3.3). During the second rift phase, Early to Middle Pleistocene, uplift of the East Xylokastro footwall caused progressive destruction of the lake Corinth (Gawthorpe et al., 2017a). During the Middle to Late Pleistocene uplift and erosion of the East Xylokastro footwall led to the present day exposures of the down-stepping deltas investigated in this study (Gawthorpe et al., 2017a).
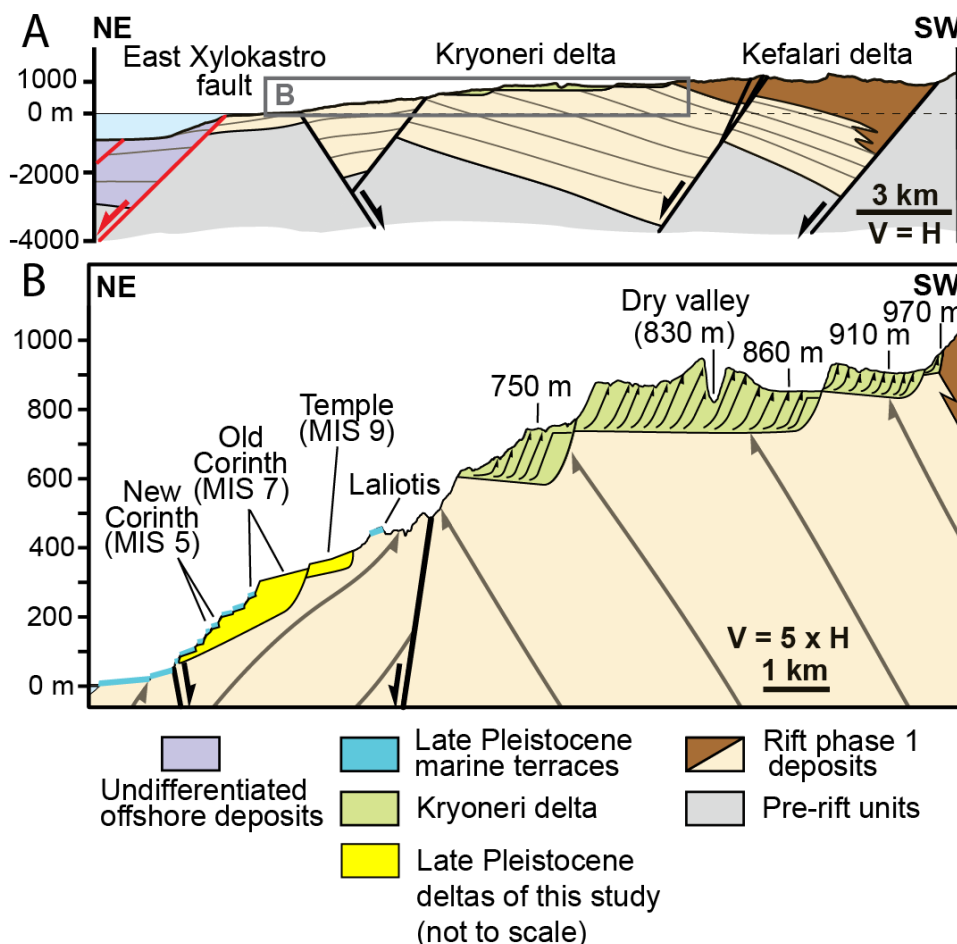


**Fig. 3.3**: Tectonic setting of the study area. The Late Pleistocene deltas investigated in this study are drawn in yellow (not to scale). The black lines with an arrow are illustrating inactive normal faults from the first phase of rifting. The red lines are illustrating active normal faults that initiated during the first phase of rifting. The beige colored unit is illustrating the Rethi-Dendro formation. The delta deposits are unconformably overlying the Rethi-Dendro formation. The figure is modified from Gawthorpe et al. (2017b).

## 3.2 General stratigraphy of the Corinth Rift Basin

The Corinth Rift Basin comprises pre-rift units of Mesozoic age (e.g., Le Pourhiet et al., 2003, Skourtsos and Kranis, 2009) and Miocene to present day syn-rift deposits (Rohais et al., 2007b). The syn and pre-rift deposits are separated by an unconformity with a time gap of approximately 15-20 Myr (Ford et al., 2013).

### 3.2.1 Pre-rift stratigraphy

The pre-rift basement comprises several thrust-sheet units which formed during the formation of the Hellenides (Le Pourhiet et al., 2003). The highly deformed Hellenide thrust sheets are divided in three main units: the Zarouchla complex, the Gavrovo-Tripoliza unit and the Pindos unit (Ford et al., 2013). The Zarouchla complex includes the Phyllites-Quartzites unit, which consists of quartzites, schists and phyllites  (e.g., Ford et al., 2013, Gawthorpe et al., 2017a). The Gavrovo-Tripoliza unit is composed of carbonate-dominated thrust sheets (Ford et al., 2013). The Pindos unit is the dominant pre-rift substratum and it is composed of pelagic carbonate from Triassic-Jurassic age and sandy turbidite deposits from Cretaceous-Tertiary age (e.g., Degnan and Robertson, 1998, Skourlis and Doutsos, 2003).

### 3.2.2 Syn-rift stratigraphy

In previous studies the syn-rift stratigraphy was subdivided into three groups (Fig. 3.4) (e.g., Ford et al., 2007, Rohais et al., 2007a). The lower group is characterized by fluvio-lacustrine deposits (e.g., Rohais et al., 2007a, Backert et al., 2010, Ford et al., 2013). The middle group comprises thick Gilbert-type fan deltas, deposits from hemipelagic settling and distal turbidite deposits (e.g., Rohais et al., 2007a, Ford et al., 2013). The upper group is characterized by Gilbert-type fan deltas and terraces deposited during uplift of the northern Peloponnesus (e.g., Rohais et al., 2007a, Ford et al., 2013).

Recent studies conducted by Gawthorpe et al. (2017a) suggest a subdivision related to the two phases of rifting. The lower and most of the middle group correspond to the first rift

phase and the top of the middle group and the upper group corresponds to the second rift phase (Fig. 3.4)

In this study the Rethi-Dendro formation is regarded as a marker for the base of the investigated delta units (Fig. 3.4, 3.5). The Rethi-Dendro Formation comprises marlstones, siltstones, sandstones and conglomerates. The boundary between the deltas investigated in this study and the Rethi-Dendro Formation is characterized by an angular unconformity. Several coarse-grained deltas have been mapped at the southern margin of the Corinth Rift (Fig. 3.5) (e.g., Rohais et al., 2008, Backert et al., 2010, Gobo et al., 2015). Some of the coarse-grained deltas are age-equivalent to the syn-rift units and others are younger (Gawthorpe et al., 2017a).
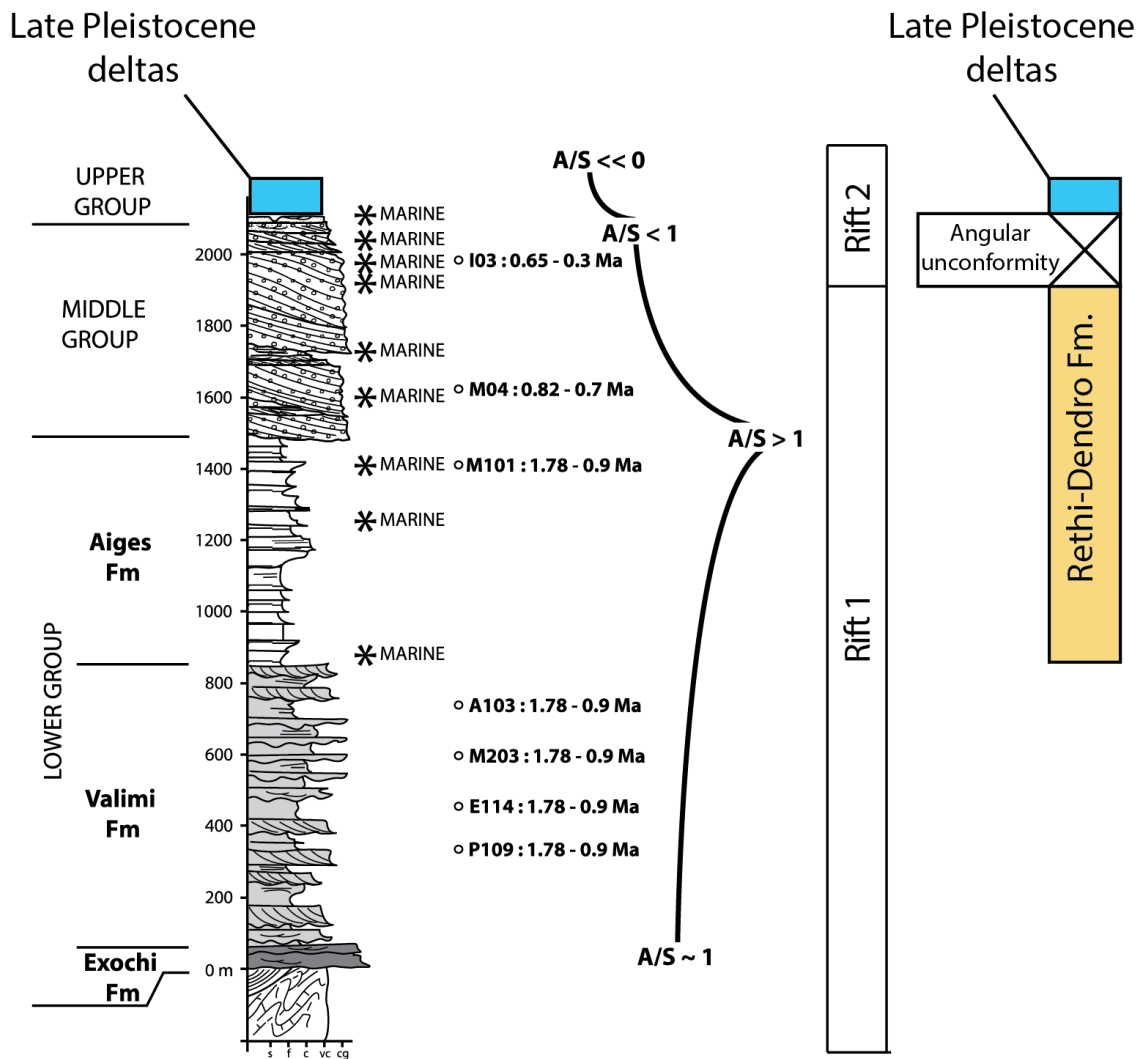
**Fig. 3.4:** General stratigraphic column for the southern margin of the Corinth Rift. Rohais et al. (2007a) suggested a subdivision into three groups: the lower group, the middle group and the upper group. More recent studies have suggested a subdivision based on the two phases of rifting (Gawthorpe et al., 2017a) , which is illustrated by the "Rift 1" and "Rift 2" boxes in the figure. The Rethi-Dendro Fm is equivalent to the Aiges Formation and is regarded as a marker for the base of the deltas investigated in this study and the boundary is characterized by an angular unconformity. Modified from Rohais et al. (2007b).
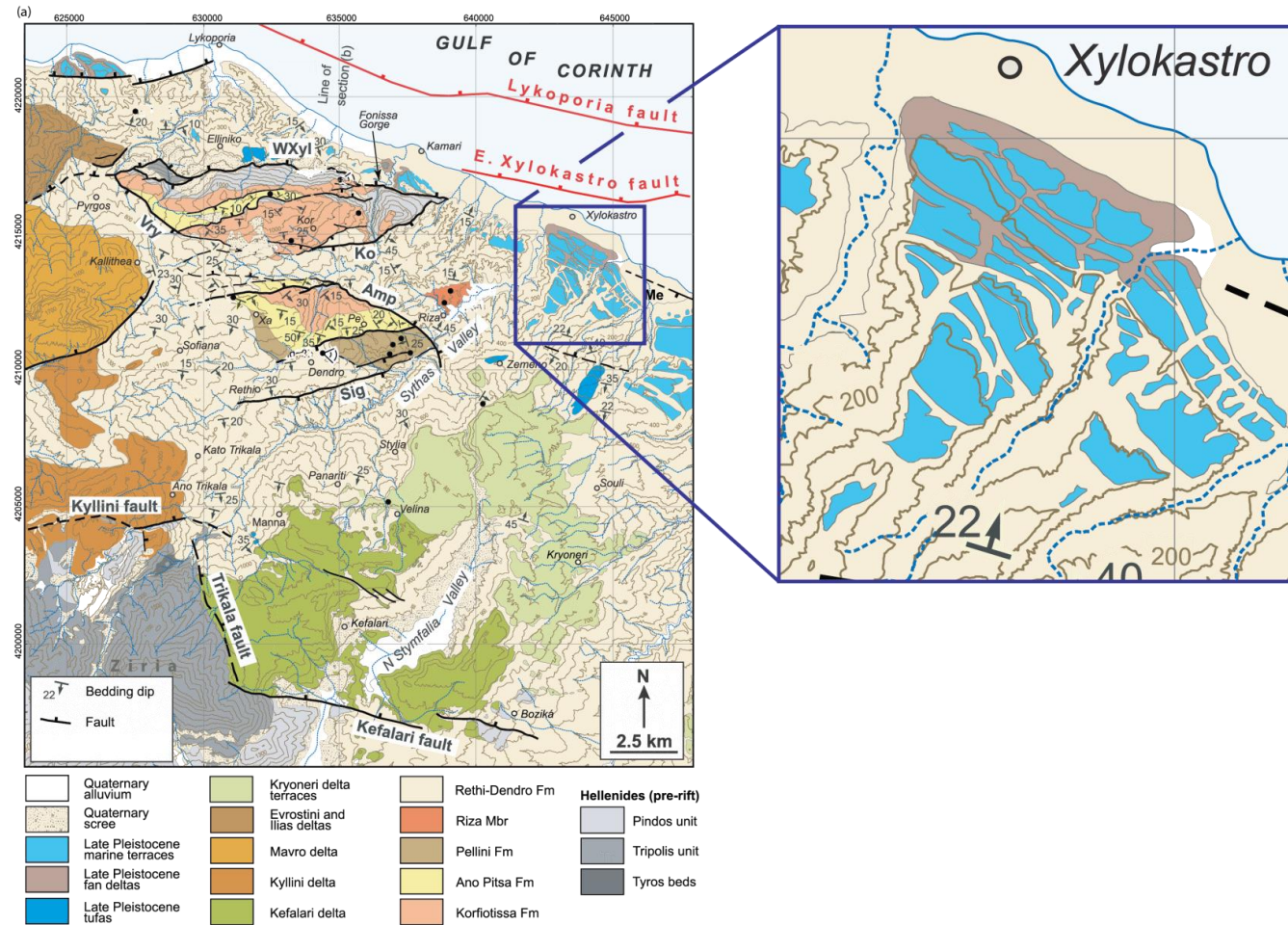
**Fig. 3.5:** Geological map of the study area. The location of the study area is marked by the blue square and the enlarged square illustrates the previous interpretation of the study area. In Chapter 5 a geological map with the new interpretation of the study area will be presented. The different formations are related to the two phases of rifting. Rift phase 1: Korfiotissa Fm, Ano Pitsa Fm, Pellini Fm, Riza Mbr, Rethi-Dendro Fm, Kefalari delta, Kyllini delta, Mavro delta. Rift phase 2: Evrostini delta, Ilias delta, Kryoneri delta, Late Pleistocene tufas, Late Pleistocene fan deltas, Late Pleistocene marine terracs.

# 4 Methodology

## 4.1 Data acquisition

The data of this study were collected during two field seasons in Greece, from 13.05.2017-30.05.2017 and 03.10.2017-25.10.2017. The field observations are complemented by LiDAR datasets and Photogrammetry analysis. In this study, the emphasis is placed on the different delta units. Master student Sandra Eriksson is investigating the marine terraces of the study area in her master thesis.

### 4.1.1 Field work

Traditional sedimentological field techniques were used, including logging and precise geological mapping of the delta bodies. Particular emphasis was placed on lithologies, textures, boundaries, architectural elements and delta geometries. Standard field equipment such as compass, measuring tape, binoculars, geological hammer, GPS, camera and grain size chart were used. Laser rangefinder and drone were used to collect data from inaccessible outcrops. Most of the outcrops were accessed by car and short walks, but access to some outcrops were restricted due to steep cliffs and impenetrable vegetation.

### 4.1.2 LiDAR

In the westernmost part of the study area, LiDAR data was acquired by my supervisor Martin Muravchik and his collaborators while working on a different project in the area. LiDAR (light detection and ranging) is a modern laser technique that allows researchers to capture detailed spatial information from geological outcrops (e.g., Bellian et al., 2005, Buckley et al., 2008). The LiDAR instrument uses laser light to measure distances and to collect data points with individual coordinates and reflection intensity values (e.g., Bellian et al., 2005, Hodgetts, 2009, Rarity et al., 2014). Color information can be obtained with the addition of a high resolution photographic camera in order to obtain realistic digital outcrop models.

### 4.1.3 UAV – Photogrammetry data

In the easternmost part of the study area a drone was used to obtain data from exposures along a valley, parallel to the depositional dip direction of the studied succession. The drone was operated by my main supervisor Dr. Martin Muravchik. The data obtained consisted of pictures and movies used for the generation of a digital outcrop model.

## 4.2 Data analysis

### 4.2.1 Digitizing of logs and figures

The software Adobe Illustrator was used to digitize the sedimentary logs. The scale of the logs varies from 1:10 to 1:50. Adobe Illustrator was also used to create figures and cross-sections.

### 4.2.2 Digitizing of field mapping data

The digital mapping of the delta units was done in ArcMap, which is a geospatial processing software. A high resolution (pixel size = 1m) digital elevation models (DEM) was imported into ArcMAP. Polygons were created for the flat surfaces and compared to the terraces mapped by Armijo et al. (1996). Field data, such as field maps, strike- and dip measurements and sedimentological logs were precisely located in the ArcMap project, by using their coordinates obtained with GPS. The DEM's from ArcMap were used combined with field data to create the cross-sections of the study area.

### 4.2.3 Photogrammetry

A virtual outcrop model was obtained from a combination of photogrammetry techniques using the following software: Visual SFM, Meshlab and CloudCompare. The virtual outcrop model was made by my supervisor Dr. Martin Muravchik. The geological interpretation of the virtual outcrop model was done in CloudCompare in order to identify the different delta units and to investigate the geometrical relations between them.

### 4.2.4 LiDAR

An already existing LiDAR dataset of the eastern margin of the Sythas valley was used to analyse the geometrical relation between the different delta units of the westernmost exposures in the study area.

# 5 Sedimentology and facies analysis

In total six different deltas were identified in the study area (Fig. 5.1, 5.2). Eleven main facies are identified within the different deltas and the interpretation of each facies is given in Table 1. The facies classification is based on sedimentary logs that can be found in the Appendix. The logs are describing the lithology, texture and sedimentary structures observed in the delta deposits. The facies interpretations are based on transport and depositional processes. The different facies are organized into five different facies associations given in Table 2.

## 5.1 Facies

The deltaic deposits comprise conglomerates, sandstones and mudstones. Clast-supported conglomerates are generally massive or crudely stratified with variable amounts of matrix. Matrix supported conglomerates are typically massive or planar parallel stratified. The sandstones are either massive or contain sedimentary structures such as cross-stratification and planar parallel stratification. The sedimentary structures are associated with a range of depositional processes. The mudstones are generally massive or planar parallel stratified.
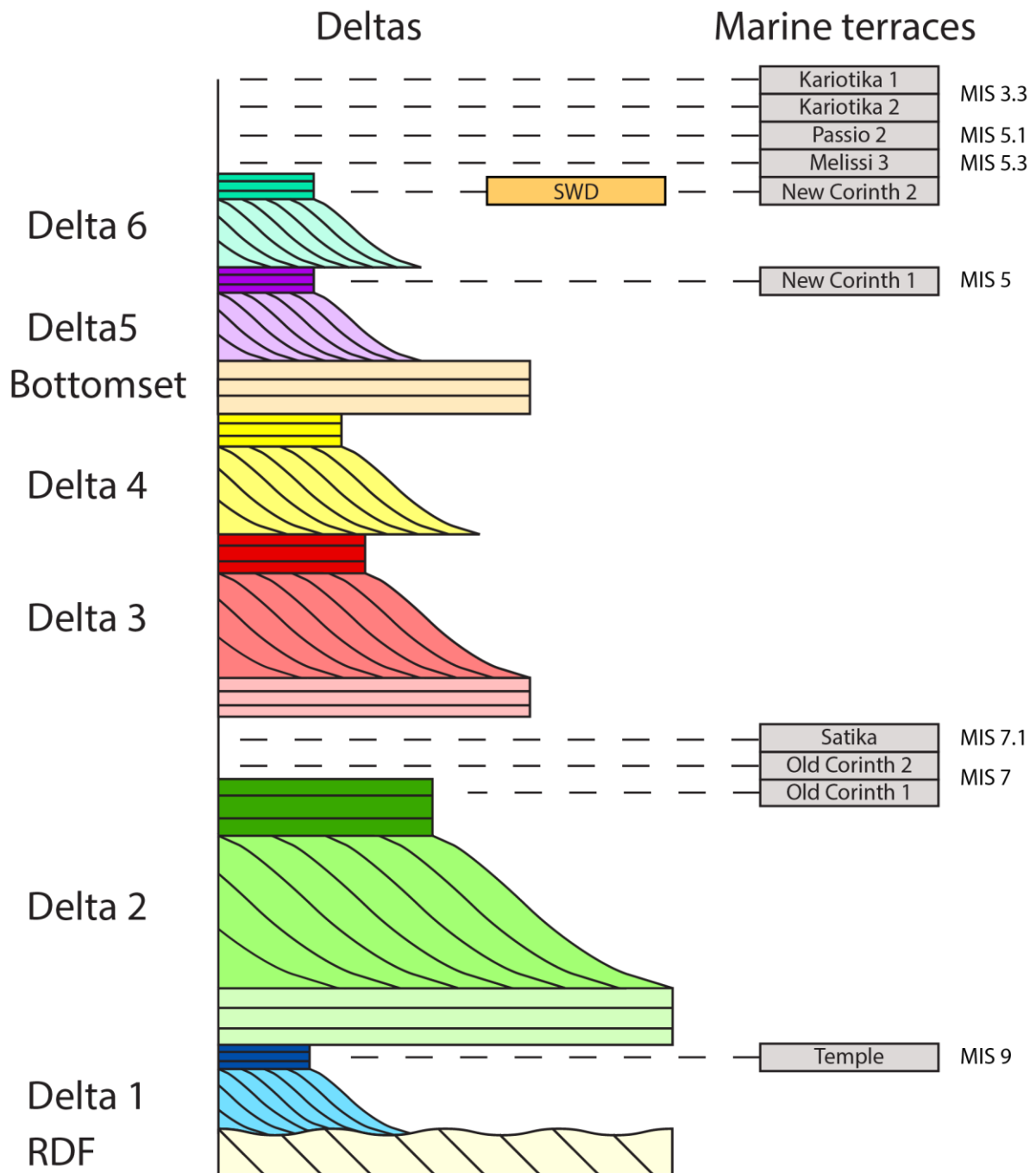
**Fig. 5.1:** Stratigraphic column illustrating the stratigraphy of the study area. The deltas are not drawn to scale. Abbreviations: RDF: Rethi-Dendro formation, SWD: slackwater deposits (Table2), MIS: Marine Istotope Stage. The boundary between the deltas and RDF is characterized by an angular unconformity. Color legend is found in figure 5.2.
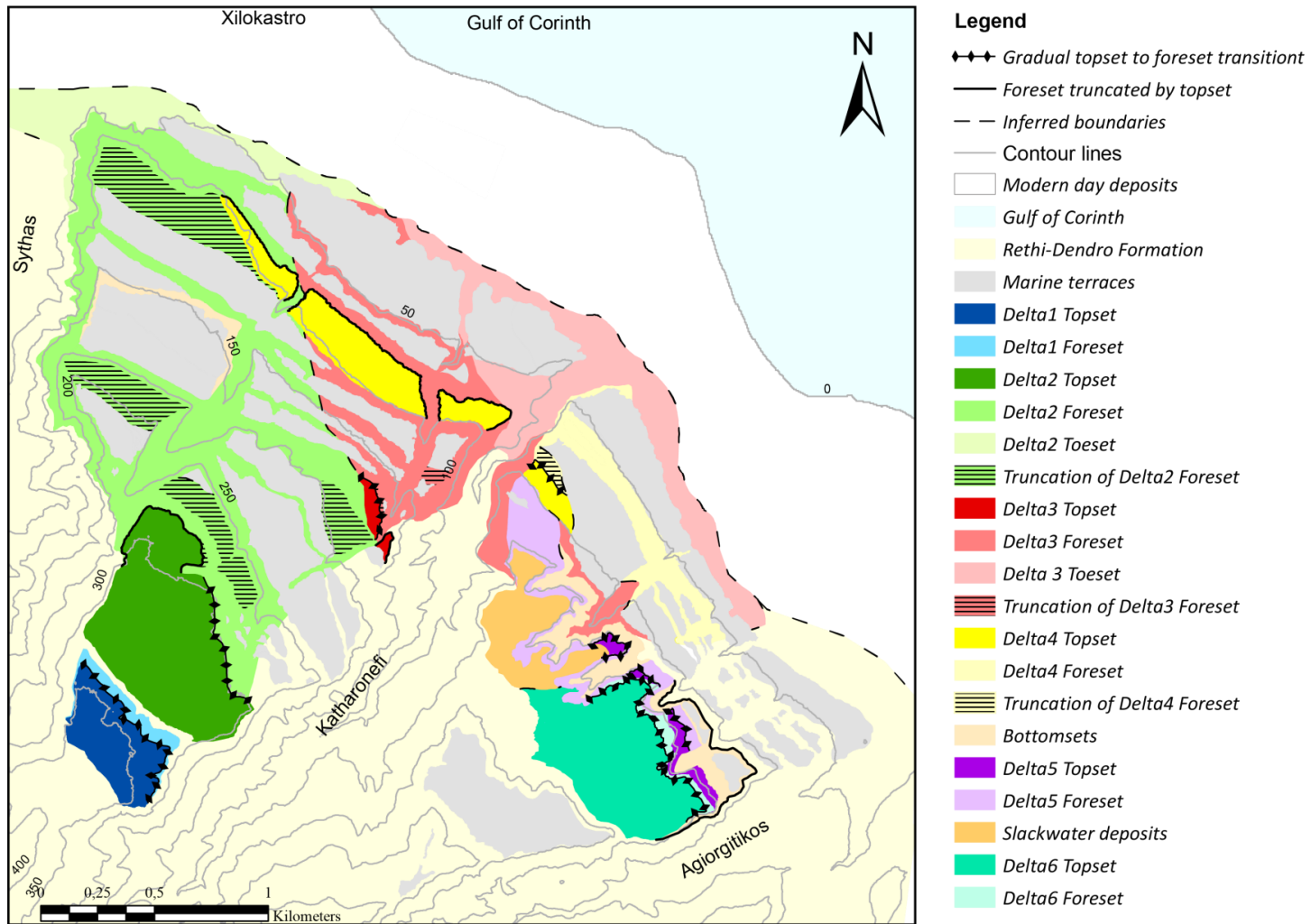
**Fig. 5.2:** Geological map of the study area showing the different delta units and marine terraces of the study area.

**Table 1:** Facies table with description and interpretation of the different facies. Facies abbreviations: G: conglomerates, S: sandstones, F: mudstones. For facies pictures see Fig. 5.3.

| Facies | Lithology and texture | Thickness | Geometry | Sedimentary structures | Interpretation and processes |
|---|---|---|---|---|---|
| **Gcm**: | Clast-supported granule to cobble conglomerate, sometimes openwork framework | From 2 cm to 4 m | Tabular or lenticular bodies | Massive | Laminar flows, debris flow deposits (e.g., Dasgupta, 2003, Backert et al., 2010, Gobo et al., 2015) |
| **Gmm** | Matrix-supported granule to cobble conglomerate | From 2cm to 2 m | Tabular or lenticular bodies | Massive | |
| **Gp:** | Matrix-supported pebble to cobble conglomerate | 1-40 cm | Tabular or lenticular bodies | Planar parallel stratification | |
| **Gc:** | Clast to matrix-supported granule to pebble conglomerate | 2-5 cm | Deposited within a 2 m wide and 50 cm thick trough with an erosional concave upward base | Planar cross-stratification and normal grading | Lateral accretion of gravel bars (Miall, 2013) |
| **Sc:** | Fine to medium sandstone | 1-12 cm | Tabular or lenticular bodies with erosional or sharp bases | Planar cross-stratification | Migration of 2D ripple/dunes (Miall, 2013) |

| | | | | | |
|---|---|---|---|---|---|
| **St:** | Fine to medium sandstone. Sometimes with random floating pebbles | 2-20 cm | Tabular or lenticular bodies with erosional or sharp bases | Through cross-stratification | Migration of 3D ripple/dunes (Miall, 2013) |
| **Sm:** | Very fine to very coarse sandstone, sometimes with random floating pebbles | 1-30 cm | Tabular bodies with erosional or sharp bases | Massive | Sandy debris flow or 'subdivision A' of the Bouma sequence (e.g., Backert et al., 2010, Gobo et al., 2015) |
| **Sp:** | Very fine to medium sandstone, sometimes with random floating pebbles | 0,2-20 cm | Tabular or lenticular bodies with erosional or sharp bases | Planar parallel lamination | Upper flow-regime plane bed conditions (e.g., Backert et al., 2010, Miall, 2013) |
| **Sg:** | Fine to very coarse sandstone, frequently passing upward into planar parallel-stratified sandstone | 14-50 cm | Tabular bodies with sharp or erosional bases | Planar parallel lamination, normal grading | High-density or low-density turbidity current (Backert et al., 2010) |

| **Fm:** | Mudstone | 1-5 cm | Tabular or lenticular bodies with sharp bases | Massive | Suspension settling (Backert et al., 2010) |
|---|---|---|---|---|---|
| **Fl:** | Mudstone. Sometimes with lenses of sand and/or pebbles (pebbles: 0,7-2,0 cm) | 2-25 cm | Tabular or lenticular bodies with sharp bases | Planar parallel lamination | Suspension fallout or weak traction current (Miall, 2013) |
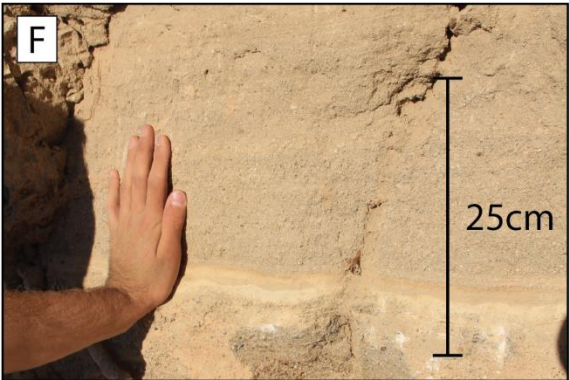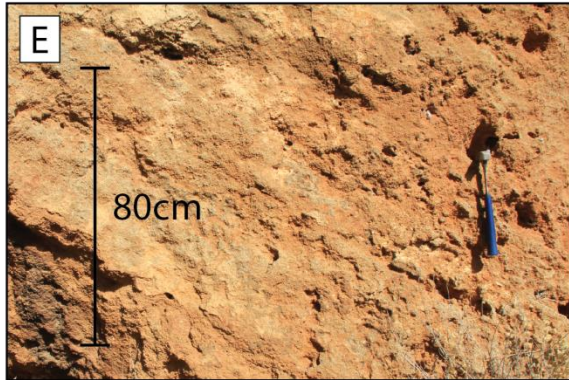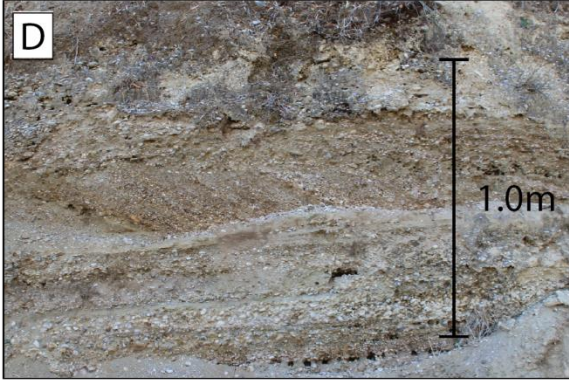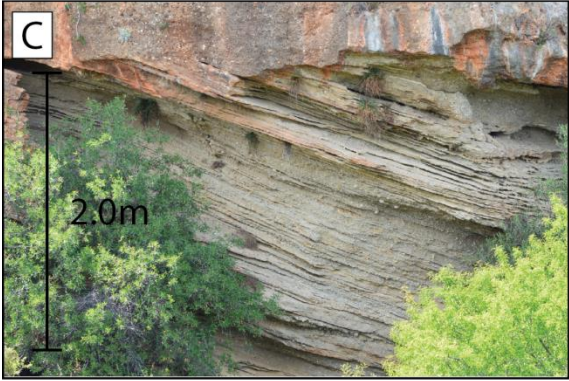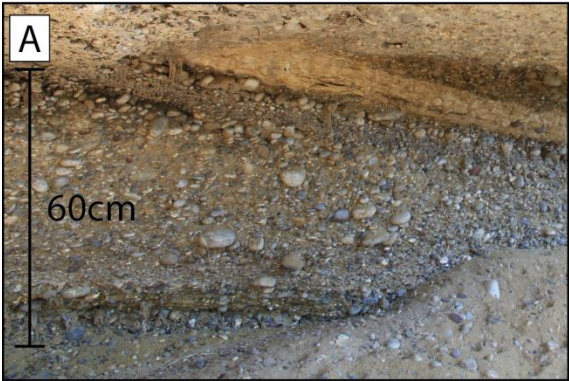
**Fig. 5.3:** Facies pictures. A: Gcm (Log 12, see appendix), B: Gmm (Log 29, see appendix), C: Gp, D: Gc (Log 39, see appendix), E: Sm (Log 22, see appendix), F: Sg (Log 41, see appendix), G: Sc (Log 13, see appendix), H: St (Log 38, see appendix) ,I: The bright colured beds are facies Fm, J: The bright colured bed is facies Fl (Log 25, see appendix).

## 5.2 Facies associations
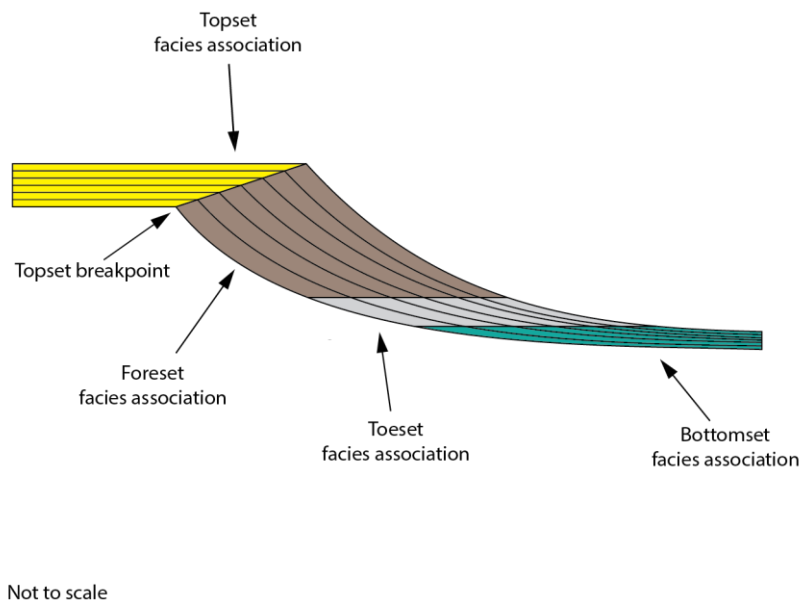


**Fig. 5.4:** Geometrical relation between the different facies associations. Modified from Backert et al. (2010)

**Table 2:** Facies associations. See Fig. 5.4 for geometrical relations.

| Facies associations: | Depositional environment | Geometry | Facies |
|---|---|---|---|
| **FA1.1 - Topset** | Subaerial - Fluvial | Horizontal to gently dipping (<10°) | Gcm, Gmm, Gp, Gc,  Sp Sc, St, Sm, Fm, Fl |
| **FA1.2 – Slackwater deposits** | Subaerial - Slackwater | Horizontal | Sm, Fm, Fl |
| **FA2 - Foreset** | Sub-aqueous | Steeply dipping, 20-33° dip. | Gcm, Gmm, Gp, Sm, Sp, Fl, Fm |
| **FA3 - Toeset** | Sub-aqueous | Gently dipping (<10°) | Gcm, Gmm, Sp, Fm |
| **FA4 – Bottomset** | Sub-aqueous | Horizontal to gently dipping (<10°) | Gcm, Sg, Fl |

### 5.2.1 Delta topset facies association – FA1.1

Description

The delta topset facies association consists of a wide range of lithofacies (Gcm, Gmm, Gp, Gc, Sp, Sc, St, Sm, Fm, Fl), typically massive clast-supported conglomerate (Gcm) organized in tabular packages (Fig.5.5). The topsets are horizontal or gently dipping in NE direction. They are tens to hundreds of meters wide in depositional dip direction and range in thickness from 1 to 20 m. In general, thicker beds are massive and poorly sorted. The thinner beds are better stratified with more prominent structures. In some of the topsets troughs with concave upward erosional bases and cross stratified conglomerates (Gc) can be observed. Laterally to the topset of Delta 6 (Fig. 5.2) the slackwater facies association is observed (Sm, Fm, Fl).

Interpretation

Through cross-stratification (Gt, St), normal-grading (Sg), cross stratification (Gc, Sc) and planar parallel lamination (Gmp, Sp) are indicators of unidirectional currents and fluvial influence (e.g., Backert et al., 2010, Miall, 2013). The massive clast-supported and lateral extensive conglomerates are interpreted to be deposits from sheet flood events and less confined flows (Rohais et al., 2008). The cross stratified deposits with concave-upward erosional bases are interpreted to be small channel features with lateral accretion of gravel bars (Miall, 2013). The topset facies association is therefore interpreted to be of fluvial origin.
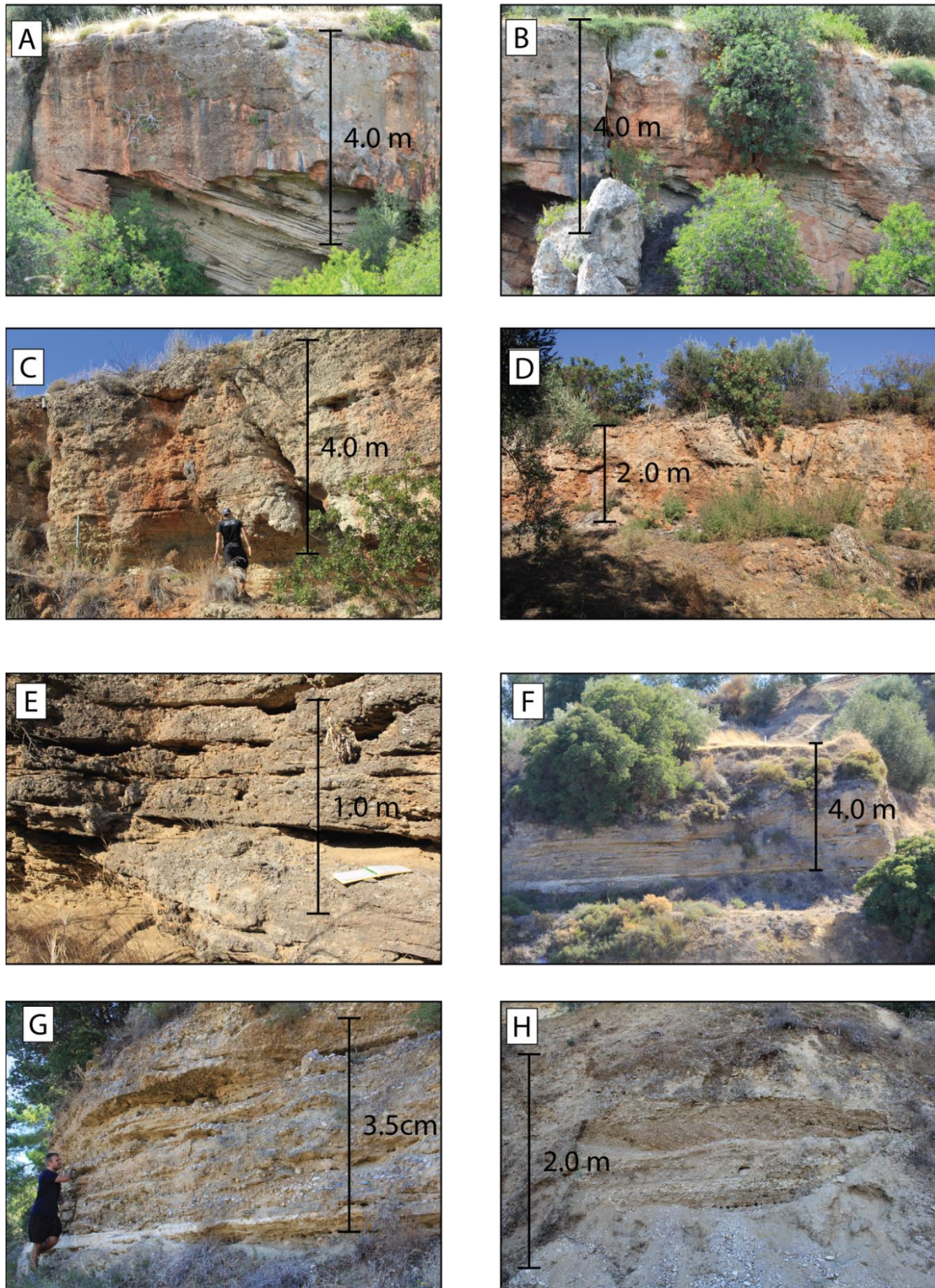
**Fig. 5.5:** Field pictures illustrating the Delta topset facies association (FA.1.1). A: Proximal parts of Delta 3 topset illustrating oblique toplap geometries. B: Distal parts of Delta 3 topset illustrating sigmoidal toplap geometries. C: Topset of Delta 6. D: Topset of Delta 1. E: Topset of Delta 5. F/G: Topset of Delta 5. H: Cross-stratified conglomerates in the topset of Delta 5.

## 5.2.2 Slackwater facies association – FA1.2

Description

The slackwater facies association consists of horizontal to gently dipping, massive sandstone and laminated/massive mudstone (Sm, Fm, Fl). It is more than 500 m wide in depositional dip direction and it is approximately 20 m in maximum thickness. This facies association is observed on top of Delta 5 topset/foreset and it is laterally equivalent to the Delta 6 topset (Fig.5.6). The transition from the finer-grained facies to the Delta 6 topset was not observed in the field as there were no exposures due to vegetation.

Interpretation

The slackwater facies association is interpreted to be age equivalent to the Delta 6 topset. The finer-grained facies (Sm, Fm, Fl) are interpreted to be slack-water deposits (e.g., Miall, 1996, Bridge, 2003).
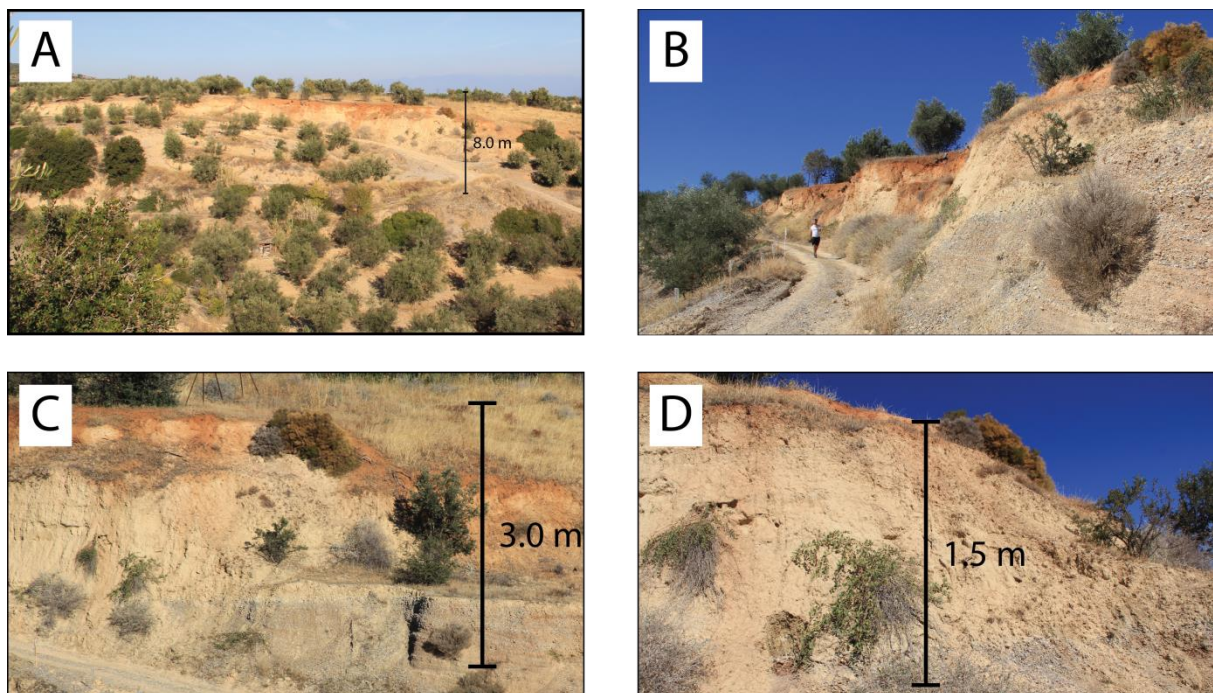


**Fig. 5.6:** A: Field pictures illustrating the Slackwater facies association (FA1.2). A, B, C and D are all pictures of the same unit at different scales. In C and D crude stratification can be observed. In the lower part of all the pictures the Delta 5 topset can be observed (conglomerates).

### 5.2.3 Delta foreset facies association – FA2

Description

The delta foreset facies association consist of several lithofacies (Gcm, Gmm, Gfm, Gmp, Sm, Sp, Fl, Fm, Fi), which can be organized in two main types (Fig. 5.7). The first type (type1) consists of massive clast-supported conglomerate up to 4 m thick. The second type (type2) consists of more well stratified, sandier conglomerates alternating with sandstones and mudstones. The delta foresets are hundreds of meters wide in depositional dip direction and range in exposed thickness from 10 to 200 m. They are steeply dipping towards NE with a dip-angle of 20-33°. Both sigmoidal (transitional) and oblique (erosional) toplap are observed. In many cases the foresets are truncated at top and overlain by marine terrace deposits (FA5). In some outcrops the foresets are eroded at the top, with no deposits on top of the truncation surfaces. In some of the deltas (Delta 2 and Delta3) the transition between the foreset and toeset is observed. In the foreset to toeset transition, the foresets are merging with the more gently-dipping and finer grained toesets (FA3).

Interpretation

The foreset facies association is interpreted to be deposits formed by subaqueous sediment-gravity flows (Falk and Dorsey, 1998). The massive sand and clast-supported conglomerates (Gcm, Gmm) are interpreted to be deposits from debris flows (e.g., Lowe, 1982, Dasgupta, 2003, Gobo et al., 2015). Well stratified and finer grained facies are interpreted to be deposits from turbidity currents or suspension fallout during episodes of low sediment discharge (e.g., Nemec, 1990, Rohais et al., 2008, Backert et al., 2010, Gobo et al., 2015). Sigmoidal and oblique toplap are interpreted to be due to relative sea-level rise and relative sea-level fall respectively (Gobo et al., 2015).

***Fig. 5.7:*** *Field picture illustrating the two types of foreset deposits. Type 1: Massive, clast-supported conglomerates up to 4 m thick, Type 2: Well stratified sand- to clast-supported conglomerates, laminated sandstone and marlstone beds, up to 5 m thick (Log 25, see appendix).*

## 5.2.4 Delta toeset facies association – FA3

Description

The toeset facies association consists of massive matrix to clast supported conglomerates (Gcm, Gmm) and planar parallel stratified sandstones (Sp), alternating with marlstone beds (Fm) (Fig. 5.8).  They are gently dipping towards NE with a dip angle of less than 10°. The total thickness and lateral extent of the delta toesets are unknown as they are not fully exposed in the study area.

Interpretation

Massive clast and matrix supported granule beds are indicators of gravity flow processes (e.g., Lowe, 1982, Dasgupta, 2003, Gobo et al., 2015). The alternation between granule beds (Gmm) and finer beds (Sp, Fm) are interpreted to be due to periods of high and low sediment discharge respectively (Rohais et al., 2008).
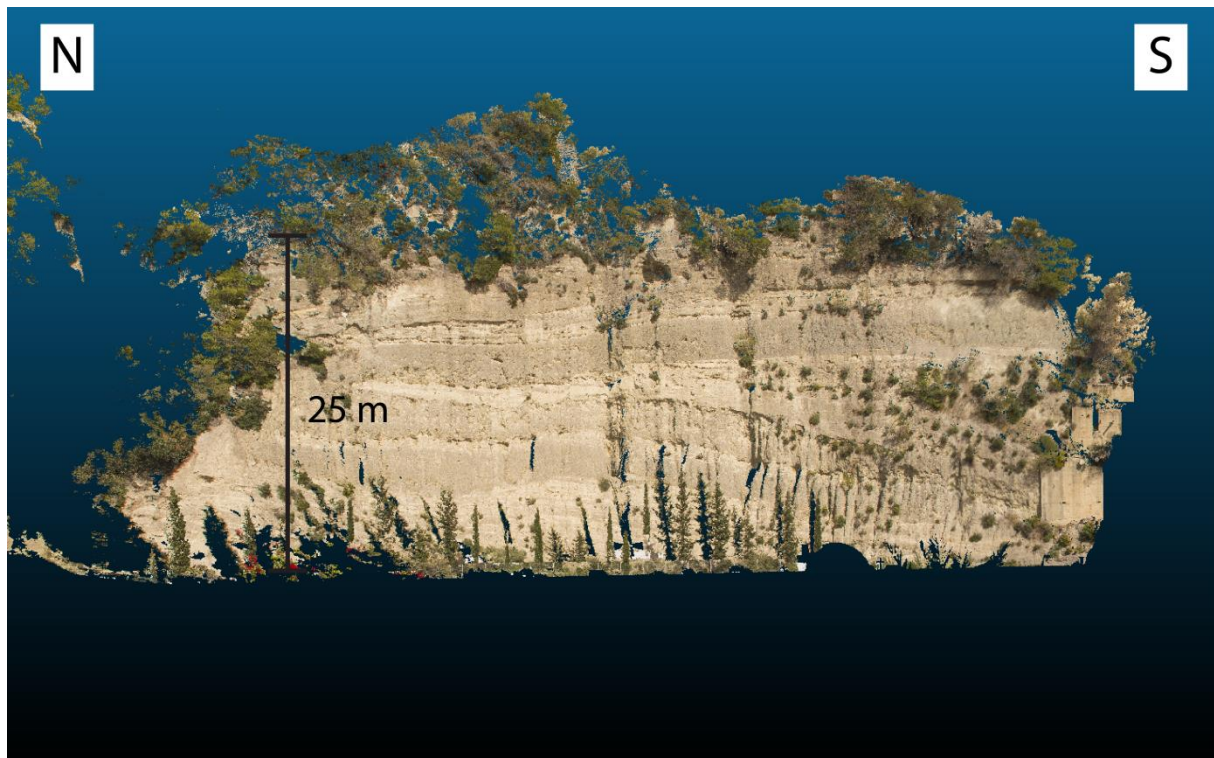


**Fig. 5.8:** Digital outcrop model illustrating the Delta toeset facies association (FA3). The alternation between conglomerates, sandstones and marlstones can be observed.

## 5.2.5 Delta bottomset facies association – FA4

Description


The delta bottomset facies association consists of mainly horizontally bedded, massive and laminated sandstone with planar parallel laminations and massive or laminated mudstone beds (Sm, Sg, Fm, Fl) (Fig. 5.9). Granule to pebble conglomerate (Gcm) can be observed at the base of the bottomset in the easternmost part of the study area. The conglomerates are eroding into the underlying Rethi-Dendro Formation. The finer grained deposits are stacked in fining upward sequences of approximately 20-40 cm. They are massive at the base and planar parallel lamination is observed towards the top of the beds. The bottomsets range in thickness from 10 to 20 m. They are more than 500 m long in depositional dip direction, but it is not possible to measure the full lateral extent of the bottomsets due to vegetation and avalanches. The delta bottomsets can only be observed in two outcrops and there is no clear link between the bottomsets and the foreset of any delta unit.


Interpretation

The massive conglomerate beds are interpreted to be debris flow deposits from a period of high sediment discharge (e.g., Lowe, 1982, Rohais et al., 2008). The finer grained facies (Sm, Sl, Fm, Fl) are interpreted to be the deposits of turbidity currents (e.g., Lowe, 1982, Nemec, 1990).
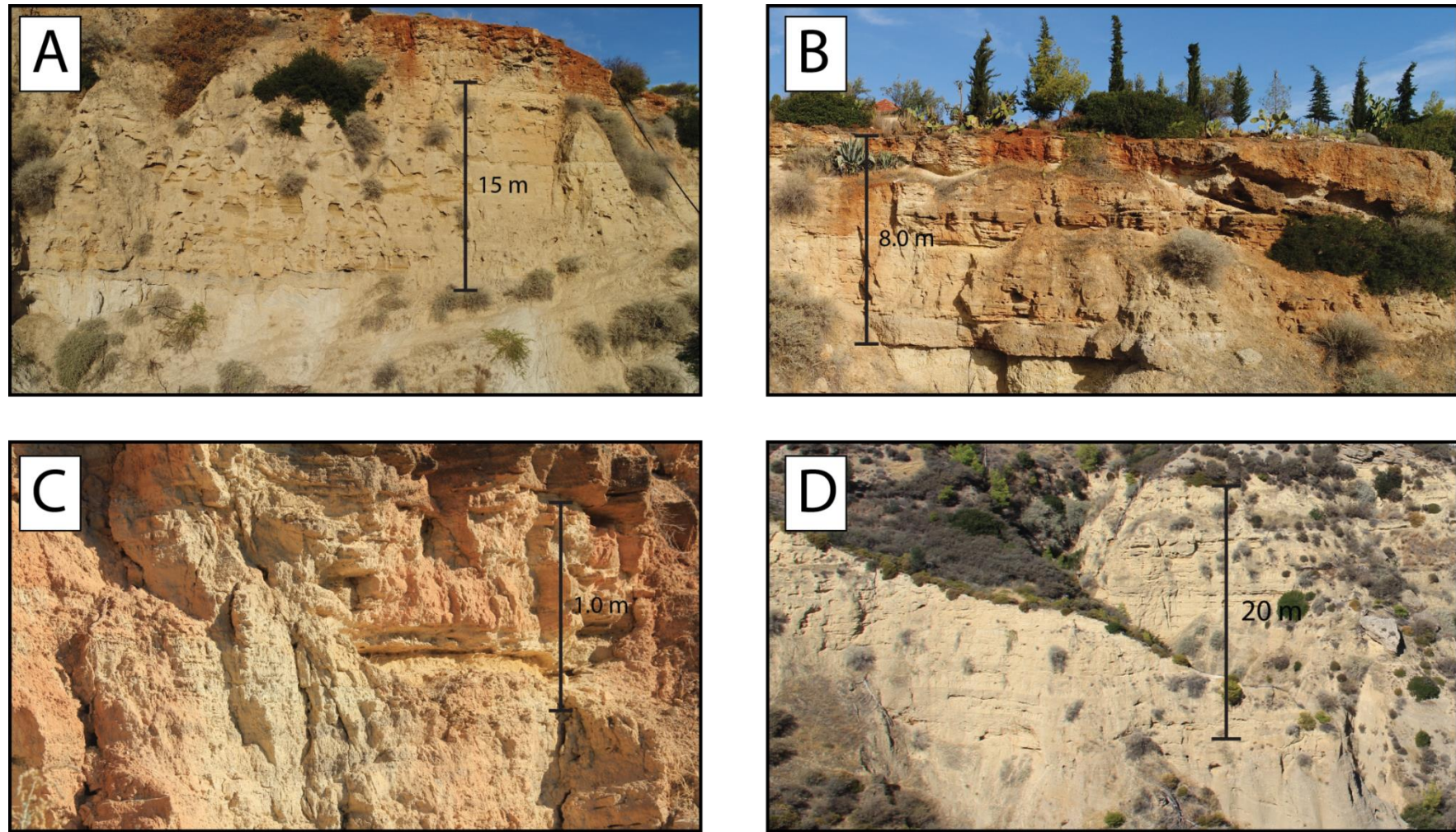
**Fig. 5.9:** Field pictures illustrating the Delta bottomset facies association (FA4). Picture A, B and C are all taken from the easternmost side of the study area and picture D is taken in a small valley east of the Katharonefi River. In picture A and B the unconformity between the bottomset and the Rethi-Dendro formation can be observed. In picture D the foreset of Delta 3 can be observed bellow the bottomset and the foreset of Delta 5 can be observed downlapping the bottomset.

## 5.2.6 Marine terrace facies association – FA5

It is not the purpose of this thesis to investigate the marine terraces of the study area. As mentioned in the Methodology chapter, master student Sandra Eriksson is writing her master thesis about the marine terraces of the study area.

Description

The marine terraces are characterized by vertically stacked tabular beds of well sorted conglomerates or sandstones (Fig. 5.10). Conglomerate lag is frequently observed at the base of the marine terrace deposits. The deposits are typically characterized by 0.5-2 m thick shoaling-upward units.

Interpretation

The marine terraces are interpreted to be wave-dominated shoreface deposits overlying transgressive ravinement surfaces (e.g., Collier, 1990, McMurray and Gawthorpe, 2000, Gawthorpe et al., 2017a).
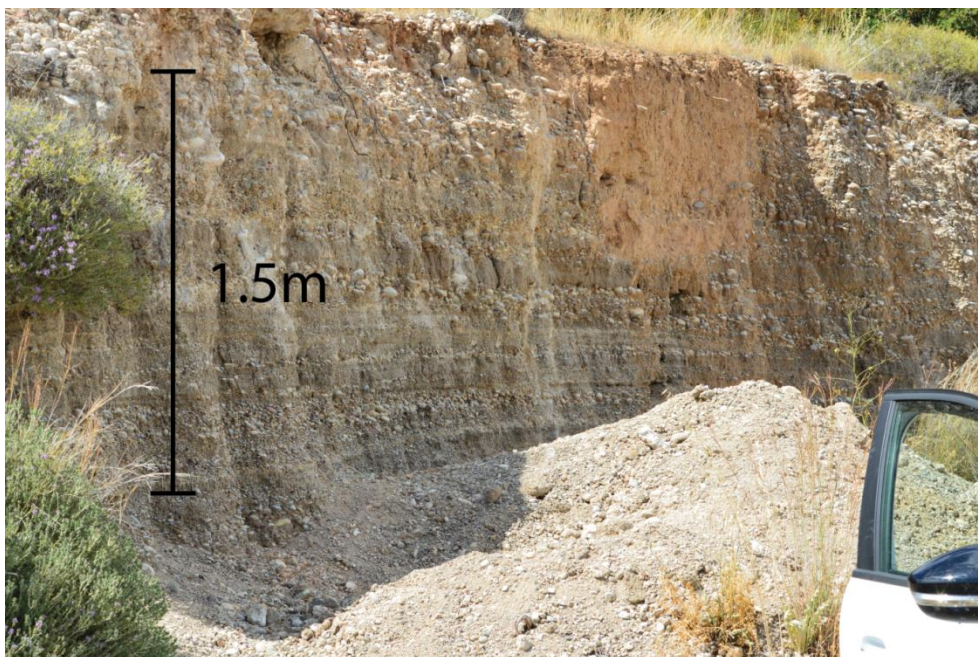


**Fig. 5.10:** Field picture illustrating the Marine terrace facies association (FA5)

# 6 Delta units

A total of six deltas were mapped in the study area (Fig. 5.2, 6.1). None of the deltas are completely preserved and there is great lateral variability across the study area. The delta architecture is illustrated in five different cross-sections of SW to NE orientation (Fig. 6.2-6.6). In general, the younger deltas are deposited topographically lower than the older deltas, except for Delta 5 and Delta 6, which are deposited on top of Delta 4 (Fig 6.1, 6.5, 6.6). The deltas are generally finer grained and smaller in terms of thickness and lateral extent in the northeastern part of the study area. The deltas are generally characterized by a lateral change from coarser to finer deposits from west towards east.
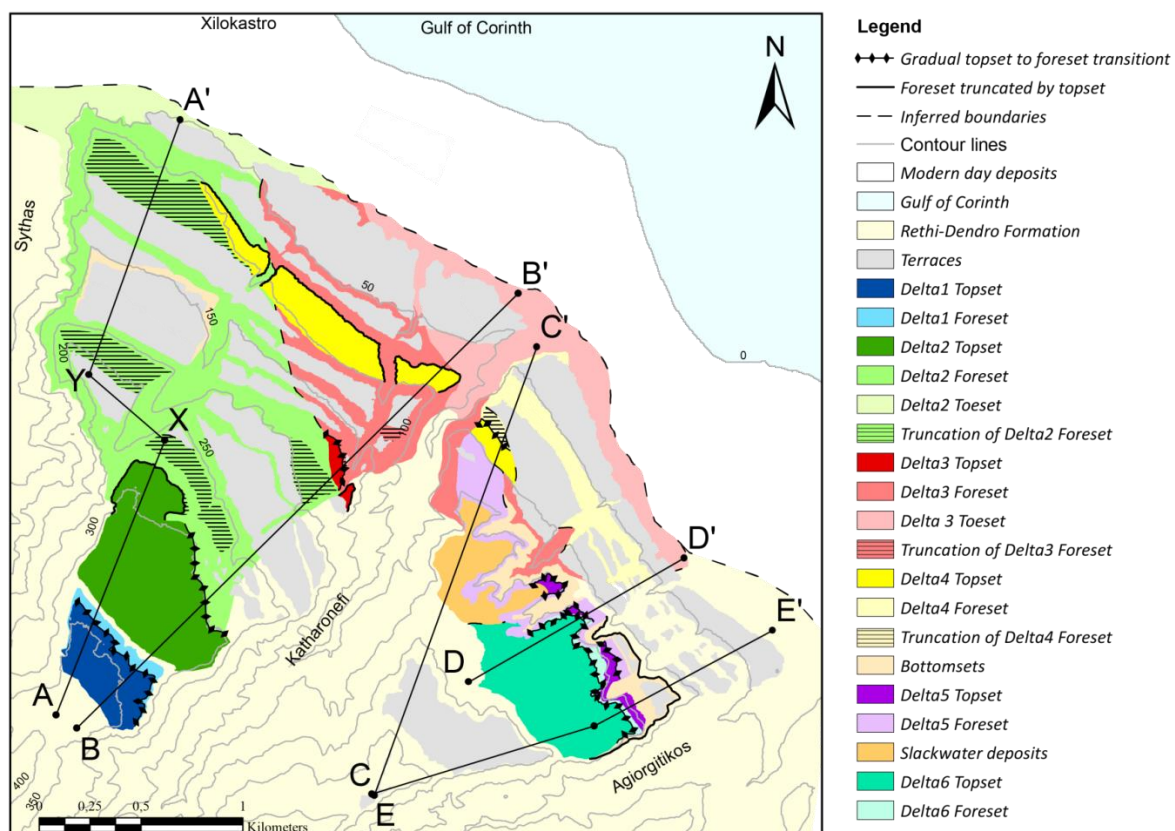


**Fig. 6.1:** Geological map of the study area. This this figure is showing the location of the following cross-sections (Fig. 6.2, 6.3, 6.4, 6.5 and 6.6).
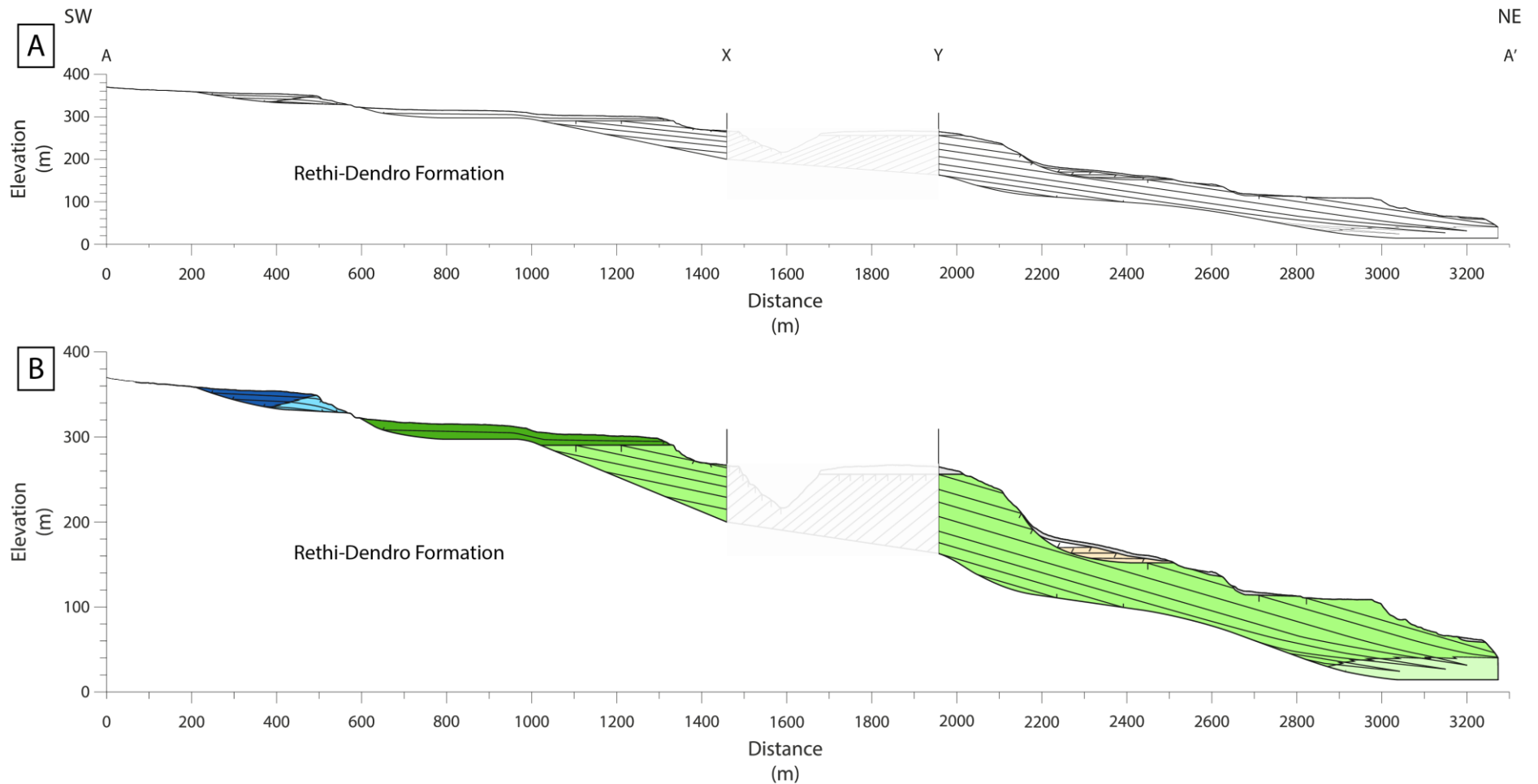
**Fig. 6.2:** Cross-section of the westernmost part of the study area (Fig. 6.1). A: To scale, B: Vertical exaggeration X2. Delta 1, Delta 2 and a bottomset unit are illustrated in this cross-section.
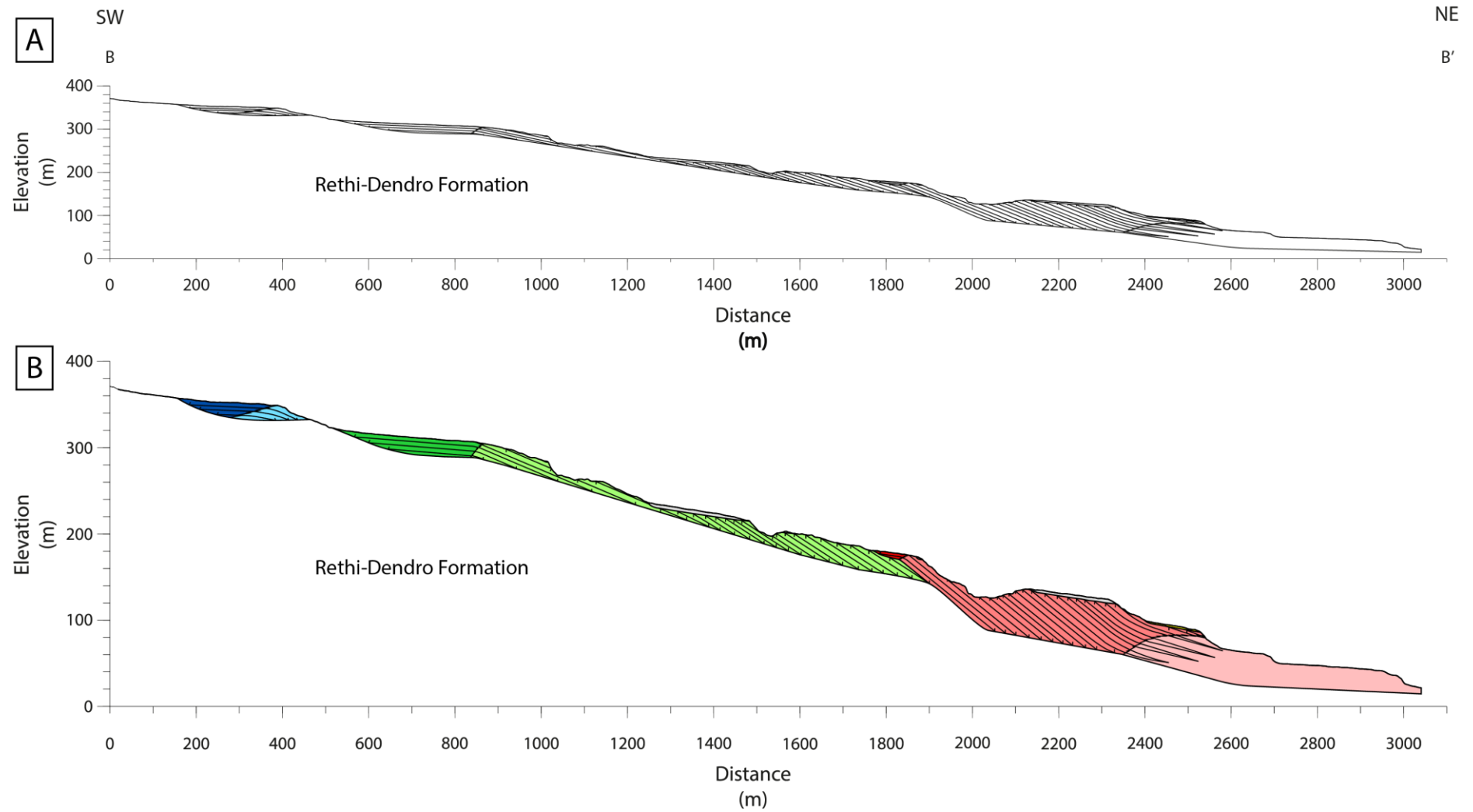
**Fig. 6.3:** Cross-section of exposures west of the Katharonefi River (Fig. 6.1). A: To scale, B: Vertical exaggeration X2. In this cross-section Delta 1, Delta 2 and Delta 3 are illustrated.
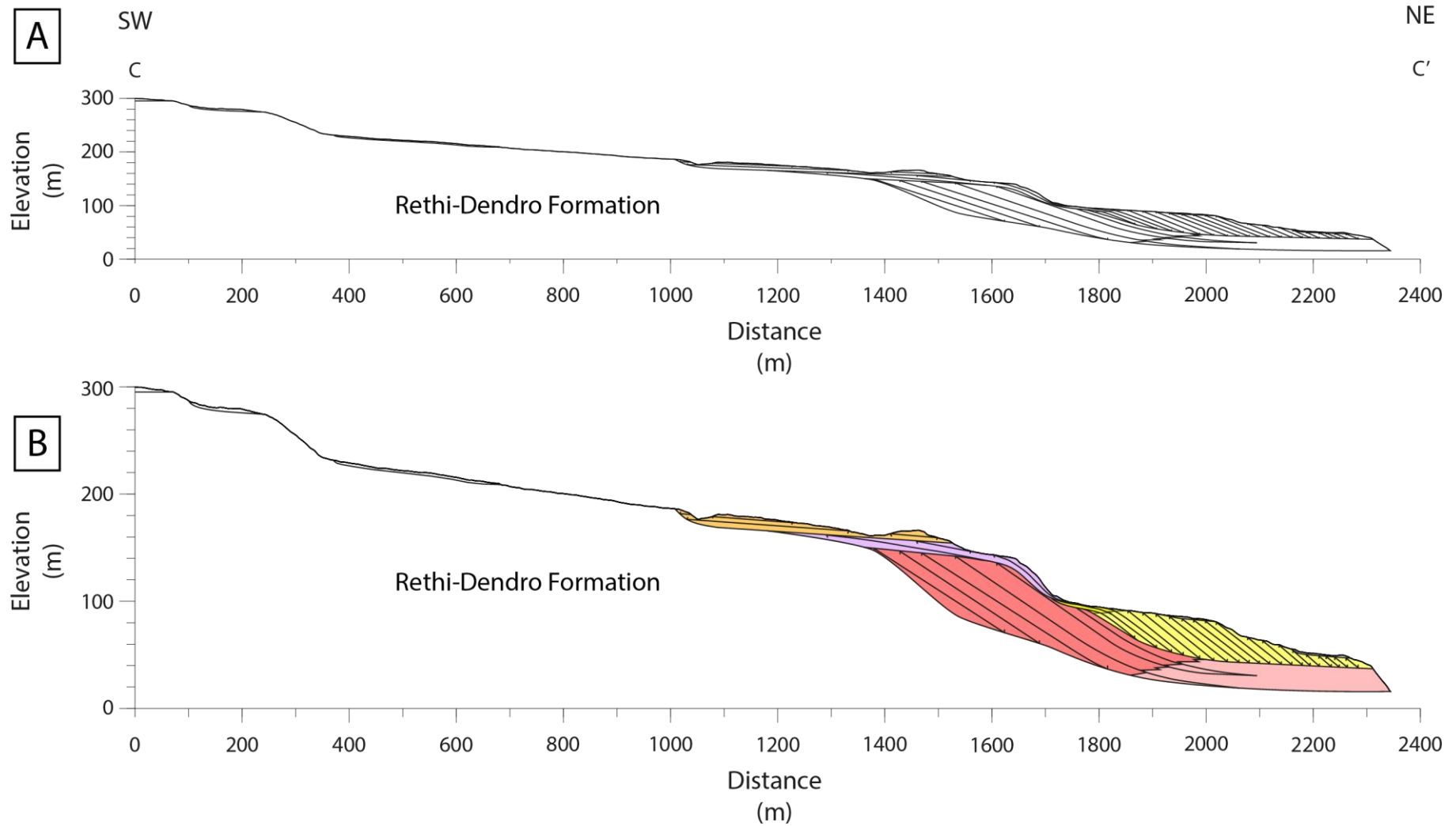
**Fig. 6.4:** Cross section of exposures east of the Katharonefi River (Fig. 6.1). A: To scale, B: Vertical exaggeration X2. In this cross-section the slackwater deposits (FA1.2), Delta 5 (foreset), Delta 3 (foreset and toeset) and Delta 4 (topset and foresets) are illustrated.
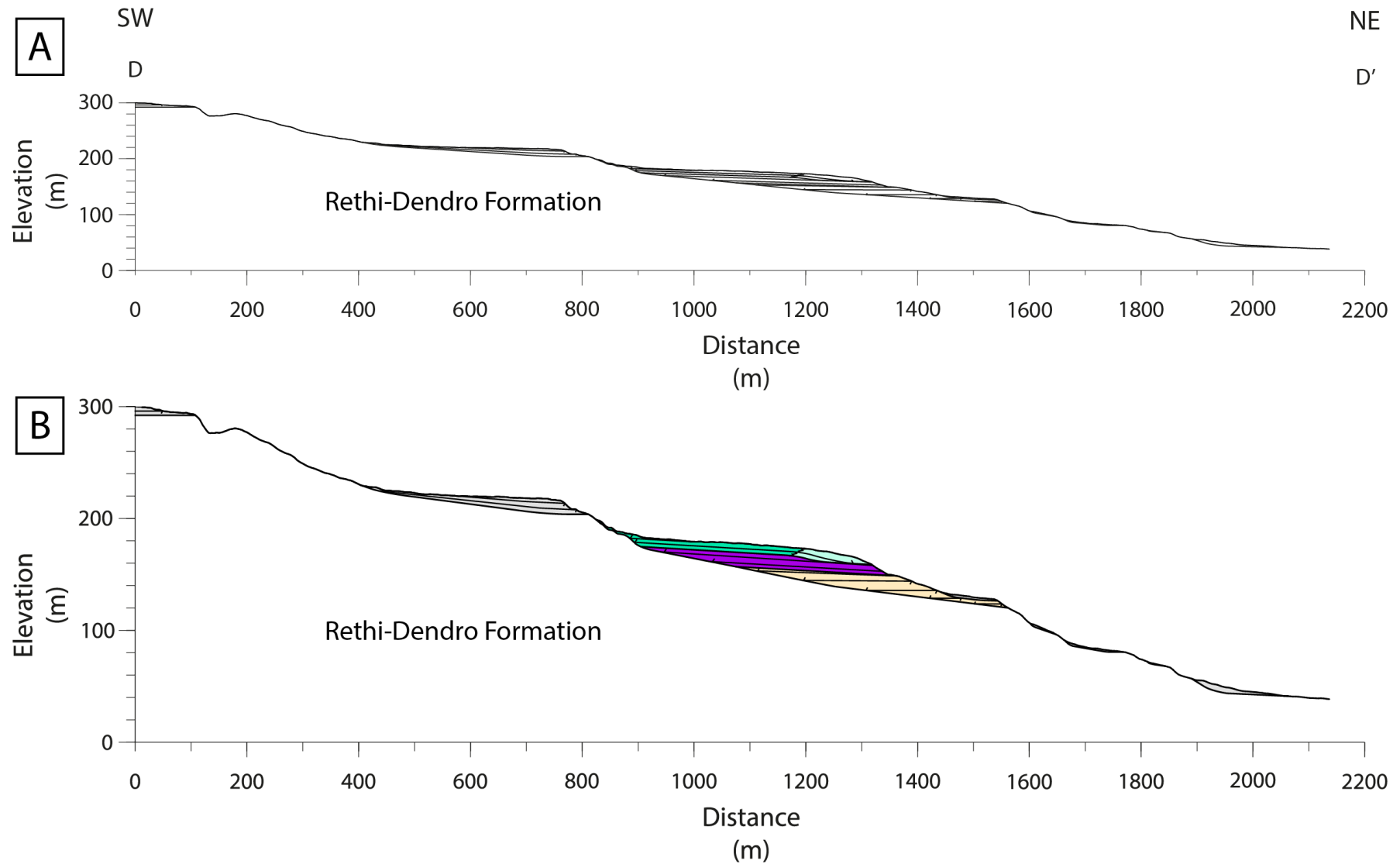
**Fig. 6.5:** Cross-section illustrating the easternmost part of the study area (Fig. 6.1). A: To scale, B: Vertical exaggeration X2. In this cross-section Delta 6 (topset and foreset), Delta 5 (topset) and a bottomset unit are shown.
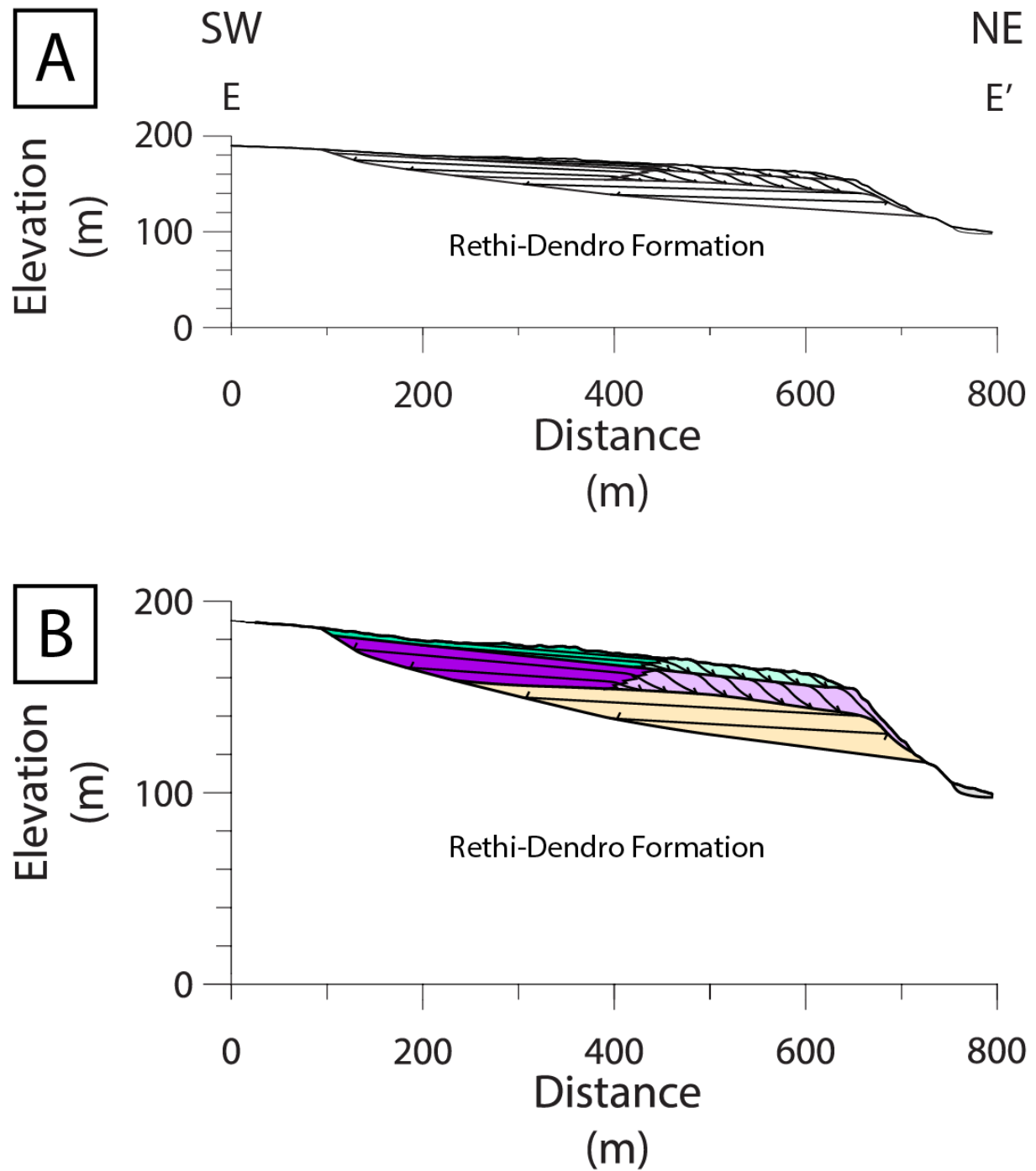
**Fig. 6.6:** Cross-section of the bottomset unit, Delta 5 and Delta 6 from a small valley east of the Katharonefi River (Fig. 6.1). A: To scale, B: Vertical exaggeration X2.

## 6.1 Delta 1

Delta 1 is deposited in the southwesternmost part of the study area (Fig. 6.1). The delta consists of delta topset (FA1) and delta foreset (FA2) deposits. The toeset of Delta 1 is not exposed in the study area. The topset is approximately 300 m long in depositional dip direction and 25 m thick. The foreset is approximately 200 m in depositional dip direction and 25 m in vertical thickness. The delta is relatively fine grained compared to the other deltas of this study and both topset and foreset consist of medium to coarse sandstone with some floating outsized clasts (facies Sm). The topset onlaps the Rethi-Dendro Formation towards South and the foreset downlaps the Rethi-Dendro formation towards North (Fig. 6.2, 6.3). The transition between topset and foreset in Delta 1 is gradational (sigmoidal toplap). The offlap break migration path of Delta 1 is characterized by a gradual transition from an upward to seaward migration (Fig. 6.2, 6.7).

## 6.2 Delta 2

Delta 2 is the largest delta of the study area and it is located in the westernmost part of the study area (Fig. 6.2). Topset, foreset and toeset of Delta 2 are exposed. The topset of Delta 2 is almost 800 m long in depositional dip directon and almost 300 m thicks. In terms of lithology, Delta 2 is one of the coarsest grained deltas investigated in this study. The delta consists of several lithofacies (Gcm, Gmm, Sp, Fm and Fl) and there is a general trend that the delta is coarser grained and more crudely stratified in the westernmost part and finer grained with more prominent stratification in the easternmost part. The delta topset onlaps the Rethi-Dendro formation towards the south and the toeset downlaps the Rethi-Dendro Formation towards the north. In terms of toplap geometries, the following variations are observed: In the westernmost part the topset is truncating the delta foresets (oblique toplap) (Fig. 6.1, 6.2) and in the easternmost part there is a transitional relationship between topset and foresets (sigmoidal toplap) (Fig. 6.1, 6.3, 6.8). The offlap break migration path of Delta 2 is characterized by a gradual transition from an upward to a more basinward migration. NE of the Delta 1 topset, the offlap break migration path is shifting from horizontal to slightly inclined seawards (Fig. 6.3, 6.8).
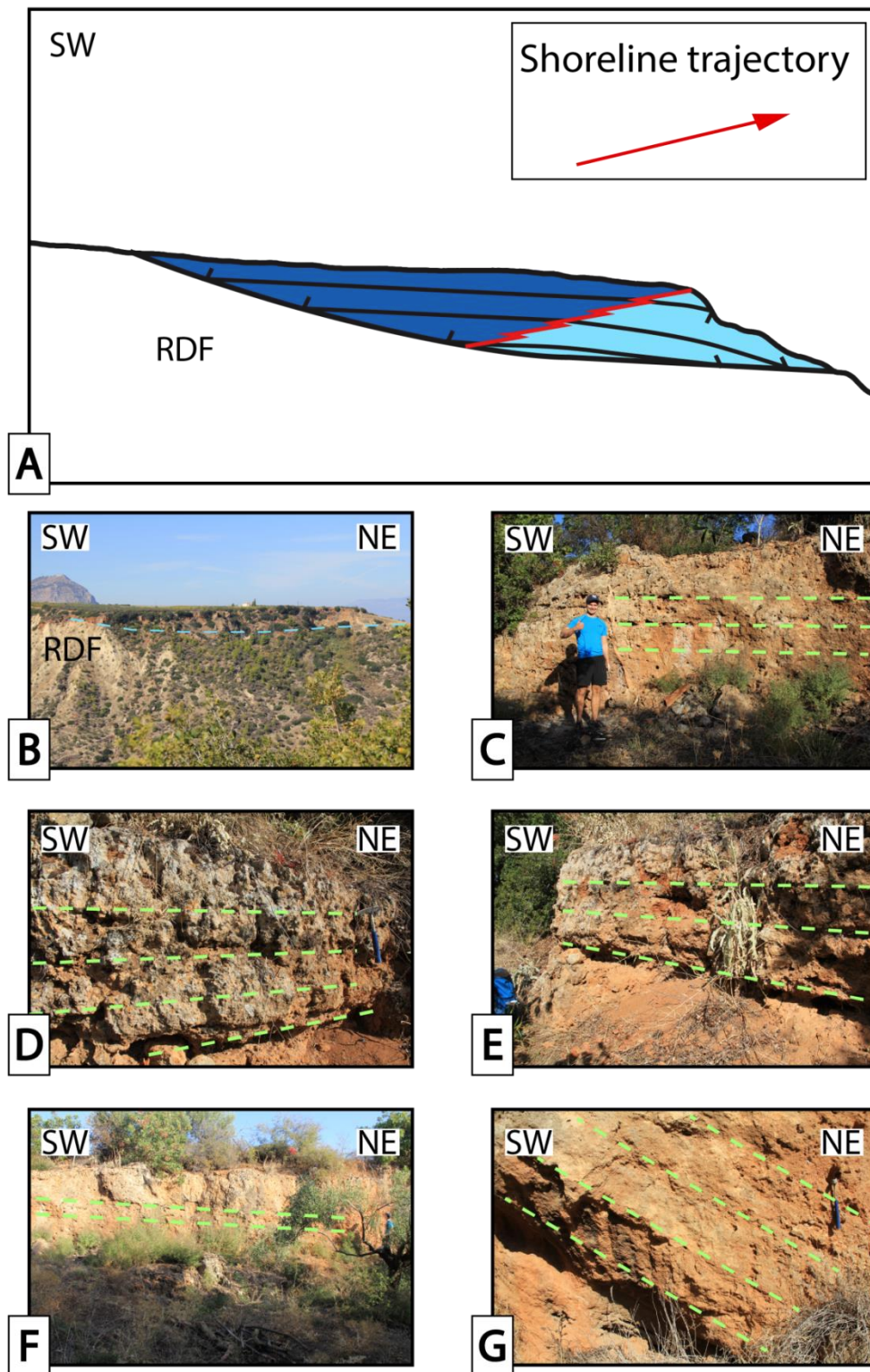
**Fig. 6.7:** Zoomed in cross-section (A, B) and field pictures illustrating the topset and foreset of Delta 1. The dashed blue line is illustrating the boundary with the underlying Rethi-Dendro formation. The green lines are illustrating the stratification. The red shazam line of A is illustrating the offlap break migration path. The red arrow is illustrating the shoreline trajectory migration direction. RDF: Rethi-Dendro formation. See log 21 and 22 in the appendix to see the sedimentology of the Delta 1 topset and foreset.
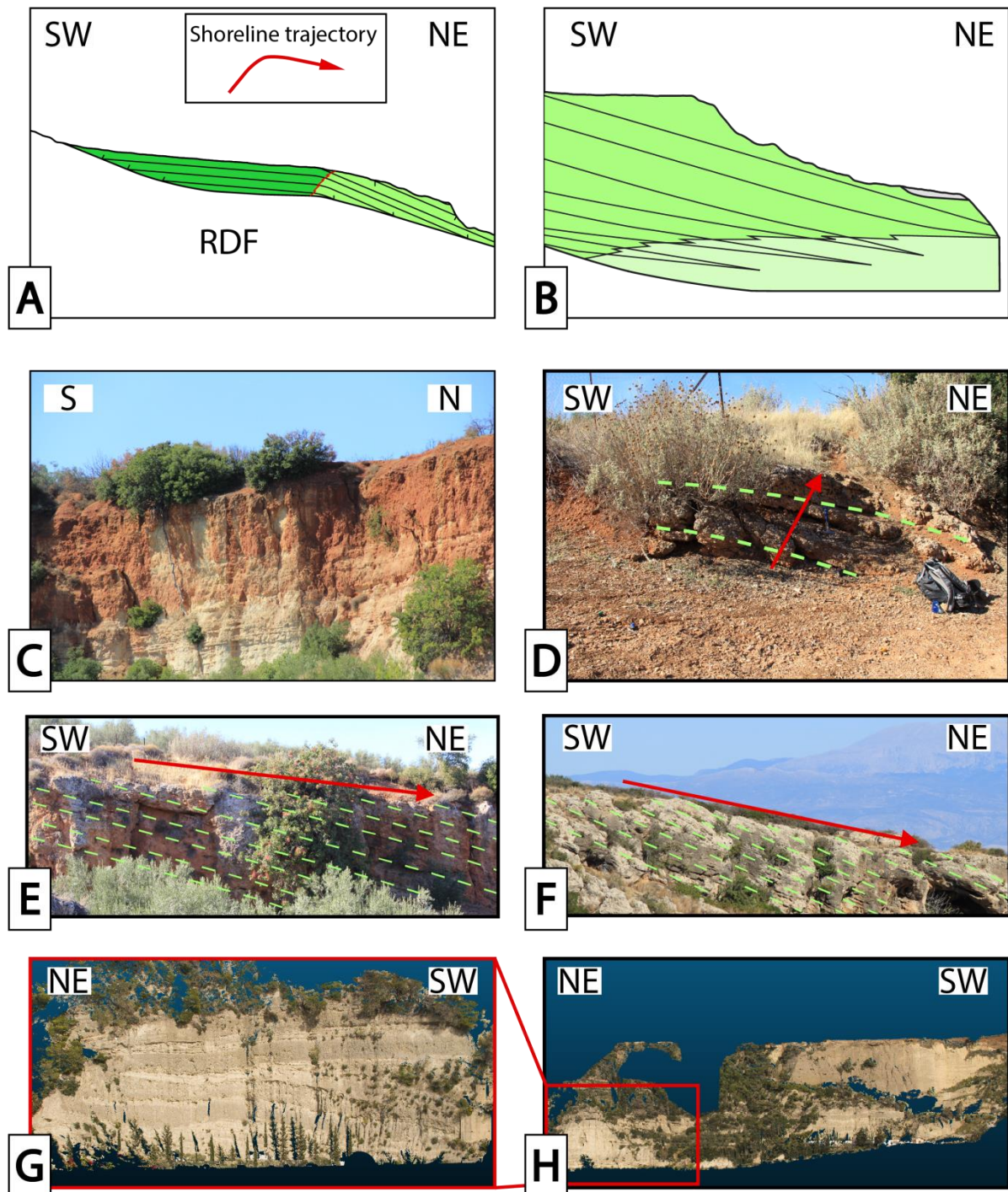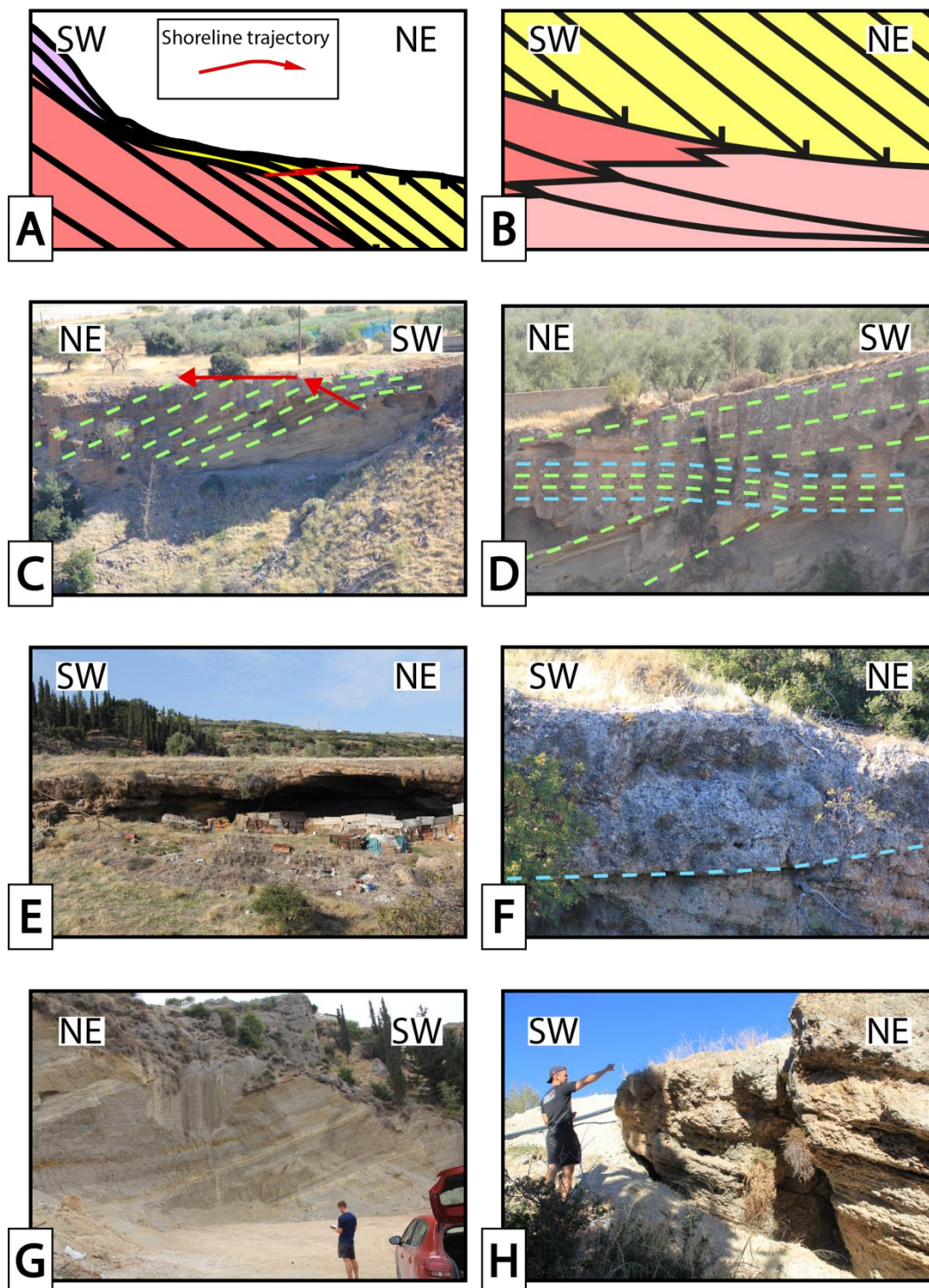
**Fig. 6.8:** Zoomed in cross-section (A, B) and field pictures illustrating the Delta 2 topset (C), delta brink (D), foreset (E, F, H) and toeset (G,H). The dashed green lines are illustrating the stratification. The red shazam line is illustrating the offlap break migration path. The Red arrows are illustrating the shoreline trajectory migration directions.Abbreviations: RDF: Rethi-Dendro formation.

## 6.3 Delta 3

Delta 3 is deposited in the middle of the study area and it is observed on both sides of the Katharonefi River (Fig. 6.1). Delta 3 topset and foreset are exposed in the study area. The topset is approximately 50 m long in depositional dip direction and 6 m thick. The foreset is approximately 600 m long in depositional dip direction and 120 m thick. In general, Delta 3 is quite similar to Delta 2 in terms of the lithology. It consists of several fine and coarse-grained facies (Gcm, Gmm, Sm, Fl). The topset onlaps and truncates the foresets of Delta 2 towards south and the toeset downlaps the Rethi-Dendro formation towards North (Fig. 6.3, 6.4). The transition from topset to foreset is gradational (sigmoidal toplap). The foreset Delta 3 is truncated by several marine terraces. The offlap break migration path of Delta 3 is characterized by a shift from an upward to seaward migration (Fig. 6.9).

## 6.4 Delta 4

Delta 4 is the northernmost delta of the study area. Only the topset and foreset of Delta 4 are exposed. The topset of Delta 4 is approximately 100 m long in depositional dip direction and 8 m thick. The foreset of Delta 4 is approximately 500 m long in depositional dip direction and 60 m thick. The lithology of Delta 4 is similar to Delta 2 and Delta 3 (Gcm, Gmm, Gp, Fl). The delta deposits are generally finer-grained towards east. The Delta 4 topset onlaps the foreset of Delta 3 towards south and the foreset downlaps the toeset of Delta 3 towards North (Fig. 6.3, 6.4). The Delta 4 topset truncates the foreset of Delta 3 west of the Katharonefi River (Fig. 6.1). East of the Katharonefi River, the transition between topset and foreset is gradational (sigmoidal toplap). The foreset of Delta 4 is truncated by several marine terraces. The offlap break migration path of Delta 4 is characterized by a shift in the migration path from upwards to seawards (Fig. 6.4, 6.10).
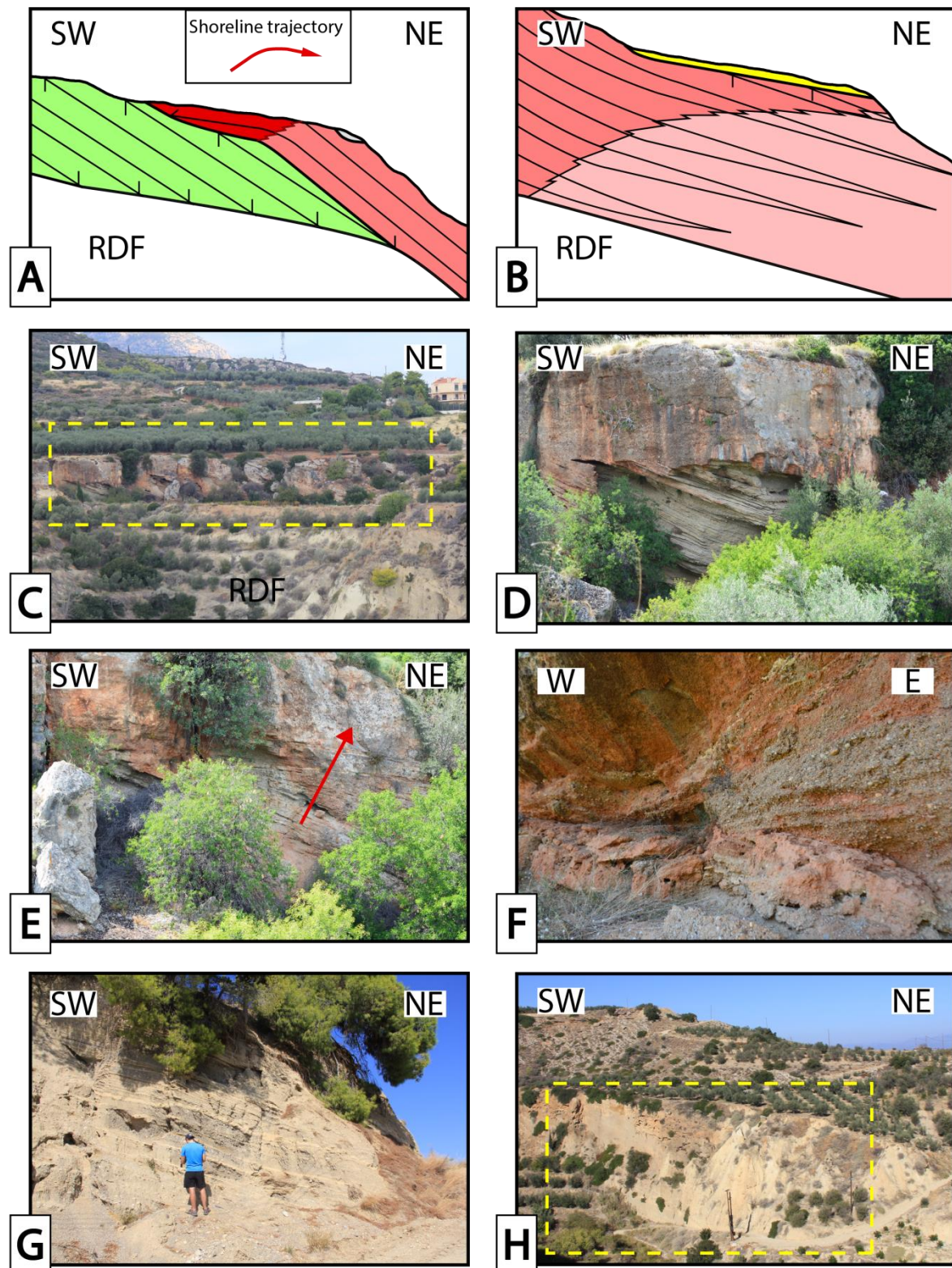
**Fig. 6.9:** Zoomed in cross-section (A, B) and field pictures illustrating the topset (C, D, and E), foreset (F, G) and toeset (H) of Delta 3.The dashed yellow squares are marking the area of interest. The red shazam line in A is illustrating the offlap break migration path. The red arrows are illustrating the shoreline trajectory migration directions. Abbreviations: RDF: Rethi-Dendro formation.

**Fig. 6.10:** Zoomed in cross-section (A, B) and field pictures illustrating the topset (C, D, E and F) and foreset (C, D, G and H) of Delta 4.The dashed blue line is illustrating the boundary between the Delta 4 topset and the foreset of Delta 3 and Delta 5. The dashed green lines are illustrating the stratification. The red shazam line (A) is illustrating the offlap break migration path. The red arrows are illustrating the shoreline trajectory migration directions.

## 6.5 Delta 5

Delta 5 is one of the smallest deltas investigated in this study. Only the topset and foreset of Delta 5 are exposed in the study area. The topset is approximately 300 m long in depositional dip direction and 20 m thick. The foreset is approximately 400 m long in depositional dip direction and 40 m thick. In terms of lithology, Delta 5 topset and foreset consists of several lithofacies (Gcm, Gc, Sm, St and Fm). The delta topset onlaps the Rethi-Dendro formation towards South and the foreset downlaps the bottomset unit towards North. The bottomset unit is deposited on top of the Rethi-Dendro formation in East and on top of the Delta 3 foreset close to the Katharonefi River (Fig. 6.4, 6.5). The transition between topset and foreset is gradational (sigmoidal). Corals are found on top of the topsets of Delta 5. These corals are surrounded by the foreset deposits of Delta 6. The offlap break migration path of Delta 5 is gradually shifting direction from upward and seaward to seaward (Fig. 6.6, 6.11).

## 6.6 Delta 6

Topset and foreset of Delta 6 are exposed in the study area. The topset is approximately 400 m long in depositional dip direction and 10 m thick. The foreset is approximately 200 m long in depositional dip direction and 10 m thick. Delta 6 is quite similar to Delta 5 in terms of dimensions and geometries. There are great lateral variations in the lithology of Delta 6. It is coarse-grained (max clast-size is 64 mm) in the western part and finer grained (fine to very coarse sand) in the eastern part of the delta. In the westernmost part facies Gcm is more frequent and in the easternmost part facies Sm is more common. The Delta 6 topset onlaps the Rethi-Dendro formation and the topset of Delta 5 towards the south and the foreset downlaps the topset of delta 5 towards North. Laterally west of the Delta 6 topset a finer grained unit, consisting of very fine sand and marls are observed (Fig. 6.1). The transition between topset and foreset of Delta 6 is gradational (sigmoidal). The offlap break migration path of Delta 6 is characterized by a gradual shift from upward and seaward to seaward (Fig. 6.6, 6.12).
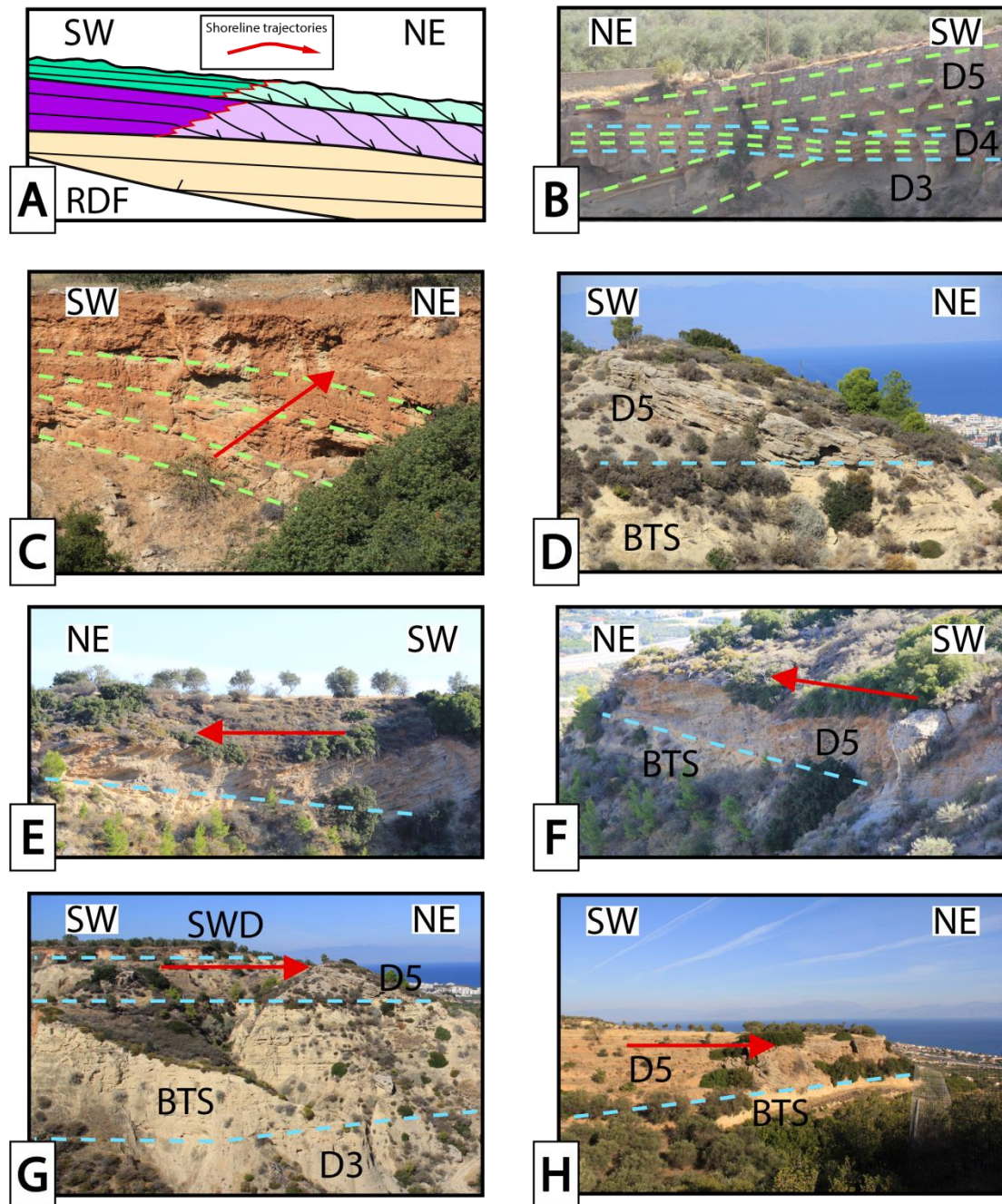
**Fig. 6.11:** Zoomed in cross-section and field pictures illustrating the Delta 5 topset and foreset. The dashed blue lines are illustrating the boundaries between the different units. The dashed green lines are illustrating the stratification. The red shazam lines (A) are illustrating the offlap break migration path. The red arrows are illustrating the shoreline trajectory migration directions. Abbreviations: SWD: slackwater deposits, BTS: bottomset, RDF: Rethi-Dendro formation, D3: Delta 3, D4: Delta 4, D5: Delta 5.
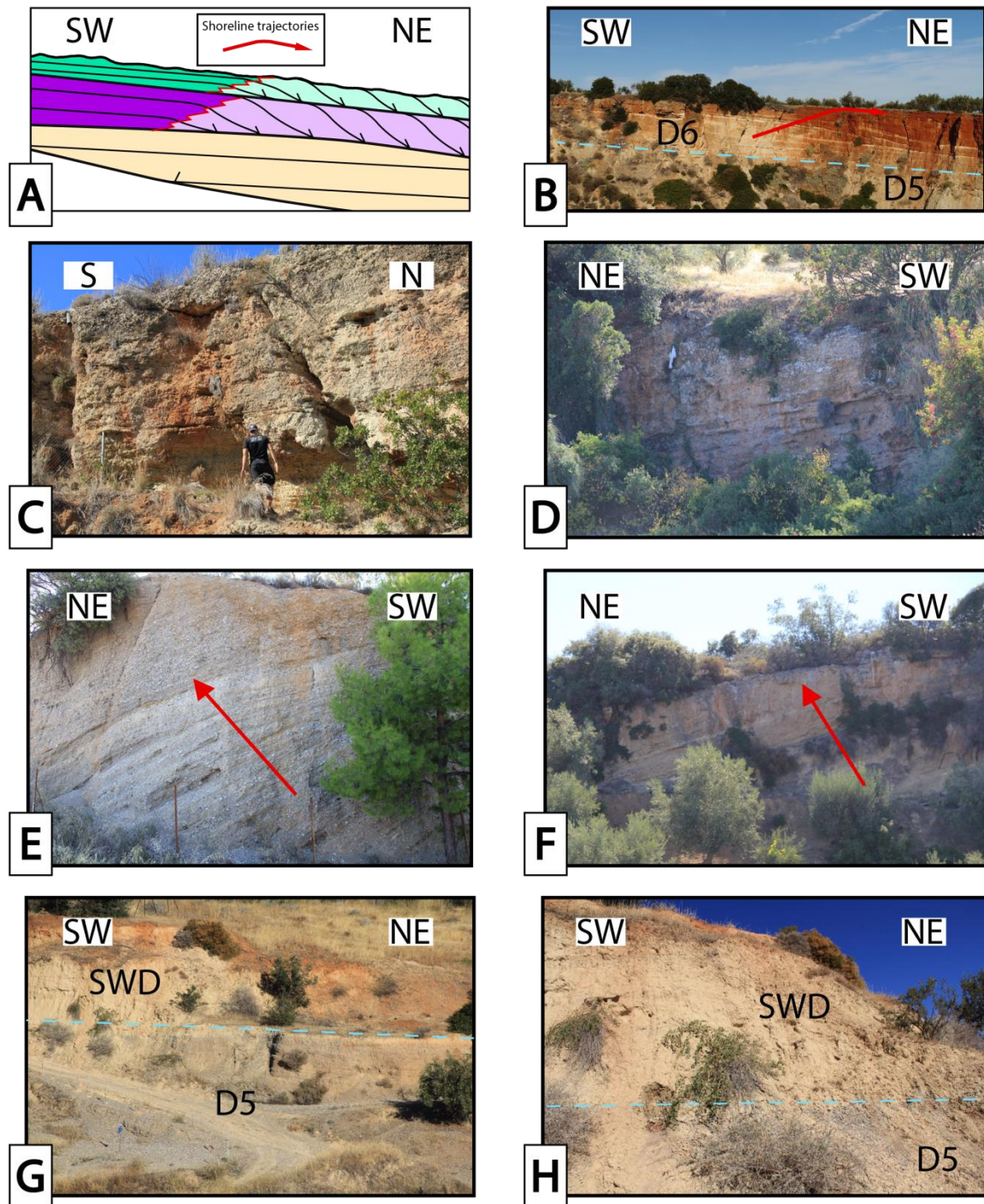
**Fig. 6.12:** Zoomed in cross-section and field pictures illustrating the topset and foreset of Delta 6. The dashed blue lines are illustrating the lower boundary of Delta 6. The shazam lines (A) are illustrating the offlap break migration path. The red arrows are illustrating the shoreline trajectory migration directions. Abbreviations: SWD: Slackwater deposits, D5: Delta 5, D6: Delta 6. The slackwater deposits (G, H) are found laterally westwards to the Delta 6 topset.

## 6.7 Interpretation of the delta units

On macroscale the deltas show a down-stepping pattern from Delta 1 to Delta 4, which is interpreted to be related to the uplift of the East Xylokastro footwall (Gawthorpe et al., 2017a). The relative age of the deltas is determined based on the termination surfaces observed in the field. The offlap break migration paths of the individual deltas can be interpreted in terms of shoreline trajectories. In general, the shoreline migrated upwards and seawards, which is interpreted to be due to a normal regression (Helland-Hansen and Martinsen, 1996). These shoreline trajectories are associated with an aggradational and progradational clinoform growth (Helland-Hansen and Hampson, 2009). In the more distal parts of Delta 5 and Delta 6 the topset is absent; however the foresets are characterized by sigmoidal toplap geometries (Fig. 6.6). This is interpreted to be due to pure progradation (Rohais et al., 2008). NE of the Delta 2 topset, the individual shoreline trajectory of Delta 2 migrates seawards and downwards, which is interpreted to be due to forced regression (Helland-Hansen and Martinsen, 1996). The distal shoreline trajectory of Delta 2 are associated with a downward clinform growth (Helland-Hansen and Hampson, 2009).

On the macro scale the shoreline trajectory between the different deltas are characterized by seaward and downward migration (Fig. 6.13), which is interpreted to be due to a relative sea-level fall as a result of the footwall uplift (Armijo et al., 1996). The shoreline trajectory between Delta 4 and Delta 6 is migrating upwards and landwards, which indicates a relative sea-level rise from Delta 4 to Delta 6 (e.g., Emery et al., 1996, Helland-Hansen and Martinsen, 1996). From Delta 6 towards the present day coastline, the shoreline trajectory is migrating seawards and downwards (Fig. 6.13).

In general, the deltas of the eastern part of the study area are finer grained than the deltas of the western part. The deltas of the eastern part of the study area are also generally smaller in terms of thickness and lateral extent than the western deltas. Most of the deltas are also finer grained internally towards east. The lateral variations from west to east are interpreted to be due to the relative distance away from the main tributary fluvial system, which is interpreted to be the Sythas River (Fig. 6.1, 6.13).
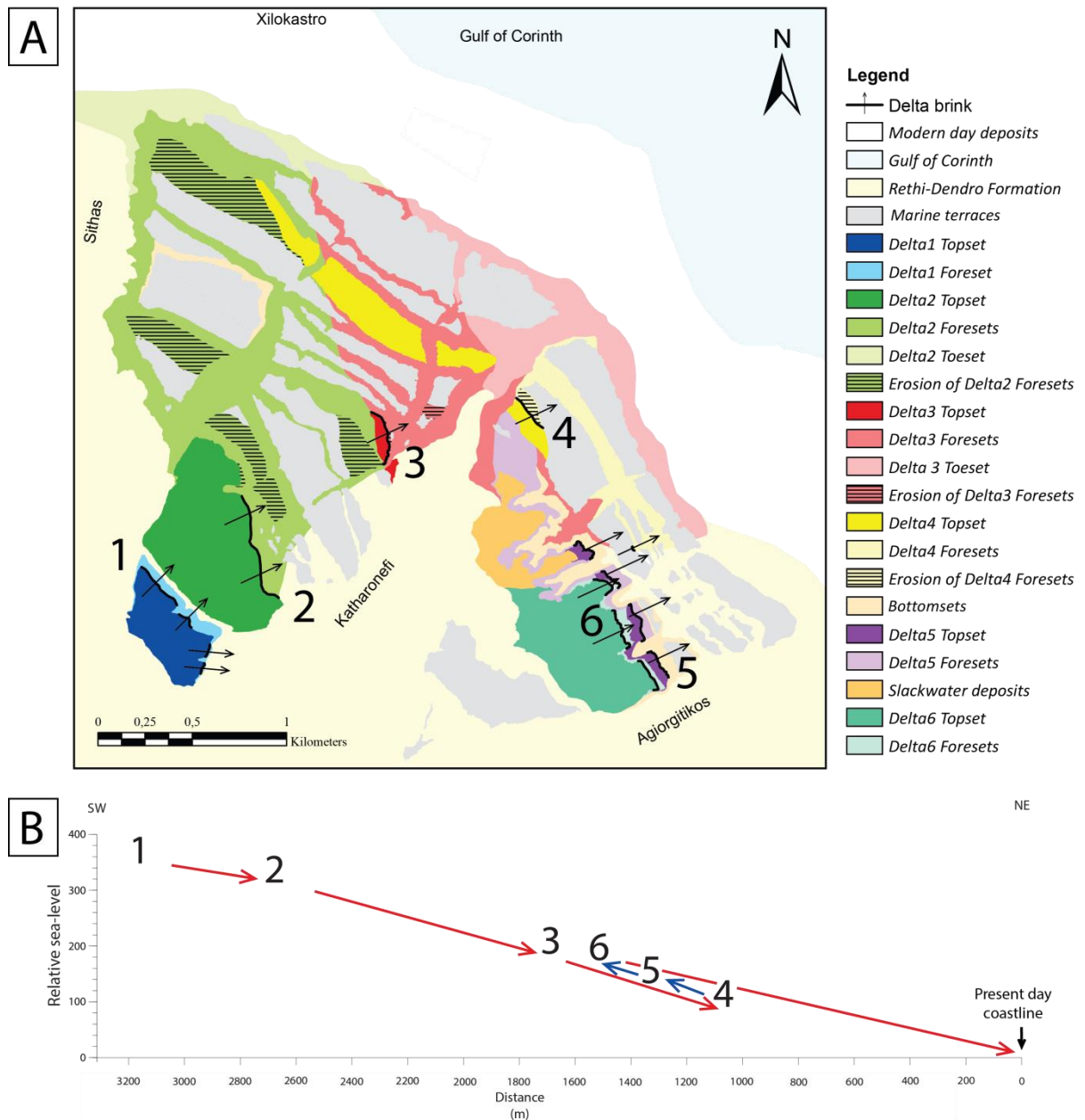
**Fig. 6.13:** A: Map illustrating the delta brink of the different deltas. B: Graph showing the relative shoreline migration path between the different deltas.

# 7 Discussion

## 7.1 Differences between giant and small-scale Gilbert-type deltas

In previous studies, great emphasis have been put on the giant Gilbert-type deltas at the southern margin of the Corinth Rift (e.g., Rohais et al., 2008, Backert et al., 2010, Gobo et al., 2015). The sedimentology and architecture of the deltas investigated in this study are not very different from the giant Gilbert-type deltas. The previously studied deltas consist of mainly massive to crudely stratified polymictic conglomerates, pebbly sandstones and small portions of sandstones and mudstones (e.g., Rohais et al., 2008, Backert et al., 2010, Gobo et al., 2015). The deltas investigated in this study consist of similar facies (Table 1). The main difference between the deltas investigated in this study and the giant Gilbert-type deltas is related to the lateral extent and thickness of the deltas. The giant Gilbert-type deltas can have a radius of more than 3 km and may exceed 1000 m in total thickness (Gawthorpe et al., 2017a). The largest delta of this study is approximately 350 m in total thickness. The differences are interpreted to be related to the location of the deltas relative to major normal faults. The previously studied giant Gilbert-type deltas are all located in the immediate hangingwall of major normal faults (e.g., Rohais et al., 2008, Backert et al., 2010, Gobo et al., 2015, Gawthorpe et al., 2017a) and they were deposited during a time period with increasing accommodation space due to hangingwall subsidence (Rohais et al., 2007a). The deltas investigated in this study are deposited on the footwall crest of the East Xylokastro fault (Fig. 7.1) and they were deposited during a time period with a decrease in accommodation space due to tectonic uplift (Rohais et al., 2007a).
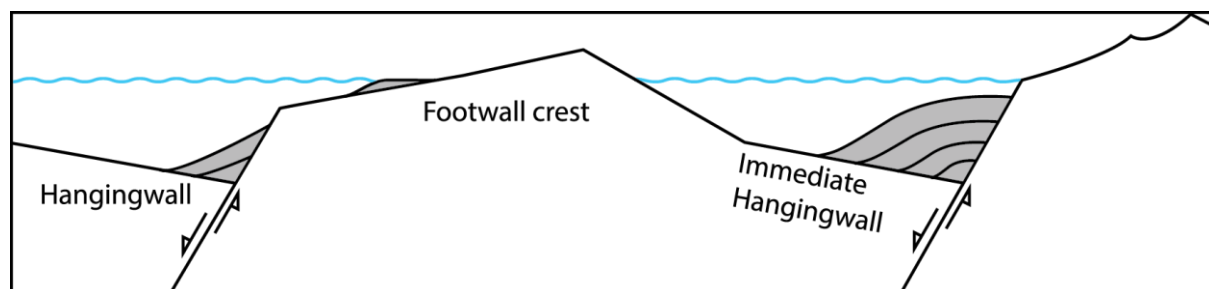


**Fig. 7.1:** Idealized cross-section of a half-graben illustrating the importance of the location of the deltaic system relative to major normal faults. The grey packages are illustrating Gilbert-type deltas. Notice the small delta on the footwall crest.

The great differences in dimensions can also be related to the rate of sediment supply. According to Gawthorpe et al. (2017a), footwall and regional uplift have progressively led to back-tilting and drainage reversal. The main rivers of the study area were flowing northwards during the first phase of rifting, but they were eventually reversed (Gawthorpe et al., 2017a).

## 7.2 Lateral variations

In total nine main terrace platforms were identified in the study area by Armijo et al. (1996). As a result of the detailed mapping conducted in this study, it was found that some of the marine terrace platforms partly correspond to delta topsets. Most of the delta topsets can be correlated laterally to marine terraces (except Delta 3 and Delta 4). It is a general trend that the deltas are relatively finer grained in the easternmost part of the study area (except Delta 1, which is one of the finest grained deltas of this study). In some of the deltas the internal deposits also fine towards east. The different deltas are also smaller in terms of thickness and lateral extent from west to east (except Delta 1, which is one of the smaller deltas of this study). The lateral variations are interpreted to be related to the relative distance away from the main tributary fluvial system. The main tributary system is interpreted to be associated with the Sythas River, which is the largest modern-day fluvial system observed in the study area (Fig. 7.2). The Katharoneri River and Agiorgitikos River are smaller fluvial systems (Fig. 7.2) and they are interpreted to be tributaries to the deltaic system in the intermediate and eastern part of the study area.
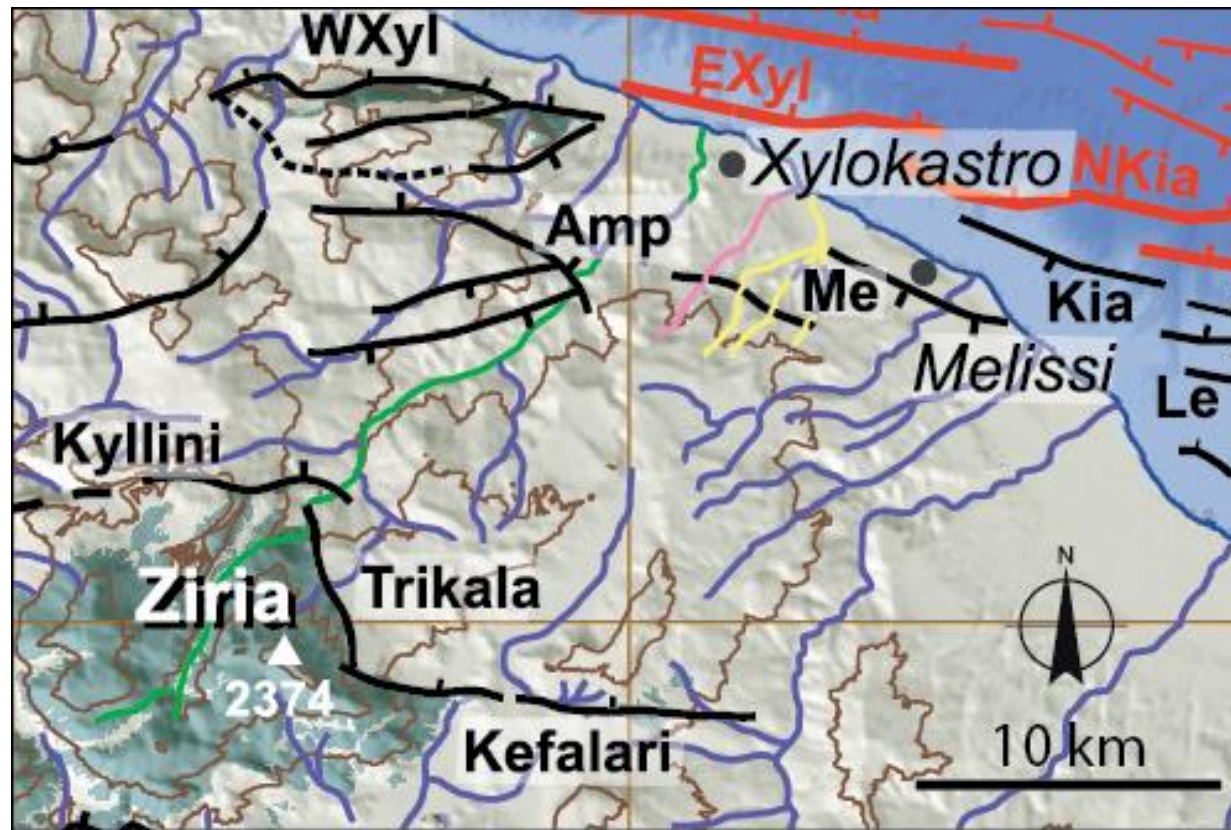
**Fig. 7.2:** The different tributary feeding systems. Green: Sythas River, Pink: Katharonefi River, Yellow: Agiorgitikos River. Modified from (Gawthorpe et al., 2017a)

## 7.3 Relative sea-level changes

It is generally agreed that the marine terraces are younger step by step downwards as the relative sea-level is falling due to tectonic uplift (Armijo et al., 1996). New evidence presented in this thesis indicates a relative sea-level rise, which is not described in previous work. The shoreline trajectories and stratal termination surfaces described in chapter 6 (Fig. 6.6, 6.7) are evidence of a relative sea-level rise from Delta 4 to Delta 6. On macroscale the deltaic system shows a seaward and downward migrating shoreline trajectory from Delta 1 to Delta 4, which is interpreted to be due to a relative sea-level fall as a result of the footwall uplift (Armijo et al., 1996). From Delta 4 to Delta 6 the shoreline trajectory indicates an upward and landward migration of the shoreline, which can possibly be related to a eustatic sea-level rise. According to the eustatic sea-level curve of Nolting et al. (2016), an eustatic sea level rise of approximately 100 m occurred between 140-120 ka (Fig. 7.3). In situ corals, dated at 127 ka by Collier et al. (1992), can be found on the New Corinth terrace (Fig. 5.1) further east of the study area (Armijo et al., 1996). The corals observed in this study are also associated with the New Corinth terrace and it can therefore be assumed that the corals are of the same age. The stratal termination surfaces are also evidence of a relative sea-level rise. Delta 5 foresets are downlapping the topset of Delta 4 and Delta 6 foreset is downlapping the topset of Delta 5. It is therefore likely that the relative sea-level rise is related to the eustatic sea-level rise between 140-120 ka.

In the eustatic sea-level curve (Fig. 7.3) by Nolting et al. (2016), eustatic sea-level rises are related to the initiation of MIS 11, MIS 9 and MIS 7. The Temple and New Corinth terraces are previously correlated to MIS 9 and MIS 7 respectively (Armijo et al., 1996). The topsets of Delta 1 and Delta 2 were initially interpreted as the Temple (MIS 9) and New Corinth (MIS 7) marine terraces respectively (Fig. 5.1) (Armijo et al., 1996). The sea-level rises at the beginning of MIS 9 and MIS 7 (Fig. 7.3) were not observed in the delta deposits. One possible explanation may be that the relative sea-level rises are balanced by the tectonic uplift of the study area. The transgression recorded between Delta 4 and Delta 6 can possibly be related to a pause or lower rate of tectonic uplift. The interpreted age of the marine terraces are based on correlation with marine terraces east of the study area. The dating of the marine terraces was conducted on terraces closer to Corinth, so the correlation is possibly wrong. It

is therefore necessary to do more accurate dating of the marine terraces and topsets of the study area to further make any conclusions.
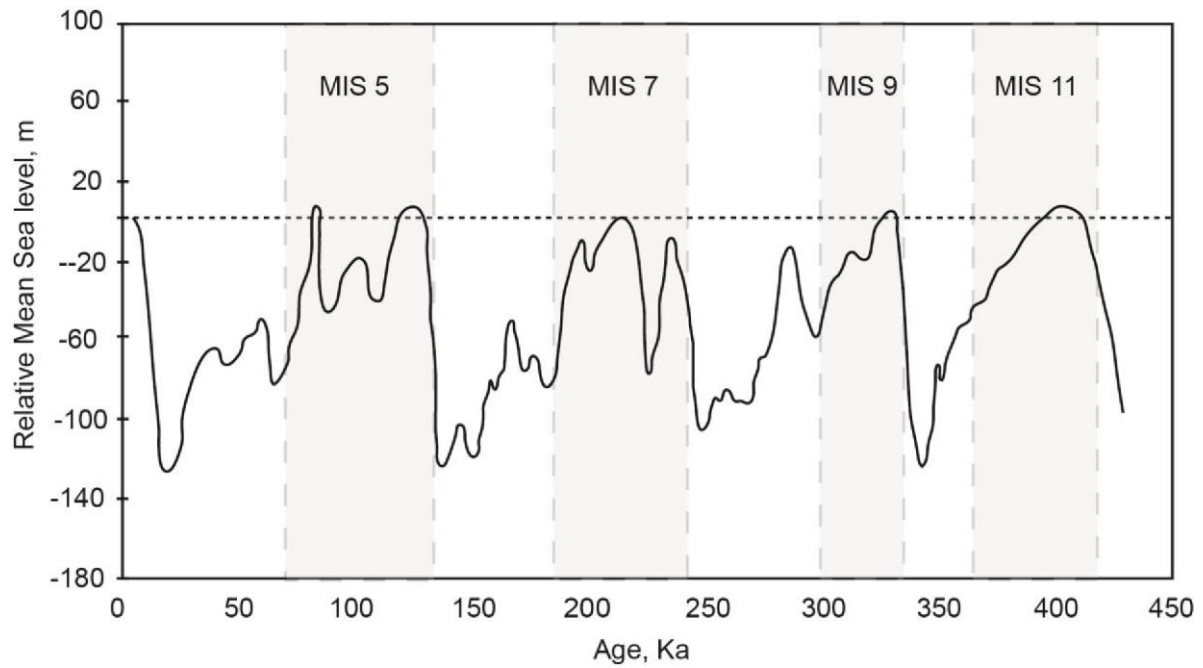


**Fig. 7.3:** Eustatic sea-level curve from Nolting et al. (2016). Abbreviations: MIS: Marine Isotope Stage. The sea-level is relative to the modern day sea-level.

# 8 Conclusions

This is the first detailed study on the sedimentology and sequence stratigraphy of the Late Pleistocene deltas on the footwall of the East Xylokastro fault. Some similarities and differences are observed from the previously studied giant Gilbert-type deltas at the southern margin of the Corinth Rift. Great lateral variations were observed between the different deltas and also internally in some of the deltas. By conducting sedimentological and sequence stratigraphic analysis of the deltas, the following conclusions have been made:

- As a result of the detailed mapping conducted in this study, it was found that some of the marine terraces interpreted by Armijo et al. (1996) partly correspond to delta topsets.

- Compared to the previously studied giant Gilbert-type deltas, the Late Pleistocene deltas of this study are relatively small in terms of thickness and lateral extent. The thickness and lateral extent of the deltas are interpreted to be related to the location relative to major normal faults. The Late Pleistocene deltas are located on the footwall crest of the East Xylokastro footwall where the generation of accommodation space is limited due to the footwall uplift. The giant Gilbert-type deltas are all located in the immediate hangingwall of major normal faults, where the generation of accommodation space is higher due to hangingwall subsidence. Another controlling factor on dimensions of the deltas is the rate of sediment supply. The sediment supply were probably reduced during the deposition of the deltas investigated in this study due to drainage reversal caused by back-tilting of the fault blocks (Gawthorpe et al., 2017a). In terms of sedimentology, the Late Pleistocene deltas investigated in this study are very similar to the giant Gilbert-type deltas.

- The overall shoreline trajectory recorded by the deltas infers a relative sea-level fall from Delta 1 to the present day sea level. New evidence presented in this study infers a relative sea-level rise from Delta 4 to Delta 6 that has not been described in previous work. The shoreline trajectory and the stratal termination surfaces recorded in the delta deposits show evidence of the transgression. This transgression is interpreted to be related to the eustatic sea-level rise that occurred in the interval

140-120 ka. This relative sea-level rise may have important implications for the understanding of the uplift history of the East Xylokastro footwall.

- Great lateral variations from west to east are observed across the study area. In general the individual delta units on the eastern part of the study area are smaller relative to the deltas on the western part of the study area. Internally in some of the deltas the deposits are coarser grained towards west and finer grained towards east. The lateral variations from west to east in the study area are interpreted to be related to the relative distance away from the main tributary fluvial system, which is interpreted to be the Sythas River. The Sythas River is the largest fluvial system in the study area (see Fig. 7.2)

# References

ARMIJO, R., MEYER, B., HUBERT, A. & BARKA, A. 1999. Westward propagation of the North Anatolian fault into the northern Aegean: Timing and kinematics. *Geology,* 27**,** 267-270.

ARMIJO, R., MEYER, B., KING, G., RIGO, A. & PAPANASTASSIOU, D. 1996. Quaternary evolution of the Corinth Rift and its implications for the Late Cenozoic evolution of the Aegean. *Geophys Journal International,* 126**,** 11-53.

BACKERT, N., FORD, M. & MALARTRE, F. 2010. Architecture and sedimentology of the Kerinitis Gilbert-type fan delta, Corinth Rift, Greece. *Sedimentology,* 57**,** 543-586.

BELL, R., MCNEILL, L. C., BULL, J., HENSTOCK, T., COLLIER, R. & LEEDER, M. 2009. Fault architecture, basin structure and evolution of the Gulf of Corinth Rift, central Greece. *Basin Res.*

BELLIAN, J. A., KERANS, C. & JENNETTE, D. C. 2005. Digital outcrop models: Applications of terrestrial scanning lidar technology in stratigraphic modeling. *Journal of Sedimentary Research,* 75**,** 166-176.

BREDA, A., MELLERE, D. & MASSARI, F. 2007. Facies and processes in a Gilbert-delta-filled incised valley (Pliocene of Ventimiglia, NW Italy). *Sedimentary geology,* 200**,** 31-55.

BRIDGE, J. S. 2003. *Rivers and floodplains: forms, processes, and sedmentary record,* Oxford, Blackwell Publishing.

BRIOLE, P., RIGO, A., LYON-CAEN, H., RUEGG, J., PAPAZISSI, K., MITSAKAKI, C., BALODIMOU, A., VEIS, G., HATZFELD, D. & DESCHAMPS, A. 2000. Active deformation of the Corinth rift, Greece: results from repeated Global Positioning System surveys between 1990 and 1995. *Journal of Geophysical Research: Solid Earth,* 105**,** 25605-25625.

BROWN JR, L. & FISHER, W. 1977. Seismic-Stratigraphic Interpretation of Depositional Systems: Examples from Brazilian Rift and Pull-Apart Basins: Section 2. Application of Seismic Reflection Configuration to Stratigraphic Interpretation. 213-248.

BUCKLEY, S. J., HOWELL, J., ENGE, H. & KURZ, T. 2008. Terrestrial laser scanning in geology: data acquisition, processing and accuracy considerations. *Journal of the Geological Society,* 165**,** 625-638.

CATUNEANU, O. 2006. *Principles of sequence stratigraphy,* Amsterdam: Oxford, Elsevier.

COE, A. L. 2003. *The Sedimentary record of sea-level change,* Cambridge, Cambridge University Press.

COLELLA, A. 1988a. Fault-controlled marine Gilbert-type fan deltas. *Geology,* 16**,** 1031-1034.

COLELLA, A. 1988b. Pliocene-Holocene fan deltas and braid deltas in the Crati Basin, South Italy: a consequence of varying tectonic conditions. *Fan deltas: Sedimentology and tectonic settings***,** 50-74.

COLELLA, A., DE BOER, P. & NIO, S. 1987. Sedimentology of a marine intermontane Pleistocene Gilbert-type fan-delta complex in the Crati Basin, Calabria, southern Italy. *Sedimentology,* 34**,** 721-736.

COLLIER, R. 1990. EUSTATIC AND TECTONIC CONTROLS UPON QUATERNARY COASTAL SEDIMENTATION IN THE CORINTH BASIN, GREECE. *J. Geol. Soc.,* 147**,** 301-314.

COLLIER, R. L., LEEDER, M., ROWE, P. & ATKINSON, T. 1992. Rates of tectonic uplift in the Corinth and Megara basins, central Greece. *Tectonics,* 11**,** 1159-1167.

DASGUPTA, P. 2003. Sediment gravity flow—the conceptual problems. *Earth-Science Reviews,* 62**,** 265-281.

DEGNAN, P. & ROBERTSON, A. 1998. Mesozoic-early Tertiary passive margin evolution of the Pindos ocean (NW Peloponnese, Greece). *Sedimentary Geology,* 117**,** 33-70.

DEWEY, J. & ŞENGÖR, A. C. L. 1979. Aegean and surrounding regions: complex multiplate and continuum tectonics in a convergent zone. *Geological Society of America Bulletin,* 90**,** 84-92.

DOUTSOS, T. & KOKKALAS, S. 2001. Stress and deformation patterns in the Aegean region. *Journal of Structural Geology,* 23**,** 455-472.

DOUTSOS, T., KONTOPOULOS, N. & POULIMENOS, G. 1988. The Corinth-Patras rift as the initial stage of continental fragmentation behind an active island arc (Greece). *Basin Research,* 1**,** 177-190.

DOUTSOS, T. & PIPER, D. J. 1990. Listric faulting, sedimentation, and morphological evolution of the Quaternary eastern Corinth rift, Greece: First stages of continental rifting. *Geological Society of America Bulletin,* 102**,** 812-829.

EMERY, D., MYERS, K. & BERTRAM, G. T. 1996. *Sequence stratigraphy,* Oxford, Blackwell Science.

FALK, P. D. & DORSEY, R. J. 1998. Rapid development of gravelly high-density turbidity currents in marine Gilbert-type fan deltas, Loreto Basin, Baja California Sur, Mexico. *Sedimentology,* 45**,** 331-349.

FORD, M., ROHAIS, S., WILLIAMS, E., BOURLANGE, S., JOUSSELIN, D., BACKERT, N. & MALARTRE, F. 2013. Tectono-sedimentary evolution of the western Corinth rift (Central Greece). *Basin Research,* 25**,** 3-25.

FORD, M., WILLIAMS, E. A., MALARTRE, F. & POPESCU, S. M. 2007. Stratigraphic architecture, sedimentology and structure of the Vouraikos Gilbert-type fan delta, Gulf of Corinth, Greece. *Sedimentary processes, environments and basins: a tribute to Peter Friend***,** 49-90.

GARCÍA-GARCÍA, F., FERNÁNDEZ, J., VISERAS, C. & SORIA, J. M. 2006. Architecture and sedimentary facies evolution in a delta stack controlled by fault growth (Betic Cordillera, southern Spain, late Tortonian). *Sedimentary Geology,* 185**,** 79-92.

GAWTHORPE, R., COLELLA, A. & PRIOR, D. 1990. Tectonic controls on coarse-grained delta depositional systems in rift basins. *Coarse-grained deltas***,** 113-127.

GAWTHORPE, R. & LEEDER, M. 2000. Tectono-sedimentary evolution of active extensional basins. *Basin Research,* 12**,** 195-218.

GAWTHORPE, R., LEEDER, M., KRANIS, H., SKOURTSOS, E., ANDREWS, J., HENSTRA, G., MACK, G., MURAVCHIK, M., TURNER, J. & STAMATAKIS, M. 2017a. Tectono-sedimentary evolution of the Plio-Pleistocene Corinth rift, Greece. *Basin Research,* 30**,** 448-479.

GAWTHORPE, R. L., ANDREWS, J. E., COLLIER, R. E., FORD, M., HENSTRA, G. A., KRANIS, H., LEEDER, M. R., MURAVCHIK, M. & SKOURTSOS, E. 2017b. Building up or out? Disparate sequence architectures along an active rift margin—Corinth rift, Greece. *Geology,* 45**,** 1111-1114.

GAWTHORPE, R. L., FRASER, A. J. & COLLIER, R. E. L. 1994. Sequence stratigraphy in active extensional basins: implications for the interpretation of ancient basin-fills. *Marine and petroleum geology,* 11**,** 642-658.

GAWTHORPE, R. L., HARDY, S. & RITCHIE, B. 2003. Numerical modelling of depositional sequences in half-graben rift basins. *Sedimentology,* 50**,** 169-185.

GILBERT, G. K. 1885. *The topographic features of lake shores*, US Government Printing Office.

GOBO, K., GHINASSI, M. & NEMEC, W. 2014. Reciprocal changes in foreset to bottomset facies in a Gilbert-type delta: response to short-term changes in base level. *Journal of Sedimentary Research,* 84**,** 1079-1095.

GOBO, K., GHINASSI, M. & NEMEC, W. 2015. Gilbert-type deltas recording short-term base-level changes: Delta-brink morphodynamics and related foreset facies. *Sedimentology,* 62**,** 1923-1949.

GUPTA, S., UNDERHILL, J., SHARP, I. & GAWTHORPE, R. 1999. Role of fault interactions in controlling synrift sediment dispersal patterns: Miocene, Abu Alaqa Group, Suez Rift, Sinai, Egypt. *Basin Research,* 11**,** 167-189.

HAMPSON, G. J., SIXSMITH, P. J., KIEFT, R. L., JACKSON, C. A. L. & JOHNSON, H. D. 2009. Quantitative analysis of net-transgressive shoreline trajectories and stratigraphic architectures: mid-to-late Jurassic of the North Sea rift basin. *Basin Research,* 21**,** 528-558.

HELLAND-HANSEN, W. & GJELBERG, J. G. 1994. Conceptual basis and variability in sequence stratigraphy: a different perspective. *Sedimentary Geology,* 92**,** 31-52.

HELLAND-HANSEN, W. & MARTINSEN, O. J. 1996. Shoreline trajectories and sequences: description of variable depositional-dip scenarios. *Journal of Sedimentary Research,* 66**,** 670-688.

HELLAND-HANSEN, W. & HAMPSON, G. 2009. Trajectory analysis: concepts and applications. *Basin Research,* 21**,** 454-483.

HENRIKSEN, S., HAMPSON, G. J., HELLAND-HANSEN, W., JOHANNESSEN, E. P. & STEEL, R. J. 2009. Shelf edge and shoreline trajectories, a dynamic approach to stratigraphic analysis. *Basin Research,* 21**,** 445-453.

HODGETTS, D. 2009. 11 LiDAR in the Environmental Sciences: Geological Applications. *Laser Scanning for the Environmental Sciences*, 165-179.

JERVEY, M. 1988. Quantitative geological modeling of siliciclastic rock sequences and their seismic expression.

KAHLE, H.-G., STRAUB, C., REILINGER, R., MCCLUSKY, S., KING, R., HURST, K., VEIS, G., KASTENS, K. & CROSS, P. 1998. The strain rate field in the eastern Mediterranean region, estimated by repeated GPS measurements. *Tectonophysics,* 294**,** 237-252.

KEMP, A. C., DUTTON, A. & RAYMO, M. E. 2015. Paleo constraints on future sea-level rise. *Current Climate Change Reports,* 1**,** 205-215.

KISSEL, C. & LAJ, C. 1988. The Tertiary geodynamical evolution of the Aegean arc: a paleomagnetic reconstruction. *Tectonophysics,* 146**,** 183-201.

KLEINHANS, M. G. 2005. Autogenic cyclicity of foreset sorting in experimental Gilbert-type deltas. *Sedimentary Geology,* 181**,** 215-224.

LE PICHON, X. & ANGELIER, J. 1979. The Hellenic arc and trench system: a key to the neotectonic evolution of the eastern Mediterranean area. *Tectonophysics,* 60**,** 1-42.

LE POURHIET, L., BUROV, E. & MORETTI, I. 2003. Initial crustal thickness geometry controls on the extension in a back arc domain: Case of the Gulf of Corinth. *Tectonics,* 22.

LONGHITANO, S. G. 2008. Sedimentary facies and sequence stratigraphy of coarse-grained Gilbert-type deltas within the Pliocene thrust-top Potenza Basin (Southern Apennines, Italy). *Sedimentary Geology,* 210**,** 87-110.

LOWE, D. R. 1982. Sediment gravity flows: II Depositional models with special reference to the deposits of high-density turbidity currents. *Journal of Sedimentary Research,* 52**,** 279-297.

LØNNE, I. & NEMEC, W. 2004. High-arctic fan delta recording deglaciation and environment disequilibrium. *Sedimentology,* 51**,** 553-589.

LØNNE, I., NEMEC, W., BLIKRA, L. & LAURITSEN, T. 2001. Sedimentary architecture and dynamic stratigraphy of a marine ice-contact system. *Journal of Sedimentary Research,* 71**,** 922-943.

MASSARI, F. 1996. Upper-flow-regime stratification types on steep-face, coarse-grained, Gilbert-type progradational wedges (Pleistocene, southern Italy). *Journal of Sedimentary Research,* 66.

MCKENZIE, D. 1972. Active tectonics of the Mediterranean region. *Geophysical Journal International,* 30**,** 109-185.

MCKENZIE, D. 1978. Active tectonics of the Alpine—Himalayan belt: the Aegean Sea and surrounding regions. *Geophysical Journal International,* 55**,** 217-254.

MCMURRAY, L. S. & GAWTHORPE, R. L. 2000. Along-strike variability of forced regressive deposits: late Quaternary, northern Peloponnesos, Greece. *Geological Society, London, Special Publications,* 172**,** 363-377.

MIALL, A. D. 1996. *The geology of fluvial deposits : sedimentary facies, basin analysis, and petroleum geology,* Berlin, Springer.

MIALL, A. D. 2013. *The geology of fluvial deposits: sedimentary facies, basin analysis, and petroleum geology*, Springer.

MITCHUM JR, R. M., VAIL, P. R. & SANGREE, J. B. 1977. Seismic stratigraphy and global changes of sea level: Part 6. Stratigraphic interpretation of seismic reflection patterns in depositional sequences: Section 2. Application of seismic reflection configuration to stratigraphic interpretation. *In:* PAYTON, C. E. (ed.) *Seismic Stratigraphy - applications to hydrocarbon exploration.* Tulsa, Oklahoma, U.S.A.: The American Association of Petroleum Geologists.

MITCHUM, R. M., VAIL, P. R. & THOMPSON III, S. 1977. Seismic Stratigraphy and Global Changes of Sea Leve, Part 2: The Depositional Sequence as a Basic Unit for Stratigraphic Analysis. 516.

MORETTI, I., SAKELLARIOU, D., LYKOUSIS, V. & MICARELLI, L. 2003. The Gulf of Corinth: an active half graben? *Journal of Geodynamics,* 36**,** 323-340.

NEMEC, W. 1990. Aspects of sediment movement on steep delta slopes. *Coarse-grained deltas,* 10**,** 29-73.

NEMEC, W., LØNNE, I. & BLIKRA, L. H. 1999. The Kregnes moraine in Gauldalen, west-central Norway: anatomy of a Younger Dryas proglacial delta in a palaeofjord basin. *Boreas,* 28**,** 454-476.

NIXON, C., MCNEILL, L., BULL, J., BELL, R., GAWTHORPE, R., HENSTOCK, T., CHRISTODOULOU, D., FORD, M., TAYLOR, B., SAKELLARIOU, D., FERENTINOS, G., PAPATHEODOROU, G., LEEDER, M., COLLIER, R., GOODLIFFE, A., SACHPAZI, M. & KRANIS, H. 2016. Rapid spatiotemporal variations in rift structure during development of the Corinth Rift, central Greece. 1225-1248.

NOLTING, A., ZAHM, C., KERANS, C. & BROOKS, D. Spatial and temporal characterization of mechanical rock properties from West Caicos, British West Indies.  50th US Rock Mechanics/Geomechanics Symposium, 2016. American Rock Mechanics Association.

ORI, G. G. 1989. Geologic history of the extensional basin of the Gulf of Corinth (? Miocene-Pleistocene), Greece. *Geology,* 17**,** 918-921.

POSAMENTIER, H. W., ALLEN, G. P., JAMES, D. P. & TESSON, M. 1992. Forced regressions in a sequence stratigraphic framework: concepts, examples, and exploration significance (1). *AAPG bulletin,* 76**,** 1687-1709.

POSTMA, G. 1984. Mass-flow conglomerates in a submarine canyon: Abrioja fan-delta, Pliocene, southeast Spain.

POSTMA, G. & ROEP, T. B. 1985. Resedimented conglomerates in the bottomsets of Gilbert-type gravel deltas. *Journal of Sedimentary Research,* 55**,** 874-885.

PRIOR, D. B., WISEMAN JR, W. J. & BRYANT, W. 1981. Submarine chutes on the slopes of fjord deltas. *Nature,* 290**,** 326.

RARITY, F., VAN LANEN, X., HODGETTS, D., GAWTHORPE, R., WILSON, P., FABUEL-PEREZ, I. & REDFERN, J. 2014. LiDAR-based digital outcrops for sedimentological analysis: workflows and techniques. *Geological Society, London, Special Publications,* 387**,** 153-183.

READING, H. 1996a. Clastic coasts. *Sedimentary Environments: process, facies and stratigraphy***,** 154-231.

READING, H. G. 1996b. *Sedimentary environments: processes, facies and stratigraphy,* Oxford, Blackwell Science.

ROBERTS, S. & JACKSON, J. 1991. Active normal faulting in central Greece: an overview. *Geological Society, London, Special Publications,* 56**,** 125-142.

ROHAIS, S., ESCHARD, R., FORD, M., GUILLOCHEAU, F. & MORETTI, I. 2007a. Stratigraphic architecture of the Plio-Pleistocene infill of the Corinth Rift: Implications for its structural evolution. *Tectonophysics,* 440**,** 5-28.

ROHAIS, S., ESCHARD, R. & GUILLOCHEAU, F. 2008. Depositional model and stratigraphic architecture of rift climax Gilbert-type fan deltas (Gulf of Corinth, Greece). *Sedimentary Geology,* 210**,** 132-145.

ROHAIS, S., JOANNIN, S., COLIN, J.-P., SUC, J.-P., GUILLOCHEAU, F. & ESCHARD, R. 2007b. Age and environmental evolution of the syn-rift fill of the southern coast of the Gulf of Corinth (Akrata-Derveni region, Greece). *Bulletin de la Société géologique de France,* 178**,** 231-243.

ROJAS, E. & LE ROUX, J. P. 2010. Sedimentary processes on a Gilbert-type delta in Lake Llanquihue, southern Chile. *Andean Geology,* 32**,** 19-32.

SKOURLIS, K. & DOUTSOS, T. 2003. The Pindos Fold-and-thrust belt (Greece): inversion kinematics of a passive continental margin. *International Journal of Earth Sciences,* 92**,** 891-903.

SKOURTSOS, E. & KRANIS, H. 2009. Structure and evolution of the western Corinth Rift, through new field data from the Northern Peloponnesus. *Geological Society, London, Special Publications,* 321**,** 119-138.

SOHN, Y., KIM, S., HWANG, I., BAHK, J., CHOE, M. & CHOUGH, S. 1997. Characteristics and depositional processes of large-scale gravelly Gilbert-type foresets in the Miocene Doumsan fan delta, Pohang Basin, SE Korea. *Journal of Sedimentary Research,* 67.

STANLEY, K. T. & SURDAM, R. C. 1978. Sedimentation on the front of Eocene Gilbert-type deltas, Washakie Basin, Wyoming. *Journal of Sedimentary Research,* 48.

TAYLOR, B., WEISS, J. R., GOODLIFFE, A. M., SACHPAZI, M., LAIGLE, M. & HIRN, A. 2011. The structures, stratigraphy and evolution of the Gulf of Corinth rift, Greece. *Geophysical Journal International,* 185**,** 1189-1219.

VAIL, P. 1991. The Stratigraphic signatures of tectonics, eustasy and sedimentology-an overview. *Cycles and events in stratigraphy.***,** 617-659.

VAN WAGONER, J., POSAMENTIER, H., MITCHUM, R., VAIL, P., SARG, J., LOUTIT, T. & HARDENBOL, J. 1988. Sea-Level Changes: An Integrated Approach. *In:* WILGUS, C. K., HASTINGS, B. S., POSAMENTIER, H. W., VAN WAGONER, J., ROSS, C. A. & KENDALL, C. G. S. C. (eds.) *An Overview of The Fundamentals of Sequence Stratigraphy and Key Definitions.* Tulsa, Oklahoma, U.S.A.: Society of Economic Paleontologists and Mineralogists.

VISERAS, C., CALVACHE, M. A. L., SORIA, J. M. & FERNÁNDEZ, J. 2003. Differential features of alluvial fans controlled by tectonic or eustatic accommodation space. Examples from the Betic Cordillera, Spain. *Geomorphology,* 50**,** 181-202.

YOUNG, M. J., GAWTHORPE, R. L. & SHARP, I. R. 2000. Sedimentology and sequence stratigraphy of a transfer zone coarse-grained delta, Miocene Suez Rift, Egypt. *Sedimentology,* 47**,** 1081-1104.

ZELILIDIS, A. & KONTOPOULOS, N. 1996. Significance of fan deltas without toe-sets within rift and piggy-back basins: examples from the Corinth graben and the Mesohellenic trough, Central Greece. *Sedimentology,* 43**,** 253-262.

Software:

https://www.adobe.com/no/products/illustrator

https://www.arcgis.com

http://www.ccwu.me/vsfm

http://www.cloudcompare.org

http://www.meshlab.net
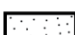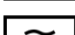
# Appendix
## Sedimentary logs

Legend

— Contour lines
*Modern day deposits*
*Gulf of Corinth*
*Rethi-Dendro Formation*
*Marine terraces*
*Delta1 Topset*
*Delta1 Foreset*
*Delta2 Topset*
*Delta2 Foreset*
*Delta2 Toeset*
*Truncation of Delta2 Foreset*
*Delta3 Topset*
*Delta3 Foreset*
*Delta 3 Toeset*
*Truncation of Delta3 Foreset*
*Delta4 Topset*
*Delta4 Foreset*
*Truncation of Delta4 Foreset*
*Bottomsets*
*Delta5 Topset*
*Delta5 Foreset*
*Slackwater deposits*
*Delta6 Topset*
*Delta6 Foreset*

## Lithology

Matrix supported conglomerate

Clast supported conglomerate

Openwork clast supported conglomerate

Sand with few floating outsized clasts

Sandstone

Marlstone
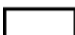
## Legend

Planar parallel stratification

Through cross-stratification

Shell fragment

Planar cross-stratification

Lenses of pebbles

## Boundaries

Sharp

Erosional

Diffuse stratification

Matrix grain size

Maximum clast size

## Facies associations

Topset facies association

Foreset facies association

Toeset facies association

Bottomset facies association

Rethi-Dendro Formation

34N  0642543
UTM 4214816

## Log 1
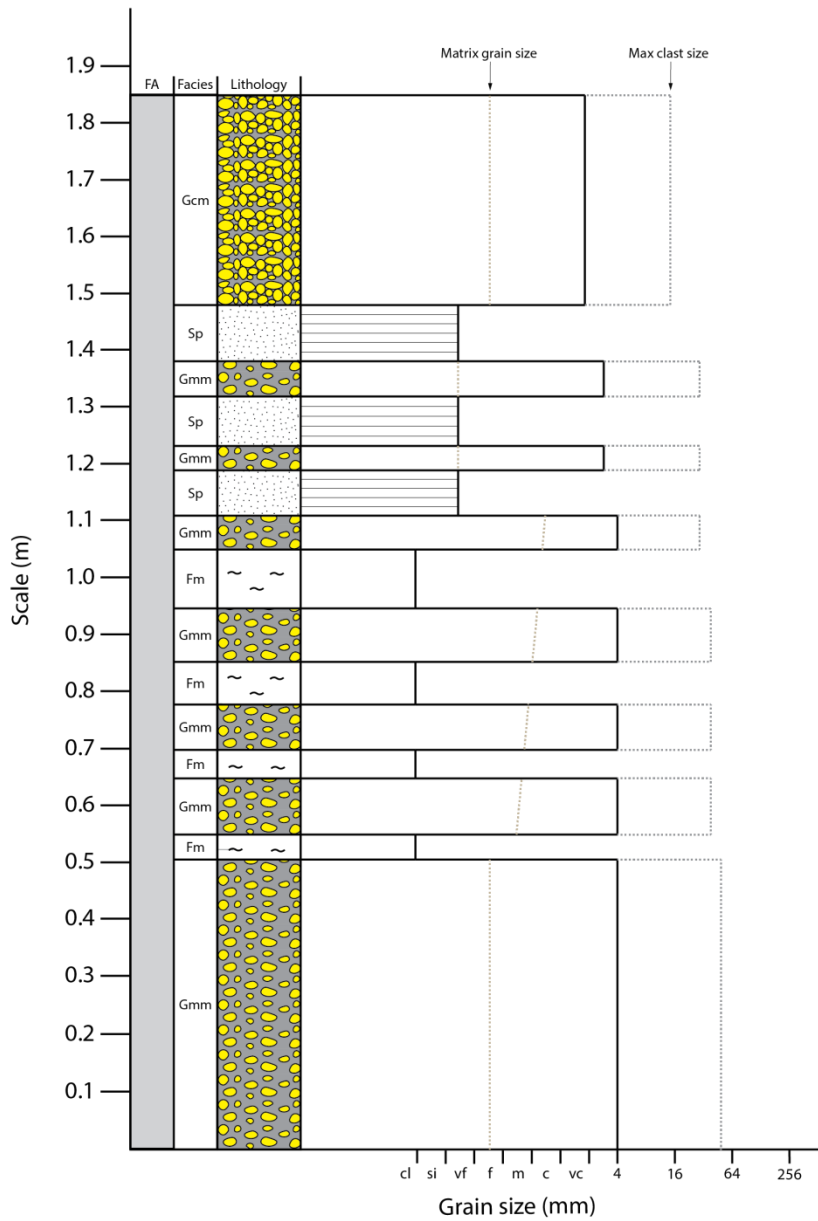
34N 0642586
UTM 4214753

## Log 2
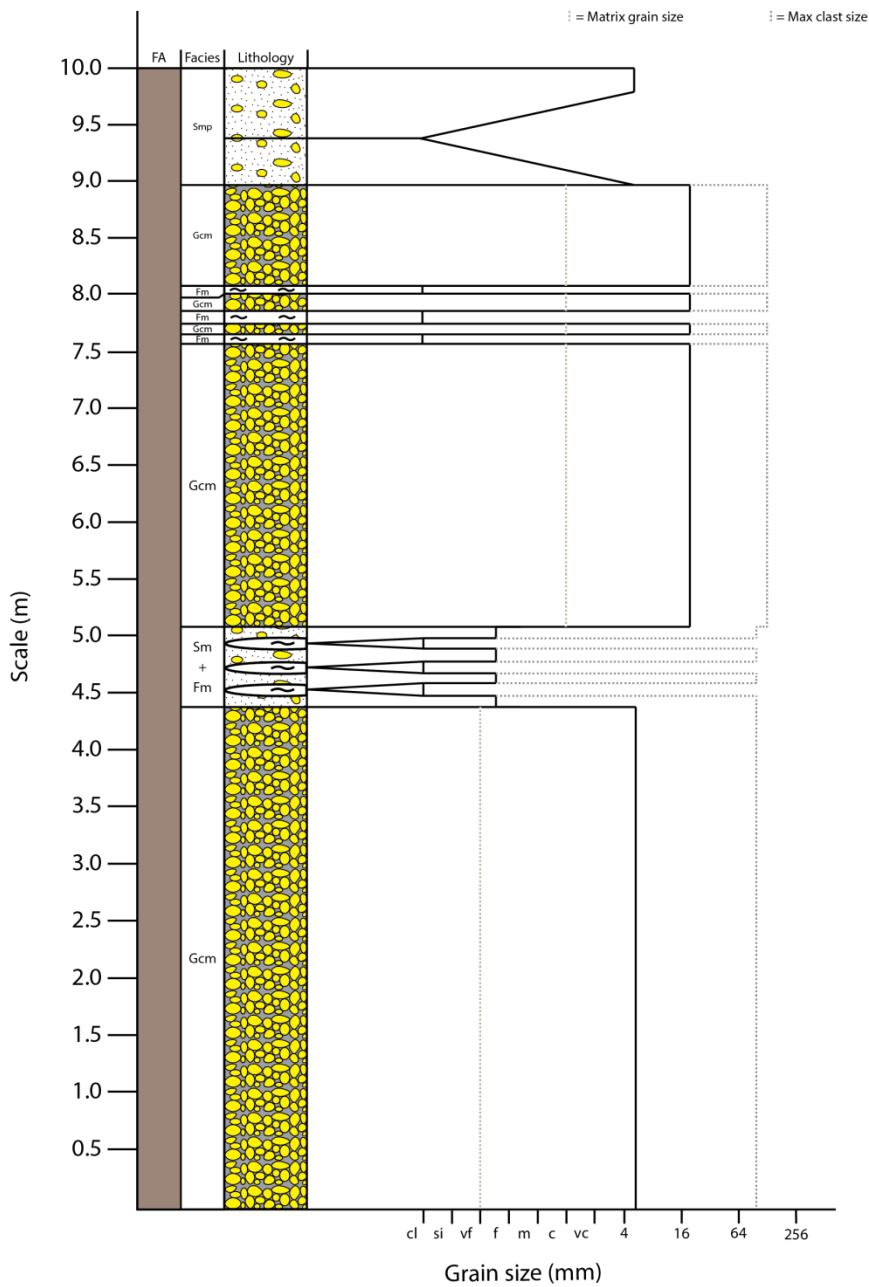
34N 0642625
UTM 4214717

## Log 3
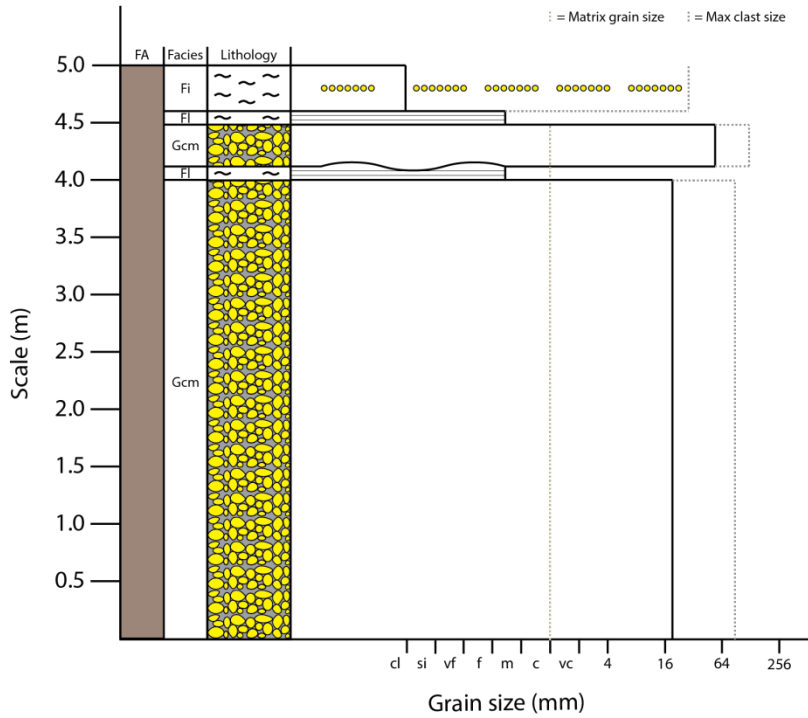


34N 0642603
UTM 4214675

## Log 4
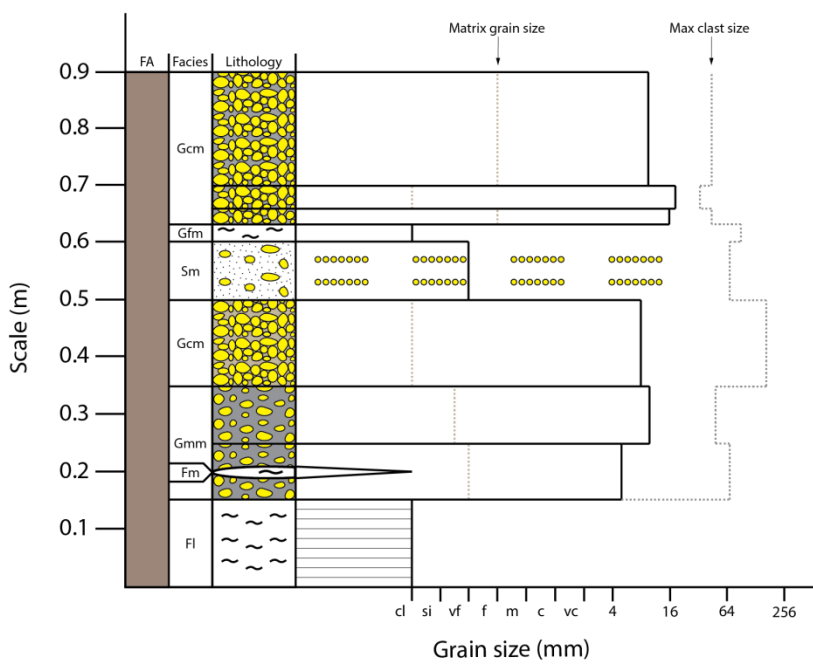
34N  0643538
UTM 4214330

## Log 5
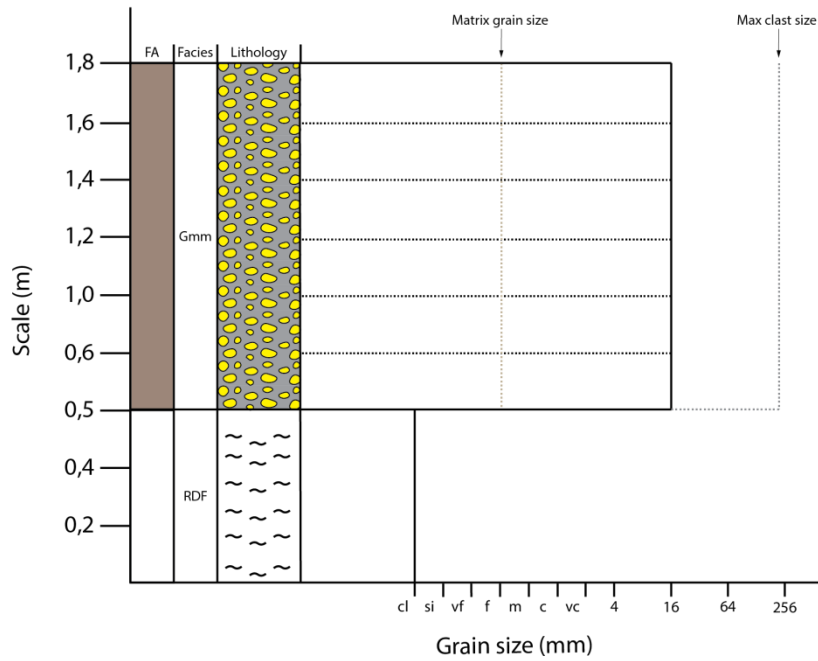


34N  0643339
UTM 4213972

## Log 6
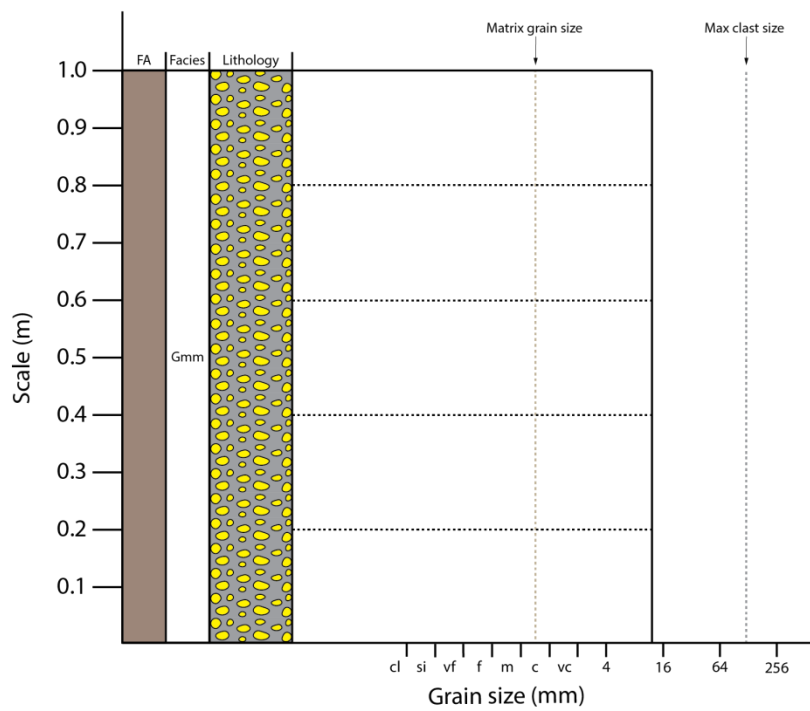
34N  0642994
UTM 4213778

## Log 7
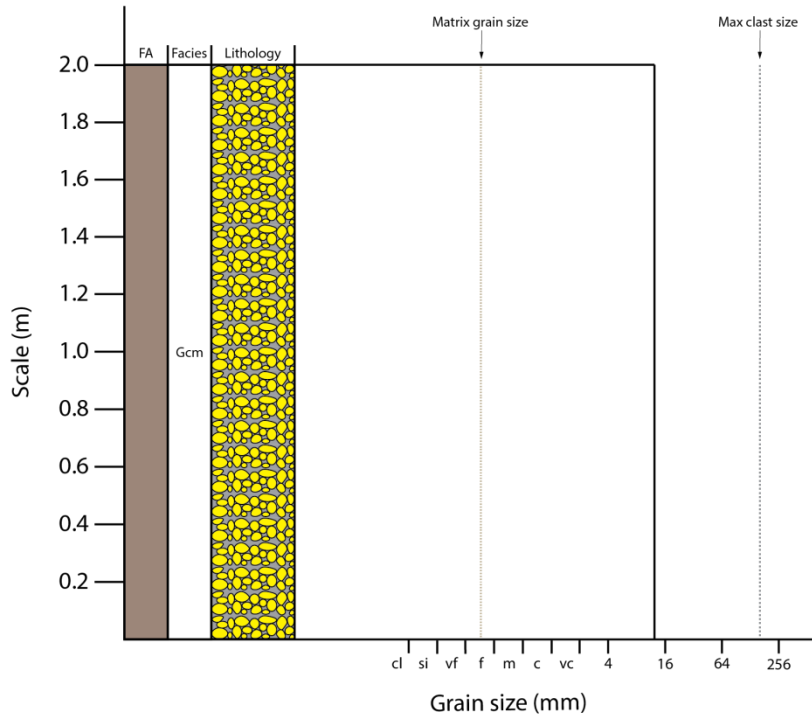


34N  0643397
UTM 4213640

## Log 8
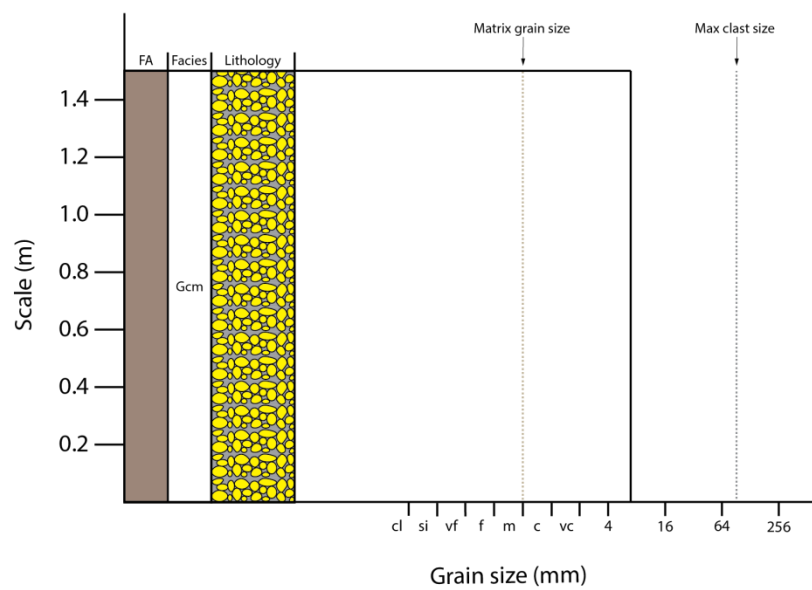
34N  0643253
UTM 4213169

## Log 9
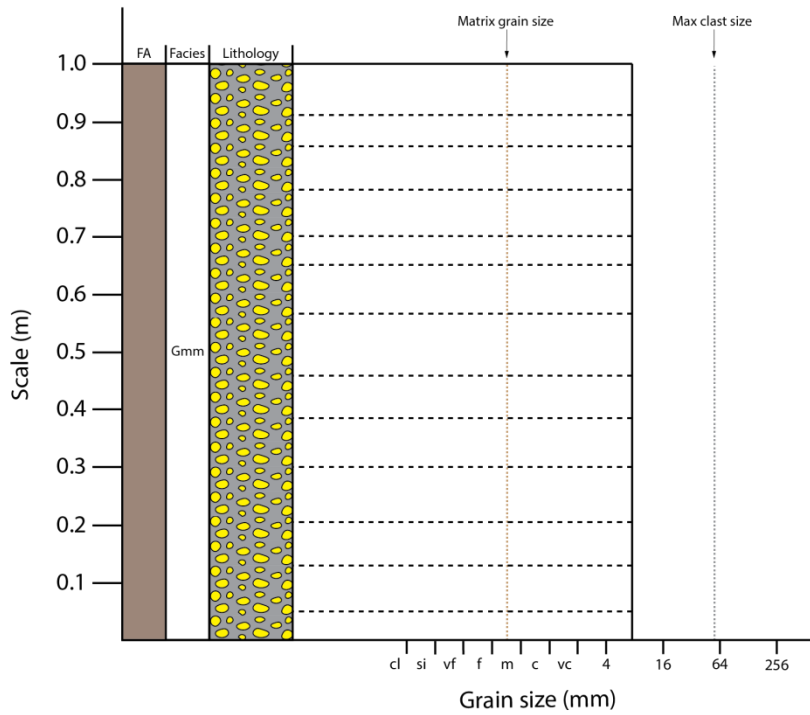


34N  0643144
UTM 4213107

## Log 10
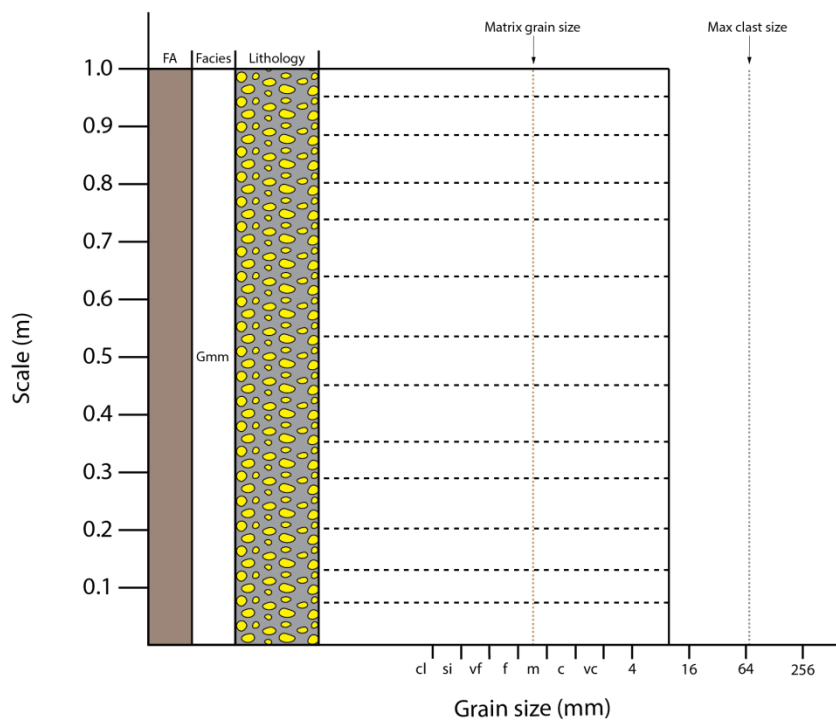
34N 0643084
UTM 4213123

## Log 11
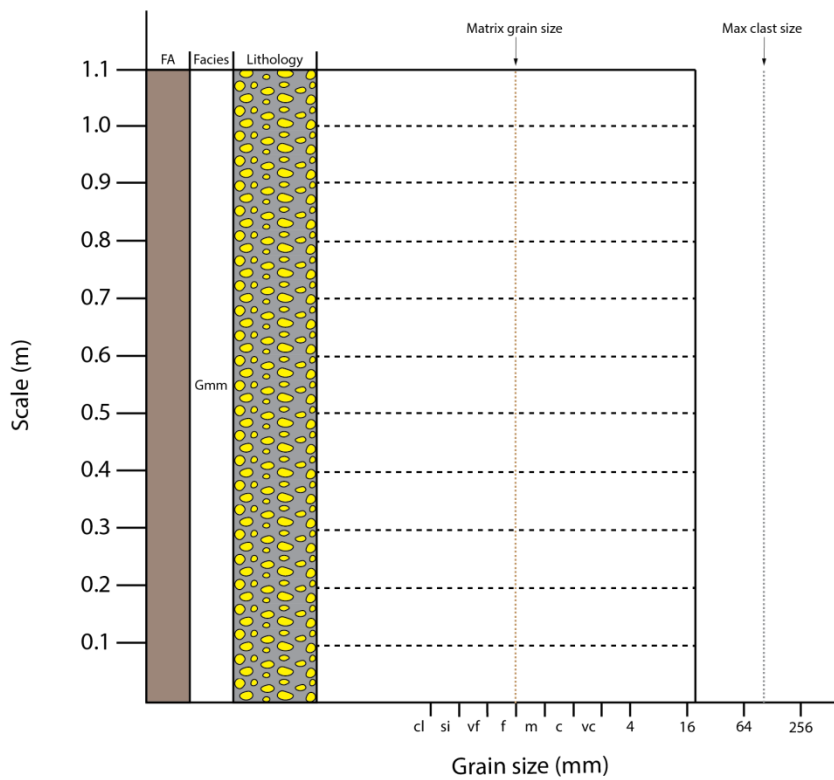
34N  0644174
UTM 4214012

## Log 12
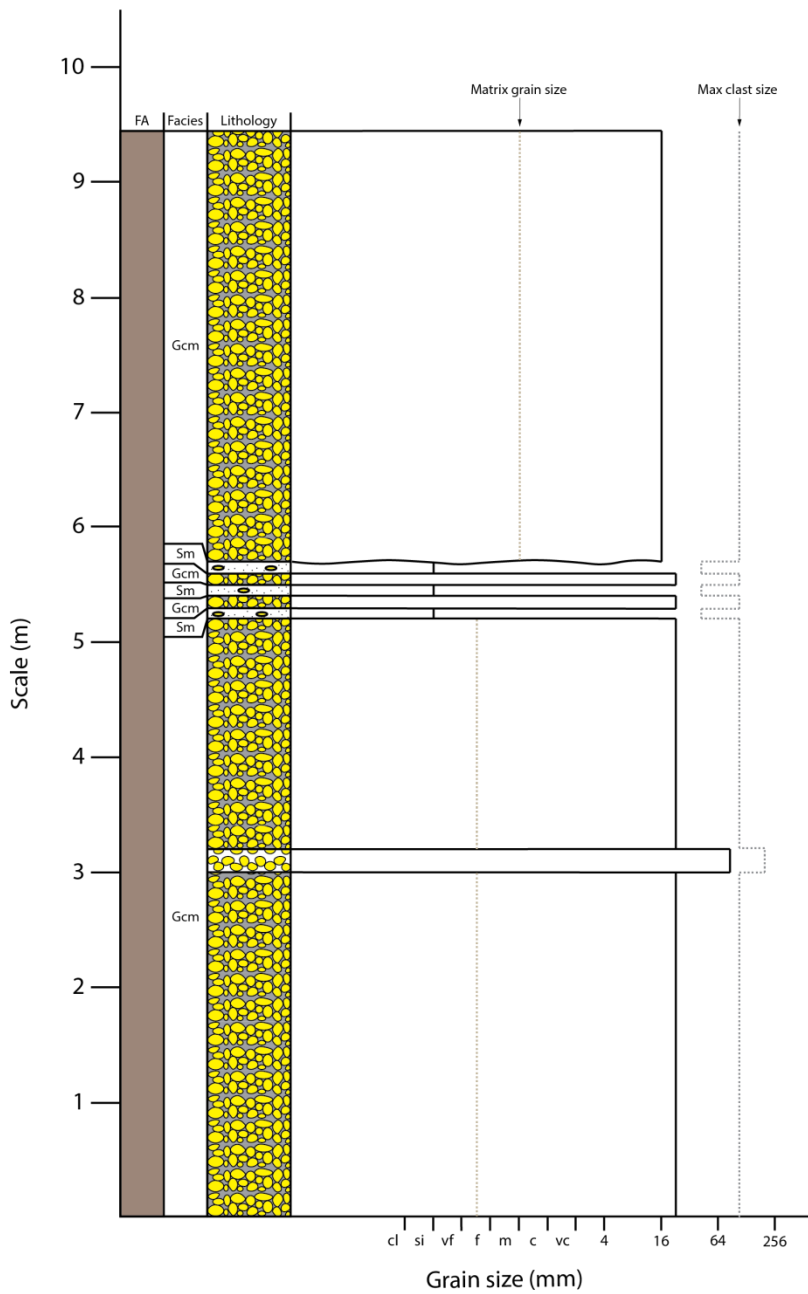
34N  0644084
UTM 4214816

Log 13
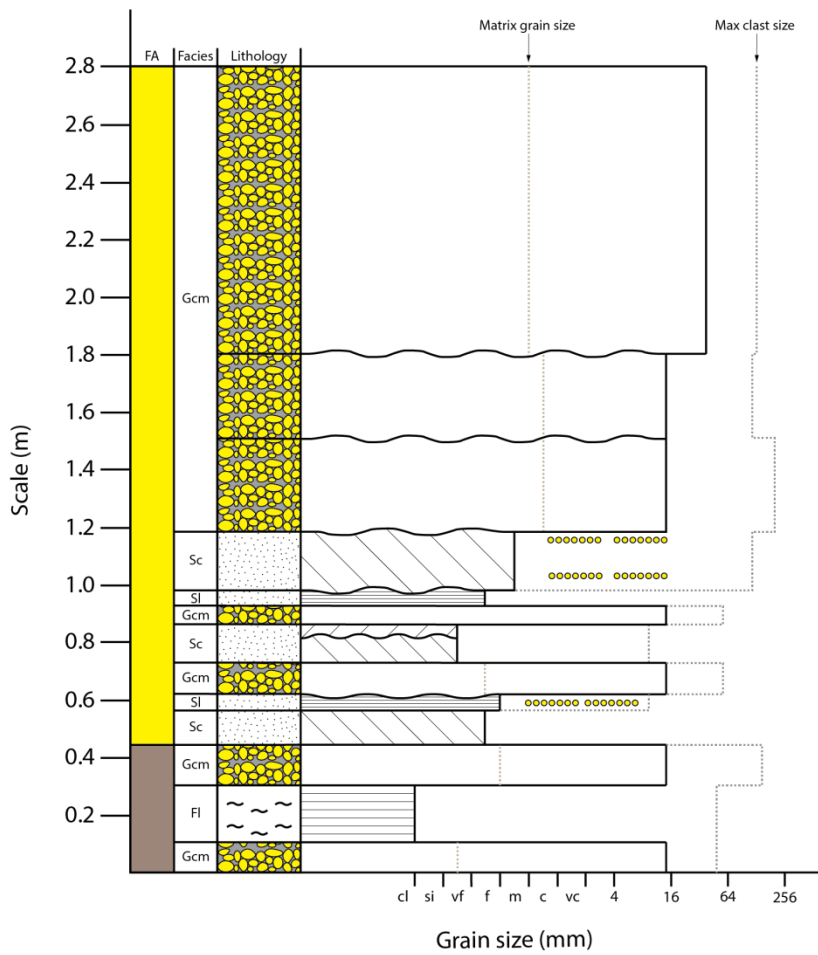
34N 0644149
UTM 4213790

## Log 14
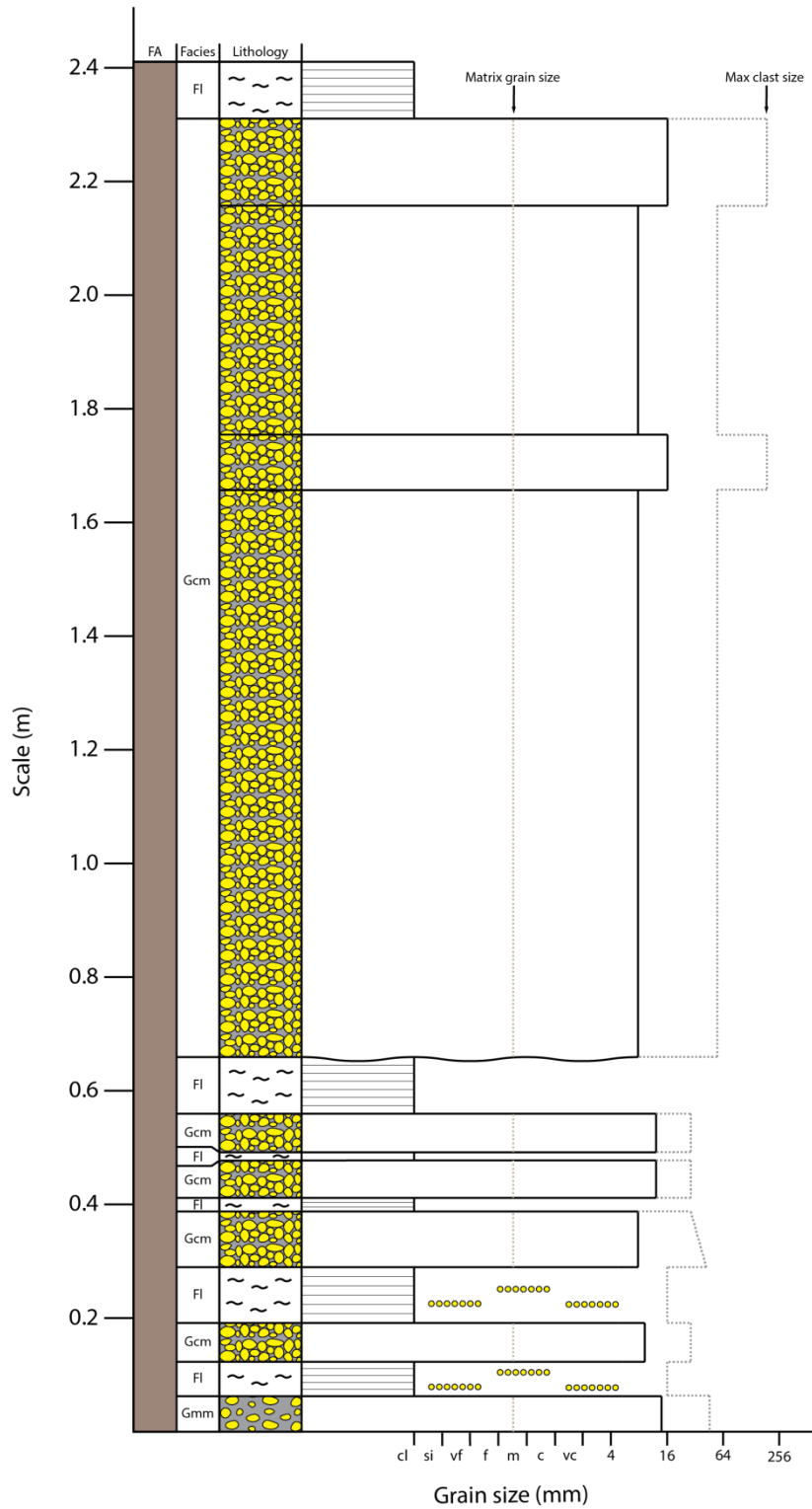
34N  0644019
UTM 4213536

## Log 15
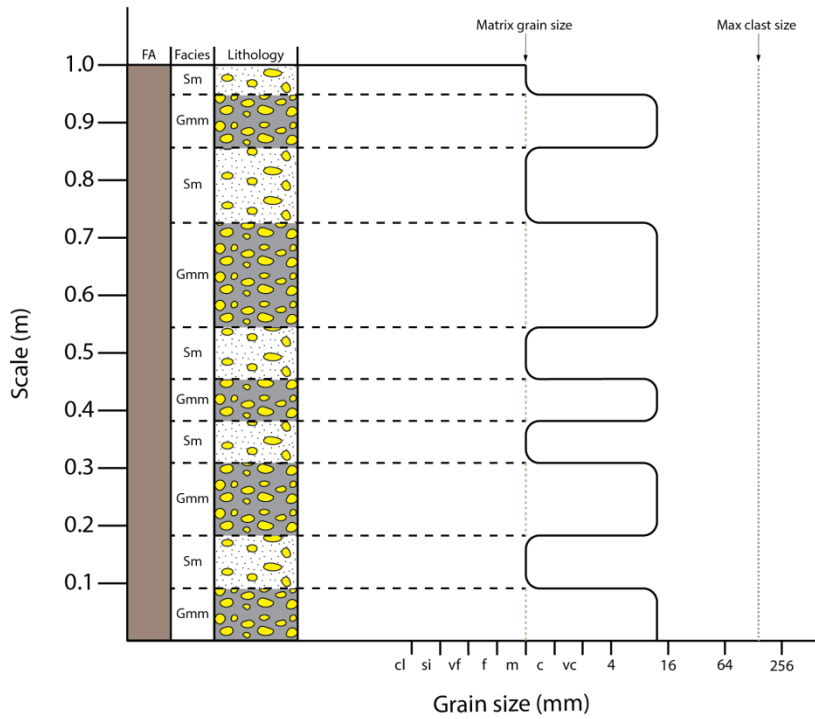


34N  0643675
UTM 4213150

## Log 16
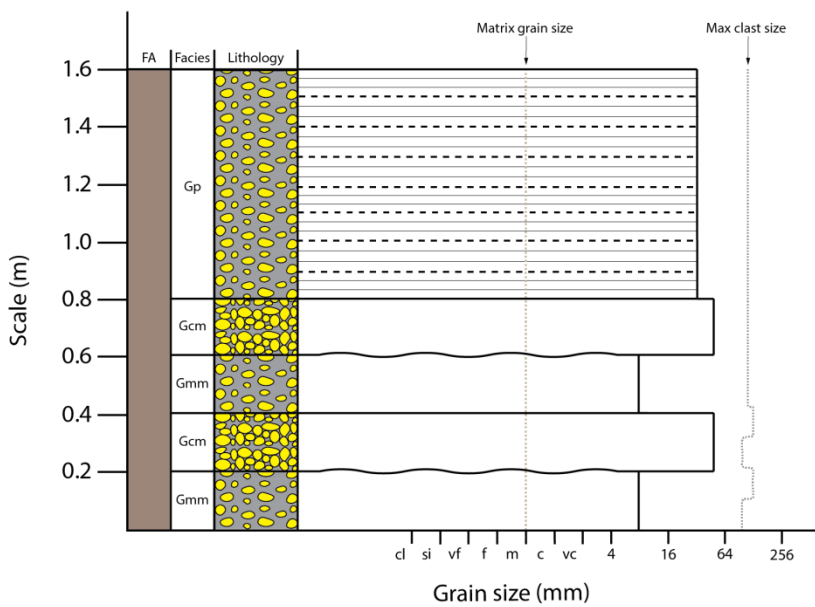
34N  0643608
UTM 4213100

## Log 17
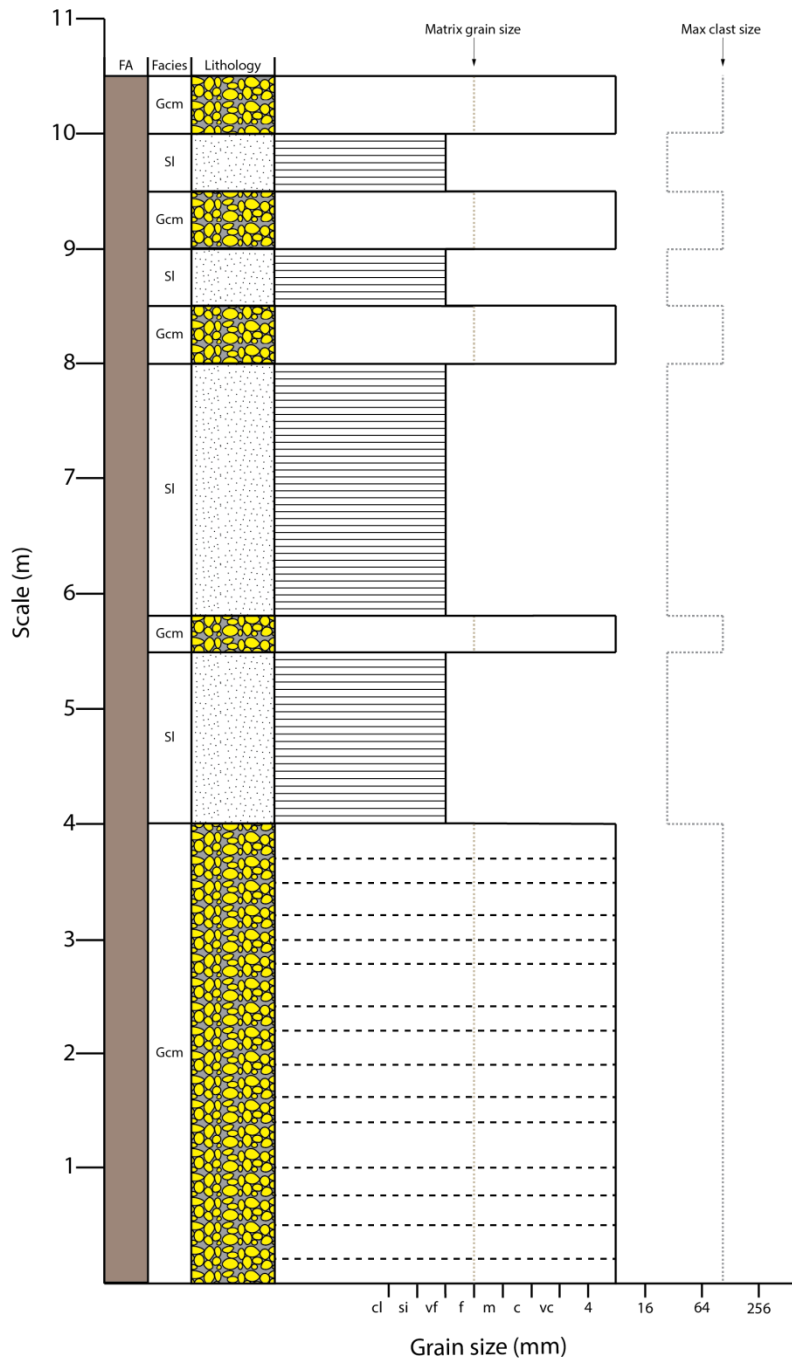
34N  0643327
UTM 4212848

Log 18
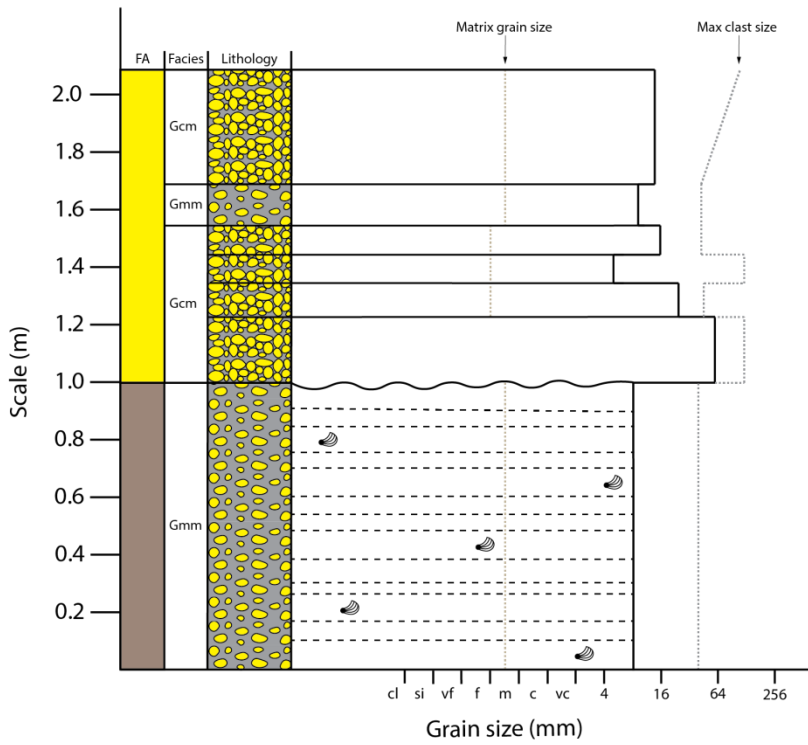


34N  0643341
UTM 4212792

Log 19
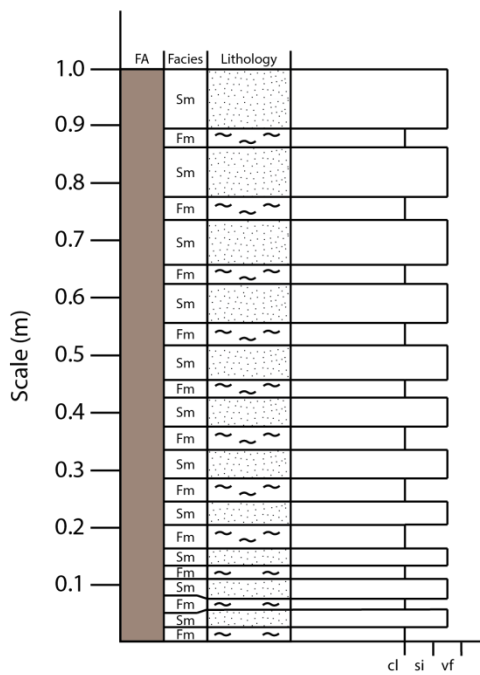
34N  0643308
UTM 4212612

Log 20
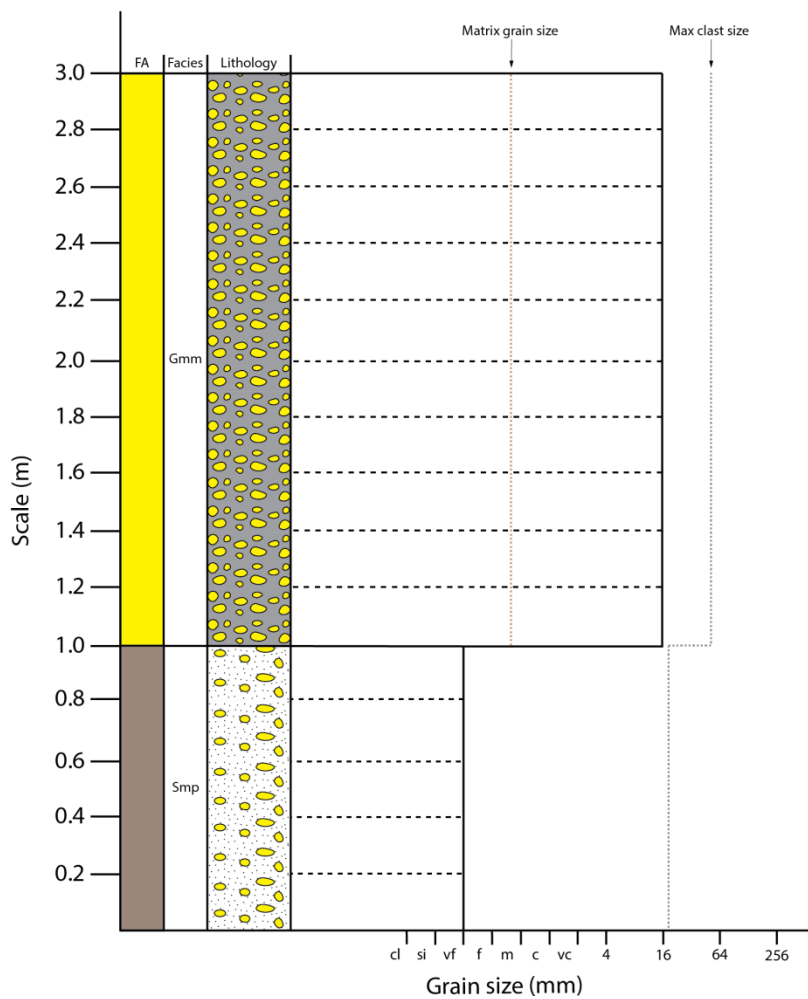
34N 0642872
UTM 4212206

## Log 21
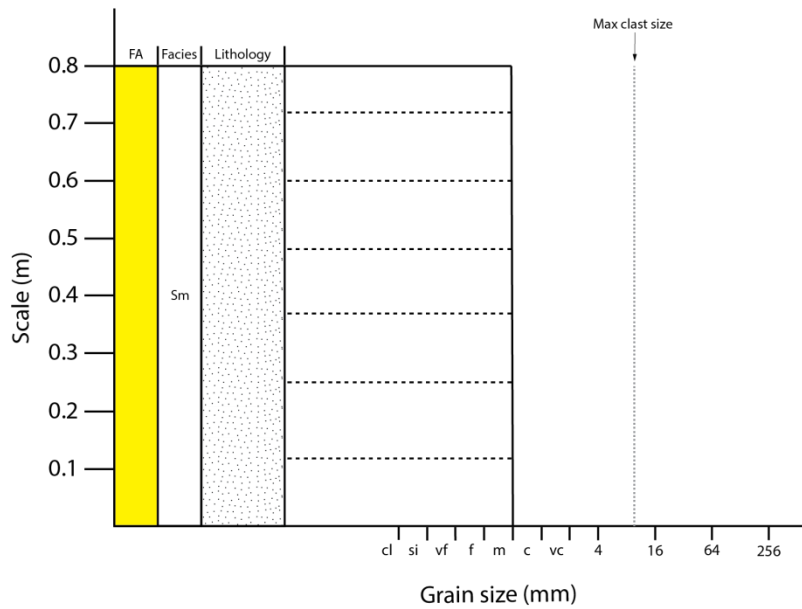


34N 0642910
UTM 4212202

## Log 22
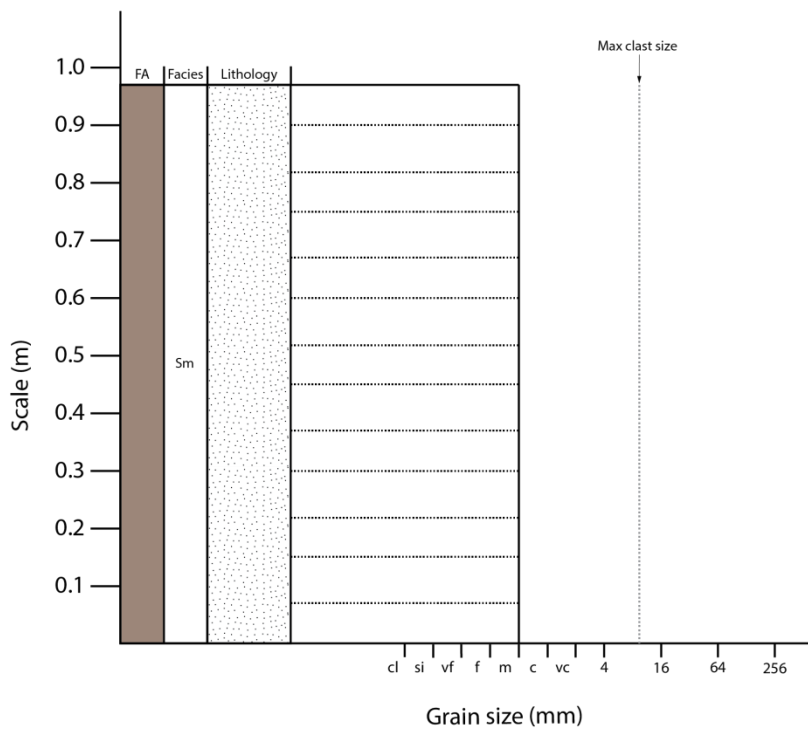
34N  0644261
UTM 4213644

## Log 23
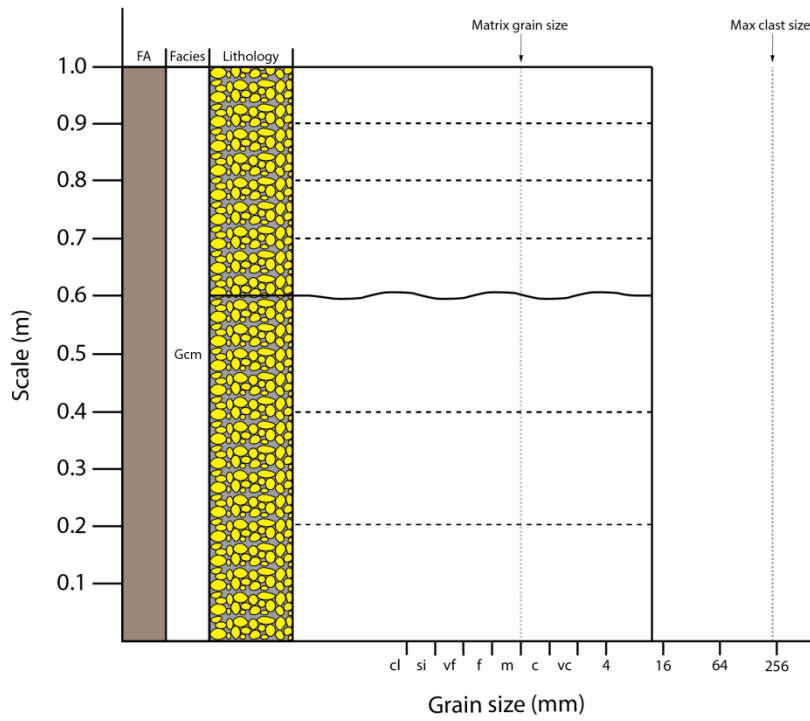
34N  0644707
UTM 4213784

## Log 24
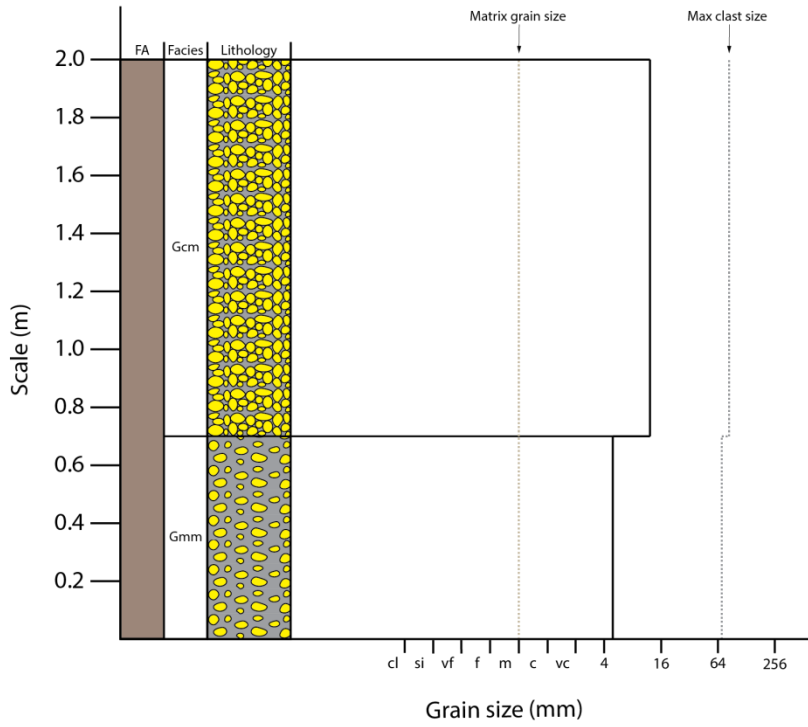
34N 0644707
UTM 4213784
Log 25
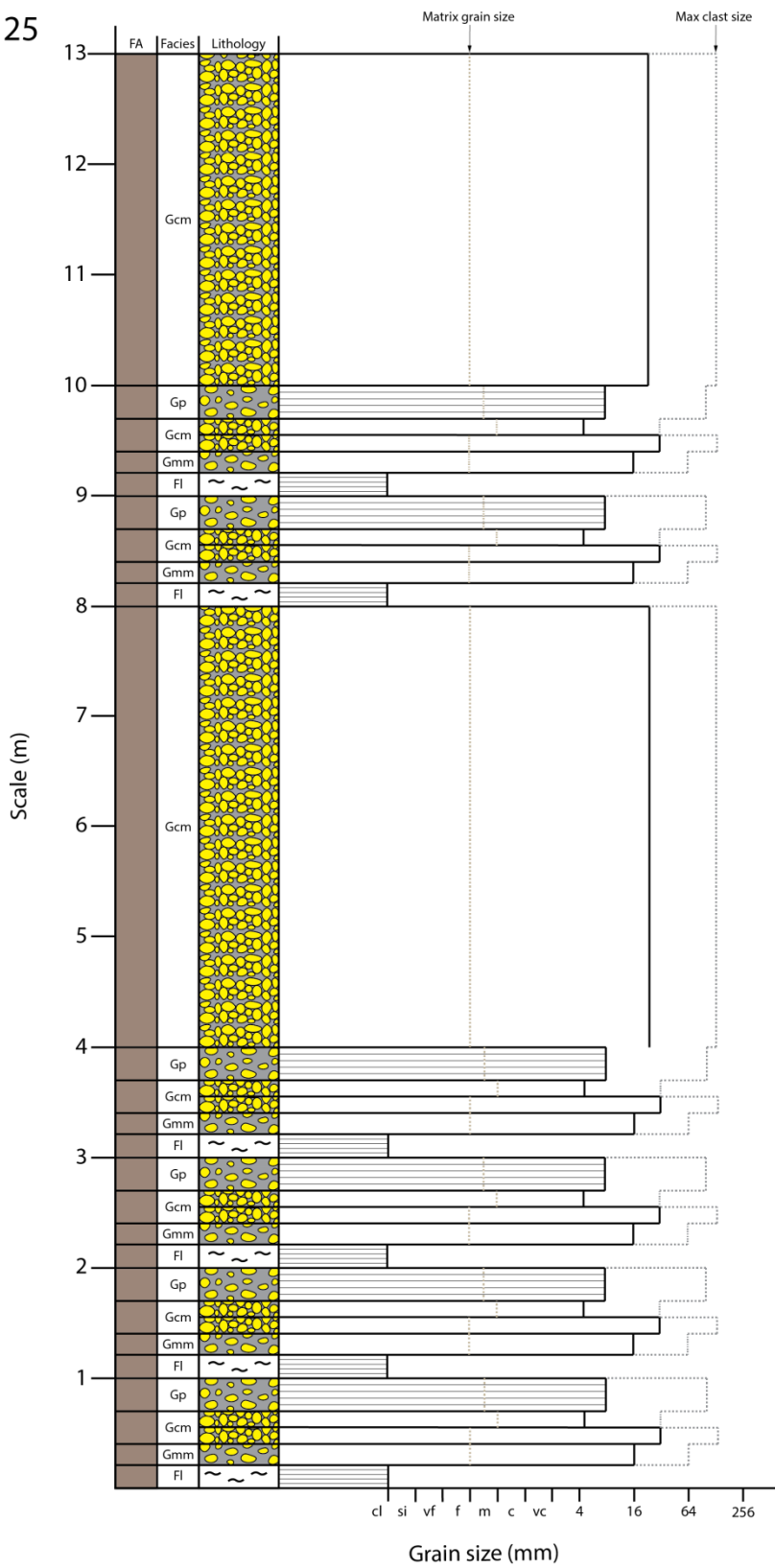
34N  0644488
UTM 4213496

## Log 26
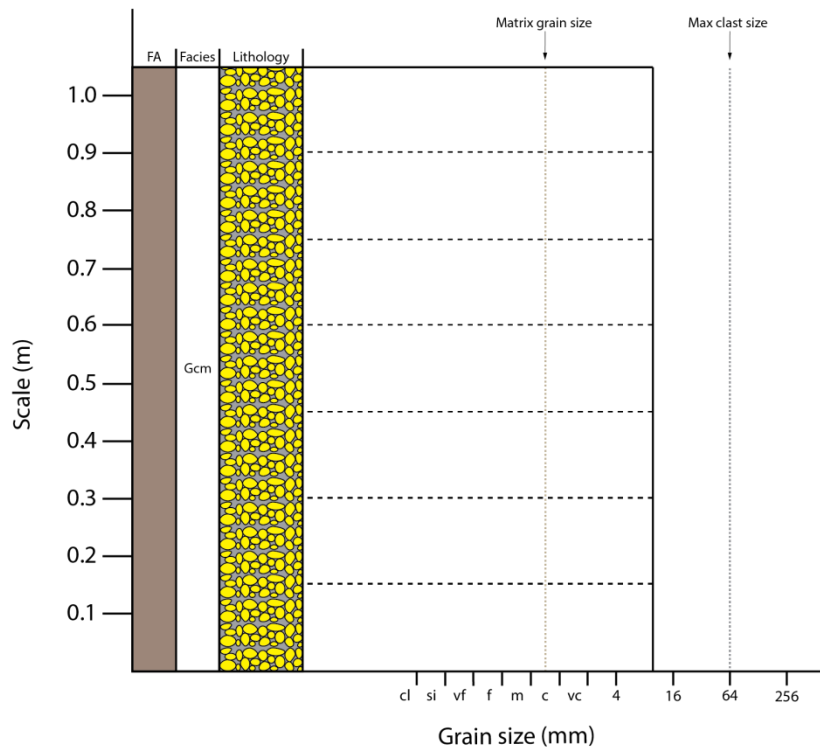


34N  0644378
UTM 4213175

## Log 27
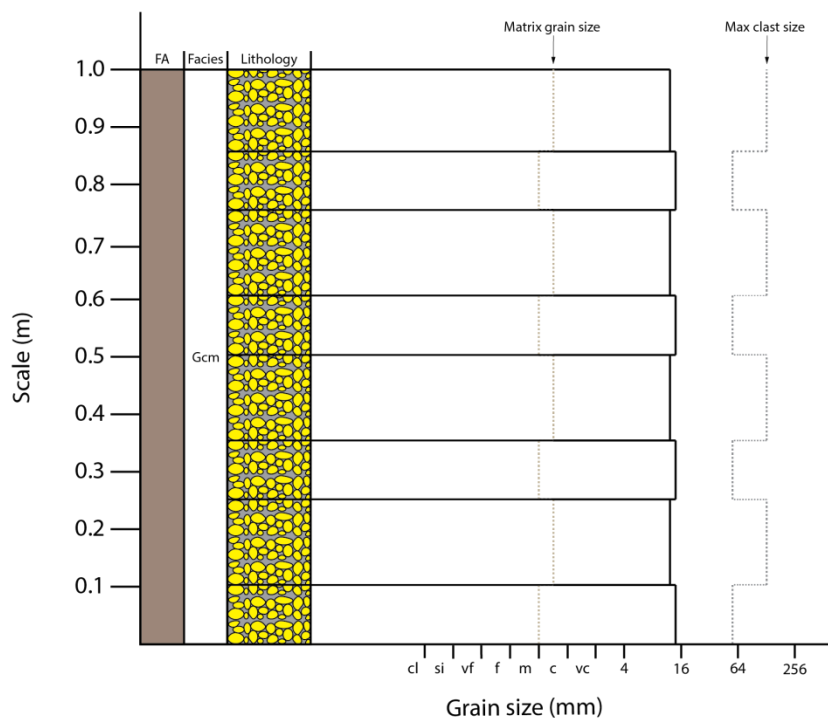
34N  0644447
UTM 4213126

Log 28
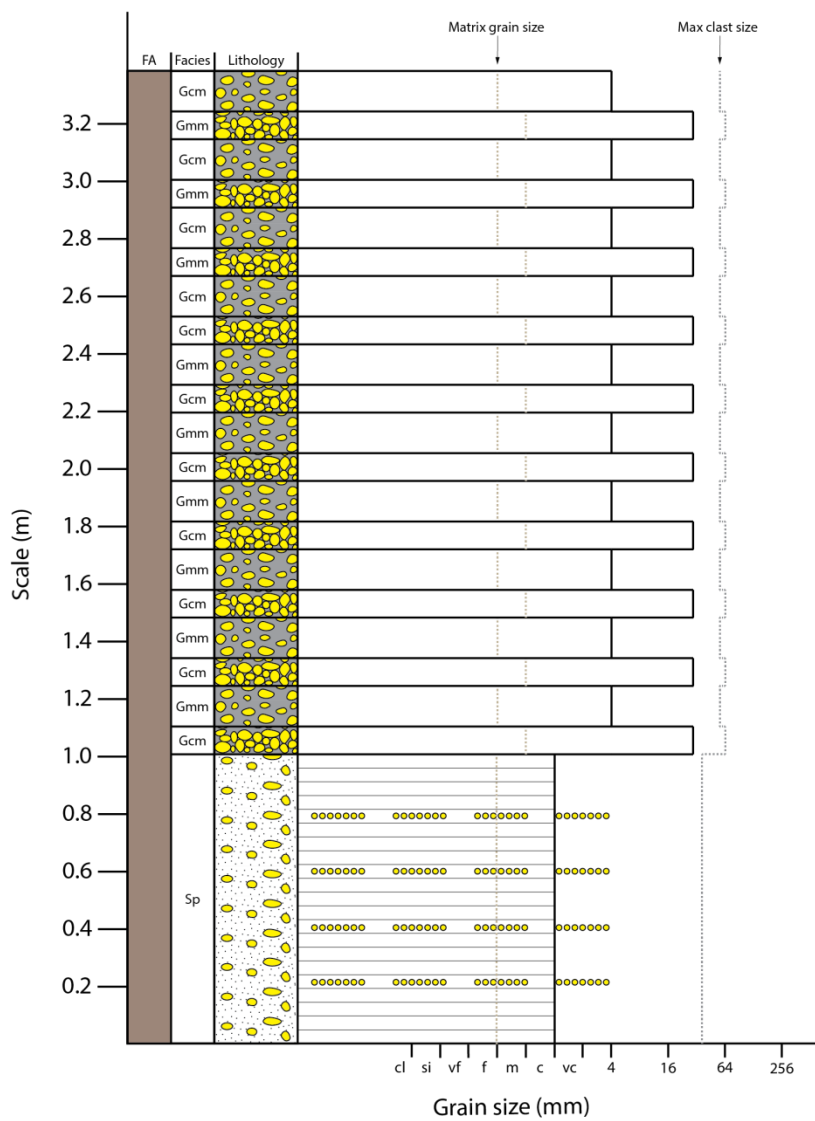
34N 0644659
UTM 4213106

Log 29
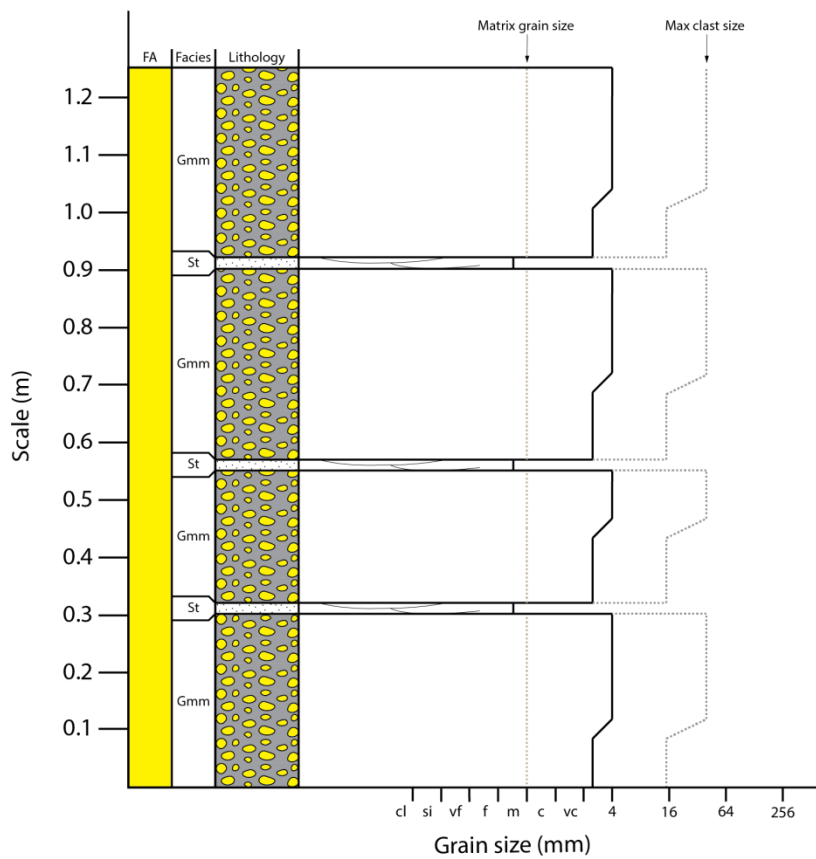
34N 0645082
UTM 4213045

Log 30
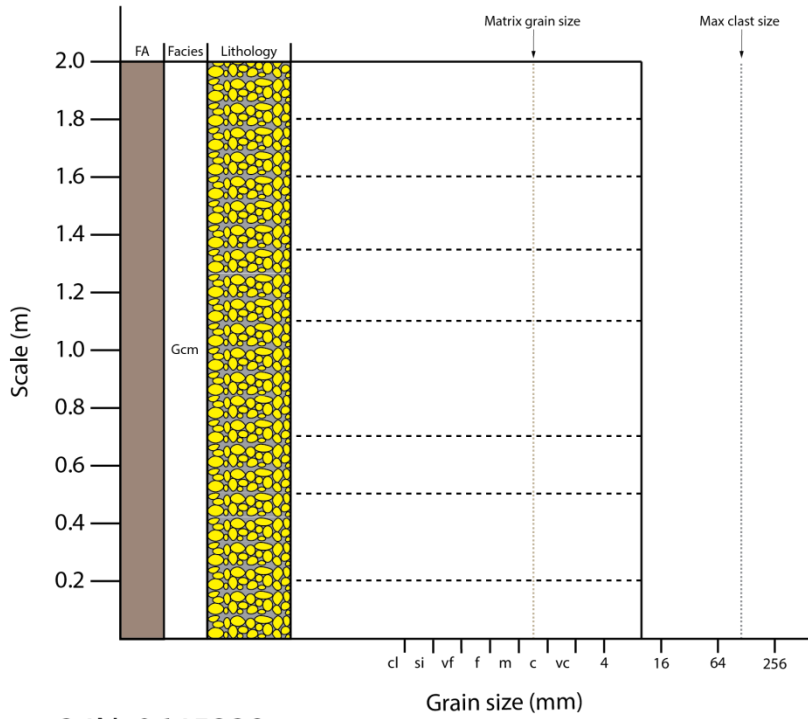


34N 0645238
UTM 4212807

Log 31
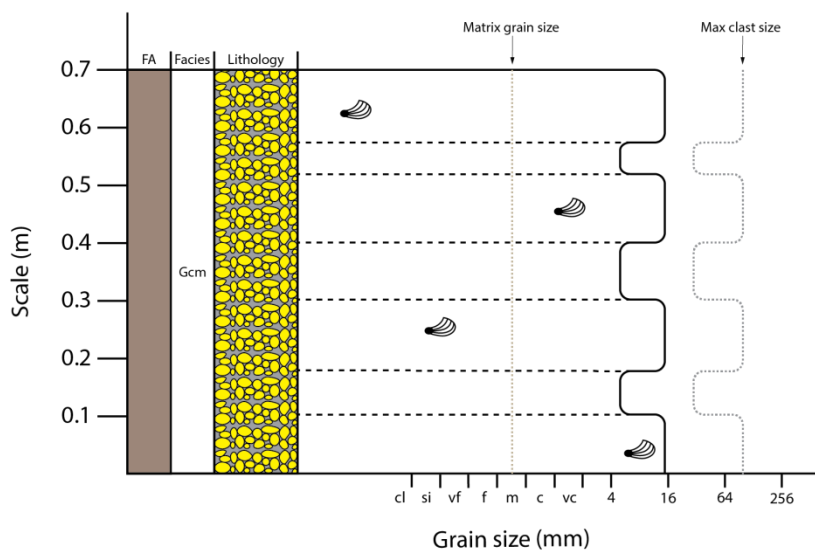
34N  0645214
UTM 4212784

Log 32
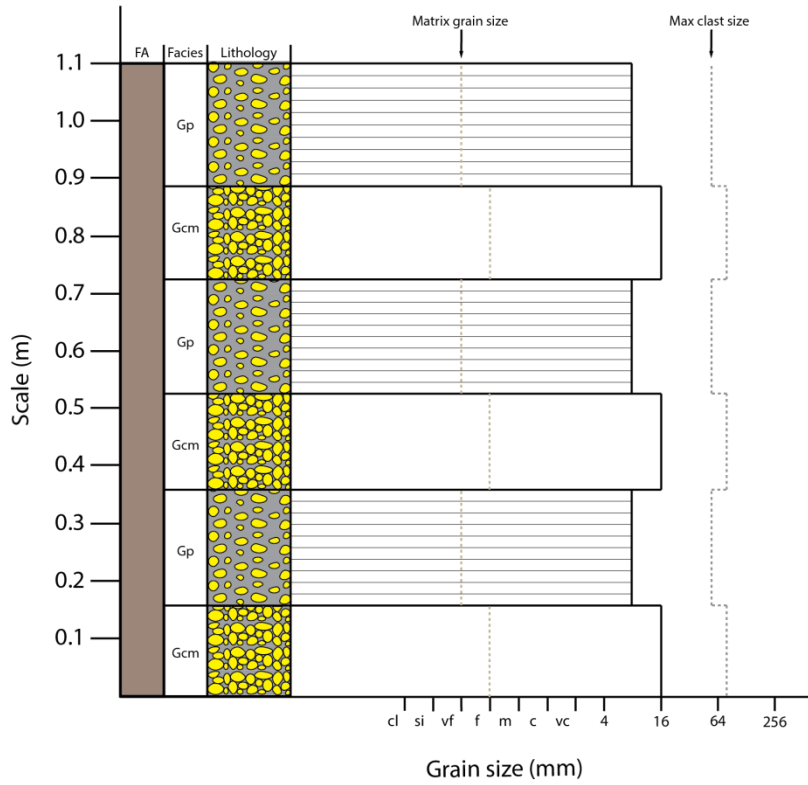
34N  0644909
UTM 4212604

## Log 33
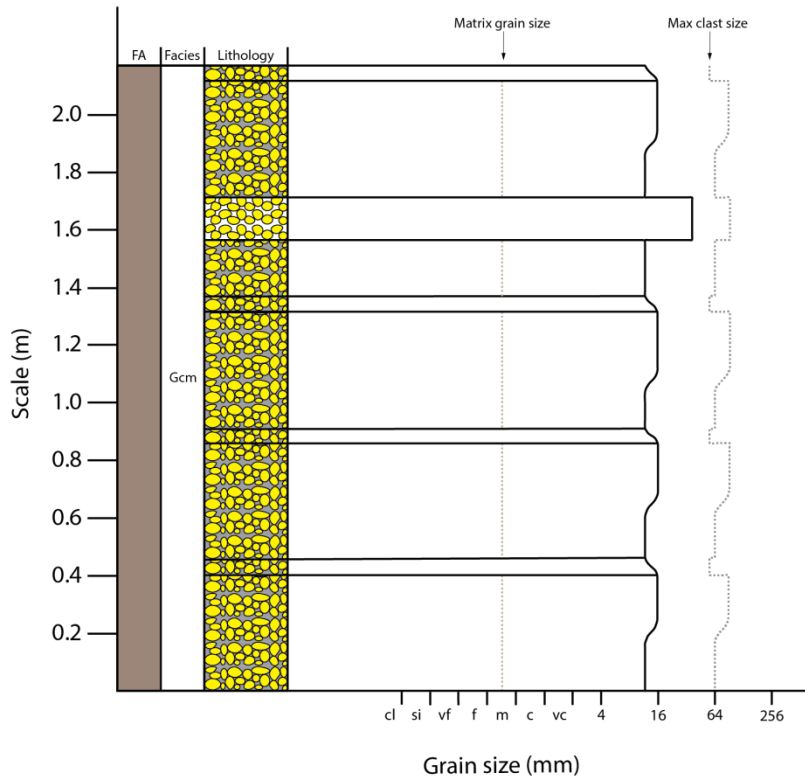
34N  0645290
UTM 4212666

Log 34
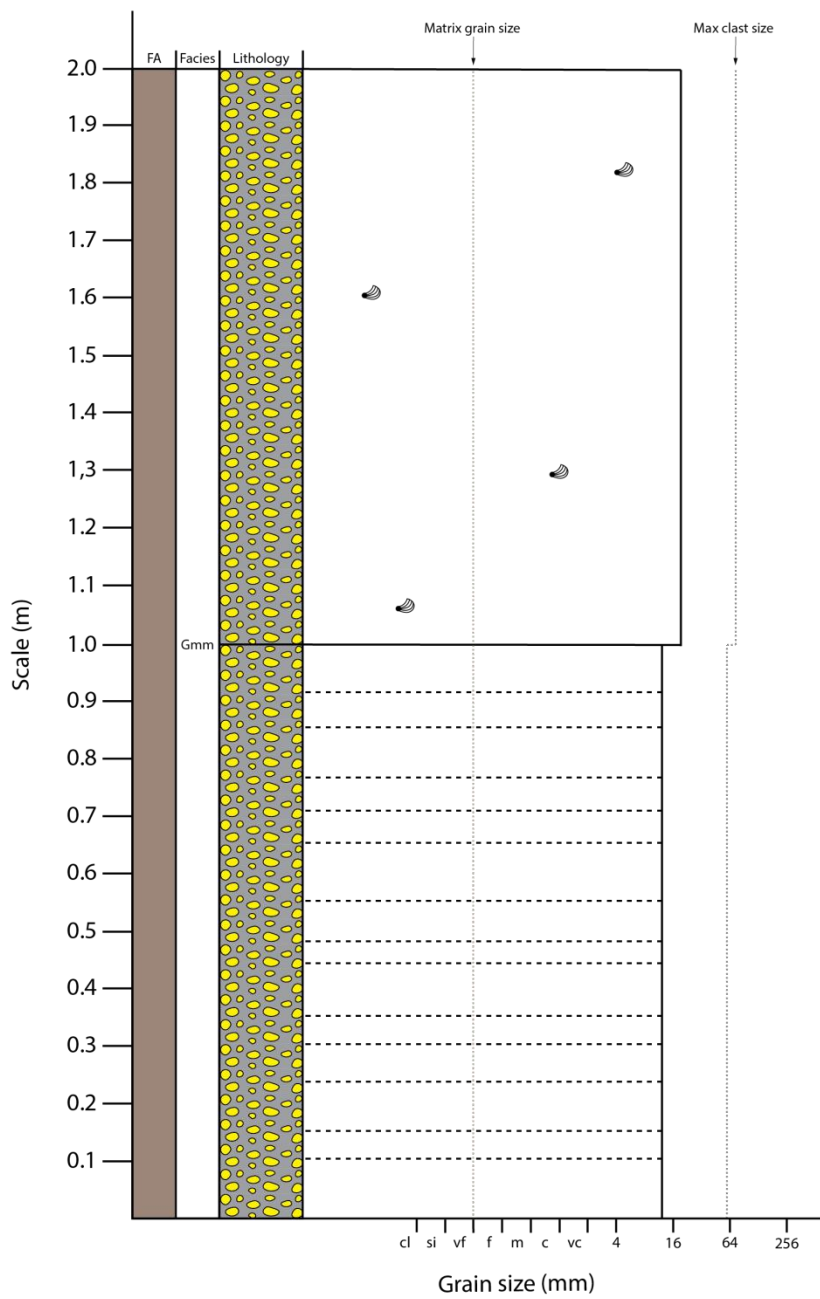
34N  0645159
UTM 4212588

Log 35
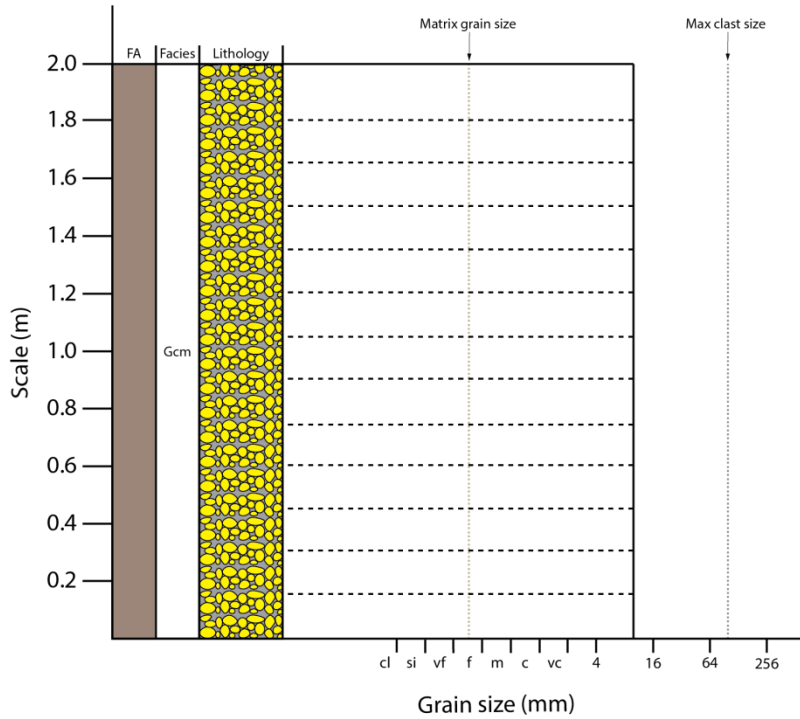
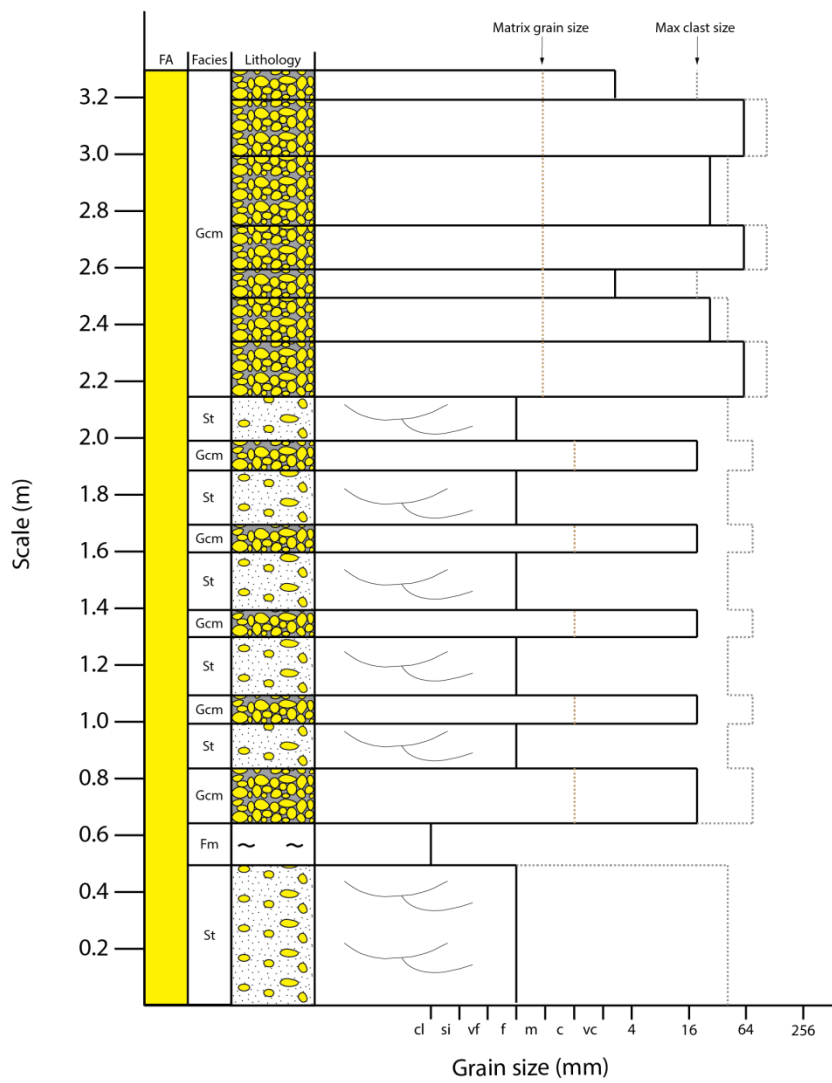

34N  0645056
UTM 4212515

Log 36
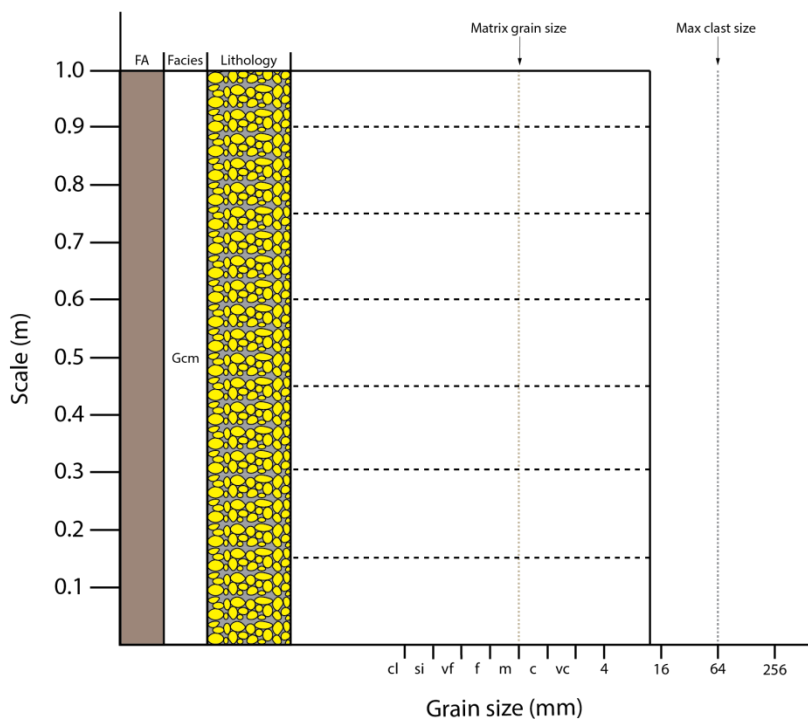
34N 0645195
UTM 4212262

Log 37
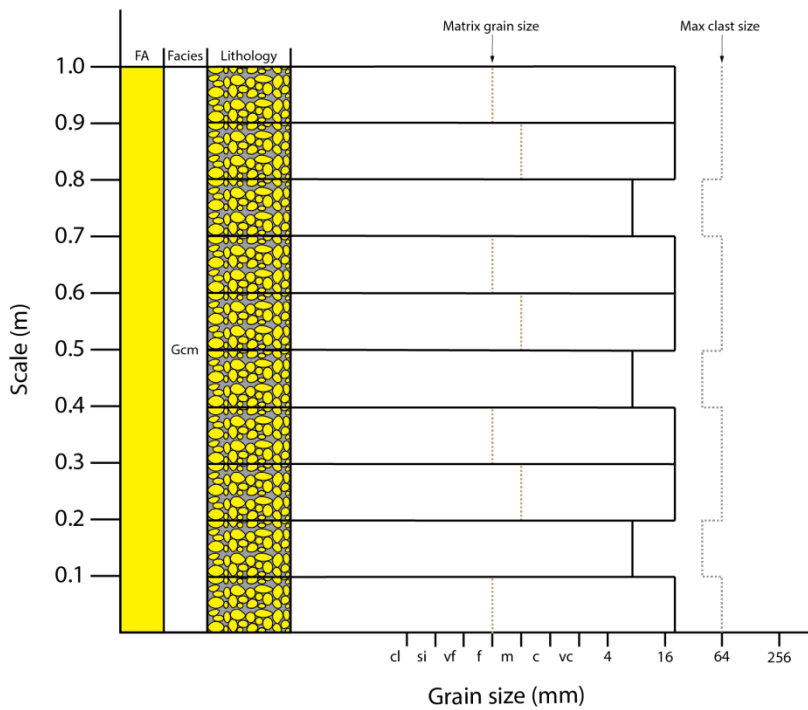
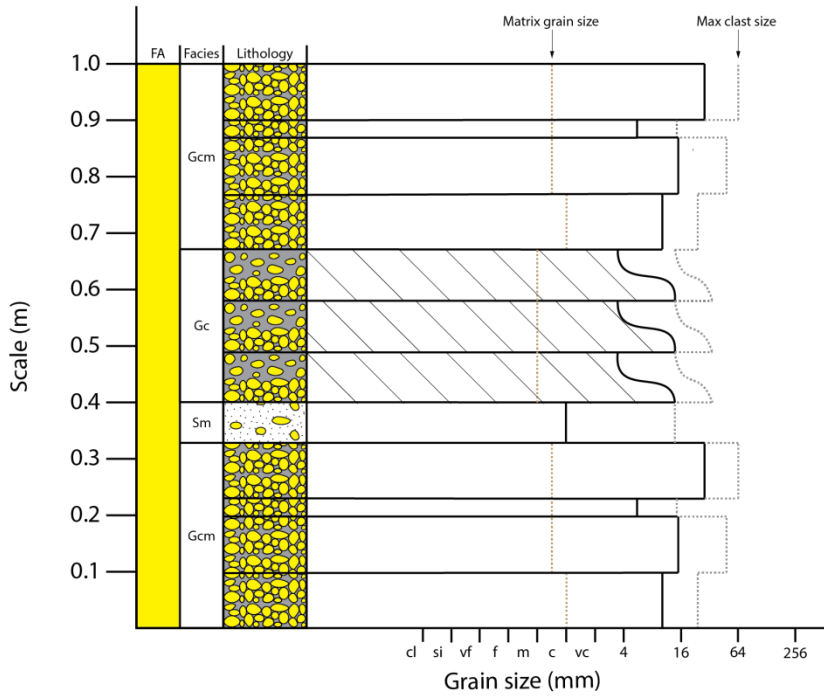34N 0645262
UTM 4212242

Log 38

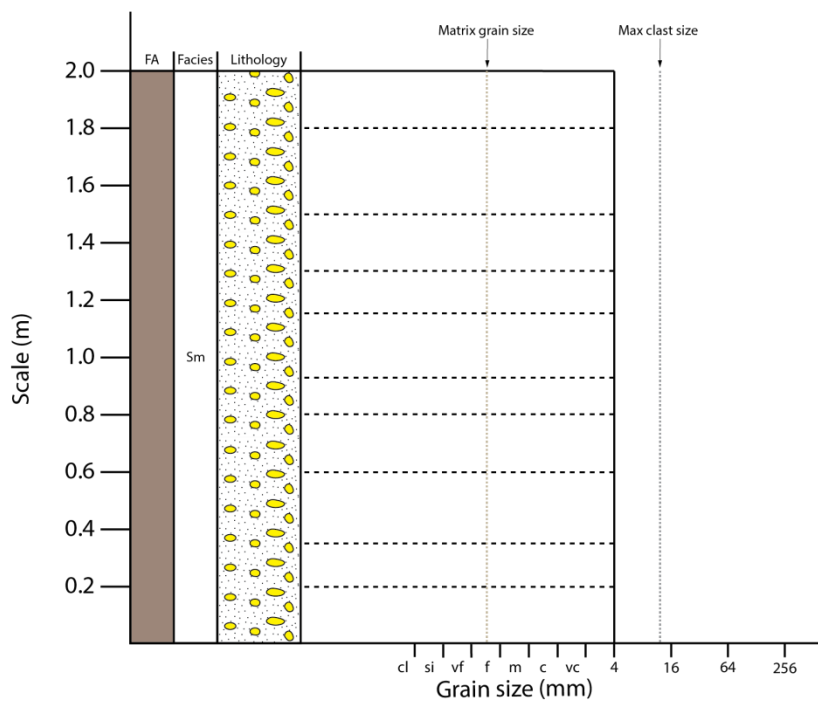34N 0645229
UTM 4212216

Log 39



34N 0645236
UTM 4212198

Log 40



106

34N  0645460
UTM 4212121

Log 41